Deliverable 2.2: Updated State of the Art on the assessment of the chemical evolution of ILW and HLW disposal cells

Work Package ACED

This project has received funding from the European Union's Horizon 2020 research and innovation programme under grant agreement N°847593.

Document information

Project Acronym	**EURAD**
Project Title	**European Joint Programme on Radioactive Waste Management**
Project Type	**European Joint Programme (EJP)**
EC grant agreement No.	**847593**
Project starting / end date	**1st June 2019 – 30 May 2024**
Work Package No.	**2**
Work Package Title	**Assessment of Chemical Evolution of ILW and HLW disposal cells**
Work Package Acronym	**ACED**
Deliverable No.	**2.2**
Deliverable Title	**Updated State of the Art on the assessment of the chemical evolution of ILW and HLW disposal cells**
Lead Beneficiary	**COVRA**
Contractual Delivery Date	**1 June 2023**
Actual Delivery Date	**15 May 2024**
Type	**Report**
Dissemination level	**PU**
Authors	**Diederik Jacques (SCK CEN), Erika Neeft (COVRA), Guido Deissmann (FZJ)**

To be cited as:

Jacques, D., Neeft, E., Deissmann, G., (2024): Updated State of the Art on the assessment of the chemical evolution of ILW and HLW disposal cells. Final version as of 15.05.2024 of deliverable D2.2 of the HORIZON 2020 project EURAD. EC Grant agreement no: 847593.

Disclaimer

Acknowledgement

This document is a deliverable of the European Joint Programme on Radioactive Waste Management (EURAD). EURAD has received funding from the European Union's Horizon 2020 research and innovation programme under grant agreement No 847593.

Status of deliverable		
	By	Date
Delivered (Lead Beneficiary)	E. Neeft (COVRA)	23 Jan 2024
Verified (WP Leader)	D. Jacques (SCK CEN)	25 Jan 2024
Reviewed (Reviewers)	K. Jantschik (GRS)	16 Feb 2024
Revised	E. Neeft (COVRA) D. Jacques (SCK CEN)	14 Mar 2024
Approved (PMO)	T. Beattie	8 May 2024
Submitted to EC (Coordinator)	Andra (Coordinator)	16/05/2024

Executive Summary

The broader scope of the work package ACED is the assessment of the chemical evolution at the disposal cell scale involving interacting materials and thermal, hydraulic and/or chemical gradients by considering Intermediate Level Waste (ILW) and High Level Waste (HLW) disposal concepts. These concepts are representative for Europe. HLW and ILW disposal cells in granitic and clay host rocks are studied in ACED. Disposal of this waste is foreseen in geological disposal facilities at a sufficient large depth to minimize the impact of climate change on the chemical evolution of these disposal cells. The waste is removed from the immediate human and dynamic, natural surface environment and the stable geological deep environment provides predictable conditions for the chemical evolution of the materials within these disposal cells. A key feature in the chemical evolution of disposal cells in the post-closure phase is the availability of water. Construction and operation can have an important influence on this availability, especially for disposal cells in indurated clays.

The focus of this report is to give an update of the state-of-the-art by highlighting the main insights obtained in ACED.

Vitrified HLW has been investigated in ACED and this waste form arises from the reprocessing of spent fuel. The produced liquid waste with a high content of radionuclides is mixed with melted borosilicate glass and the mixtures are poured in stainless steel canisters. The stainless steel canister is encapsulated in carbon steel overpack and surrounded by a buffer. The clay and granitic host rock in the vicinity of the buffer is heated for a couple of thousands of years. This buffer may control the access of water to the carbon steel overpack, especially for the bentonite buffer envisaged for a disposal cell in granitic rock. A cementitious buffer was included in the disposal cell with indurated clay. The effect of aggregates in a cementitious buffer can have a high impact on the evolution of properties for the transport of water but the indurated clay may control the access of water to the carbon steel overpack. There is contact between pore water and the vitrified waste form after fracture of this overpack. ACED has taught us that the glass alteration rate in the vicinity of steel is controlled by the corrosion rate of steel and not by a product layer of hydrated glass with passivation capacity to minimize the alteration rate. The radionuclides in the waste have decayed till such an extent that the radiotoxicity of the waste is smaller than uranium ore when the glass starts to alter.

Cemented metallic and organic ILW have been investigated in ACED. The ILW disposal vaults are larger in size than the HLW disposal tunnels. Also, more host rock damaging construction methodologies can be used for ILW disposal vaults than for HLW disposal tunnels. Construction and operation can therefore have a higher impact on the chemical evolution in ILW disposal cells than in HLW disposal cells. The metallic waste and organic waste chosen to be investigated in ACED were neutron irradiated steel and cellulosic waste contaminated with radionuclides. Influx of water from the host rock as well as carbonation of cementitious minerals by ingress of dissolved CO_2 and bicarbonate may control the degradation rate of these types of waste. For both the granitic and clay rock, the dimensions of the vaults and type and content of waste packages was assumed to be similar in the generic ILW disposal cells studied in ACED. In this case, the alteration rate of concrete and degradation rate of waste is higher for granitic rock than for indurated clay rock due to the differences in availability of water in the host rock in the vicinity of the engineered barriers.

Keywords

Vitrified, cement, steel, granite, clay

Table of content

List of figures

List of Tables

1. Introduction

Long-term management of radioactive waste includes its final destination in a disposal facility or repository. Depending on the type of waste, disposal facilities are located at the surface or close to the surface for short lived low level or intermediate level waste (low level waste, LLW), whereas deep geological disposal is the preferred solution for long lived intermediate or (heat producing) high level waste (respectively ILW or HLW). The disposal system consists of an engineered barrier system (EBS) and natural barriers (geological formations) and its objective is to isolate the waste from the accessible biopshere and contain the radionuclides in the waste. Isolation of the waste is achieved by granitic host rock and the overburden of the clay host rock and reduce substantially the likelihood of inadvertent human intrusion. The clay host rock and EBS both contribute to the containment of the radionuclides in the waste. The geological formations minimize the impact of climate change on the evolution of the EBS until the waste is no longer hazardous. The EBS consist of the waste form, waste package and buffer or backfill. Only for HLW, there is a carbon steel overpack between the waste package and buffer.

In the framework of this report, a disposal cell – as part of the disposal system – is defined as the EBS surrounded by the host rock. In most designs, the engineered barriers consist of various different materials and also the host rock will have geochemical properties (pore water composition, mineral phases) significantly different from the properties of the engineered barriers. Diffusive (and sometimes also advective) transport of solutes will introduce disequilibrium with geochemical reactions as a consequence. In addition to the multiple materials and interfaces, aspects of transient processes (heat evolution, re-saturation) cannot be neglected. As such, the geochemical conditions in a disposal cell are not static but will evolve with time.

The broad subject of this report is assessment of the chemical evolution at the disposal cell scale for ILW and HLW and is based on R&D that have been done within the work package ACED – **Assessment of the chemical evolution in ILW and HLW disposal cells** – of the EURAD project. The information is complementary to that in the original state-of-the-art reports that were written at the start of the ACED project (Deissmann et al., 2020, Neeft et al., 2020,2022).

The main **objective of ACED i**s to improve methodologies to obtain multi-scale quantitative models for the chemical model at cell disposal scale, based on experimental data and process knowledge, and to improve the description of the most relevant processes driving the chemical evolution into robust mathematical frameworks. Applications will lead to integrated process understanding at larger temporal and spatial scales compared to individual process scale studies.

1.1 Rationale of ACED

Assessing the chemical evolution at the disposal cell scale is highly relevant for different aspects in radioactive waste management:

- **Safety functions of a multi barrier disposal system**. The objectives of the multi barrier system are to contain and isolate the radioactive waste, an engineered barrier may contribute to containment by minimizing the transport of water to the waste form and minimizing the transport of dissolved radionuclides released from the waste form. The chemical evolution is specifically relevant for this containment function as it is an important trigger for release of radionuclides from the waste form and waste package, for physical and chemical degradation of the different barriers in the engineered barrier system and for the mobility of radionuclides through the disposal cell.
- **Reduction of uncertainty**. An improved description of the geochemical evolution will allow a better assessment of the long-term evolution of the disposal system – at least at the scale of a disposal cell – both in terms of performance (durability of different materials) as in terms of aqueous geochemical conditions (speciation of radionuclides and related strength of sorption). A more quantitative/semi-quantitative description of the evolution of the disposal cell will be possible in addition to the qualitative/narrative description.

- **Optimisation**. The consequences of choice of materials specifications resulting in different physical and chemical material properties on the geochemical evolution can be one of the factors taken into account for material design and optimization. Quantitative/semi-quantitative values obtained from models for the geochemical evolution may form relevant input for this.

The scientific work performed within ACED contributes to several research questions within the EURAD strategic research agenda (EURAD, 2019) including:

- **Radionuclide release from waste packages other than spent fuel** – Although release of radionuclides and radionuclide migration are not in the scope of ACED, the stability of different waste forms in disposal conditions was studied. The focus was on nuclear glass in contact with steel, bentonite or other clays and cement and cemented waste containing organics and steel. Radionuclides can be present in liquids or solutions during processing the waste. These radionuclides are to be immobilized in a waste form or matrix. We study vitrified and cemented waste forms. Through experimental (involving nuclear waste glass) and modelling, insight has been gained into the influence of geochemical conditions at the interface of the immobilization matrix and the adjacent materials and the relevance for dissolution and alterations of the immobilization matrix.
- **Waste Package interfaces** – In an experimental program processes at interfaces with steel, both clay and cement were addressed. Insights were provided on geochemical transformations at the interfaces, specifically the occurrence and nature of secondary iron corrosion products. In addition, the experimental program investigated the geochemical changes when also nuclear glass is in contact with these interfaces. Other interfaces that are relevant for waste packages were not experimentally studied but a comprehensive state-of-the-art report on phenomenology and processes made at the start of ACED provided the main input to ACED (Deissmann et al., 2020). Geochemical models accounting for processes at interfaces and geochemical changes with a material due to the interaction with another material have been and will be implemented in coupled reactive transport codes and applied at different scales including the interface scale, the waste package scale and the disposal cell scale (see section 1.2 for definitions).
- **Metallic & cementitious chemical perturbations and Bentonite and other Clay based systems** - The systems investigated within ACED always contain a metallic component which will corrode; the fate of Fe originating from the corrosion in a clay- or cementitious backfill or buffer material was elucidated by a combination of experimental and numerical techniques at the interface scale and incorporated into coupled reactive transport models at larger scales. The consequences of perturbations of cementitious materials on, for example, a clay host rock were investigated in the CEBAMA project (Duro et al., 2020) and relevant information for EURAD was also summarized in Deissmann et al. (2020). In systems with cementitious materials, its chemical perturbation or geochemical properties will affect other processes such as the rate of corrosion of steel and nuclear waste glass.
- **HLW/ILW Near-Field Evolution and THMC evolution** – The specific system studied in ACED were indeed the near-field of ILW and HLW disposal systems by its definition of ILW and HLW disposal cells, one of the most dynamic parts. One of the central elements in ACED was the modelling of the geochemical near field evolution around a disposal cell including transient states of temperature and water saturation if relevant. Modelling mechanical couplings was outside the scope of ACED.

1.2 Approach

The chemical evolution of a disposal cell depends strongly on the choice of the different (barrier) materials, their geometry and the host rocks and is thus strongly influenced by choices in national programmes. On the other hand, there are many similarities of the type of materials and the type of interfaces between different national programs (see Neeft et al. (2020) for an overview). Thus, instead of taking different national concepts, ACED defined generic disposal cells based on characteristics in national programs in Europe with interfaces between materials that are of high relevance in many

national programs. The focus was then on methods and approaches for studying the chemical evolution. **Four representative disposal cells** were selected based on interfaces between materials to ensure the evaluation of the methodologies for a wide but representative range of properties and conditions relevant for different national programs:

- For HLW, the two sequences of materials in contact with a host formation are:
  - Glass / steel / bentonite clay / granitic host rock
  - Glass / steel / cementitious materials / clay-based host rock
- For ILW, one main system of engineered barriers is defined containing organic or metallic (steel, iron) waste in contact with a:
  - Granitic host rock
  - Clay-based host rock

As processes and features on small scales may affect the chemical evolution at disposal cell scale, processes and phenomena were studied on three scales:

- ***Interface scale***: The focus of the interface scale is on two materials in contact with each other to obtain information on the geochemical evolution close to an interface in terms of chemical variables and alteration in solid phase composition at a detailed small scale. Existing information obtained in national or international projects were summarized in Deissmann et al. (2020). In addition, the scientific bases for steel in contact with cement or clay with attention to the effect of corrosion products from one material on the other was studied in detail using a number of existing and on-going experiments with steel-cement or steel-clay interfaces were combined with a few targeted new experiments such that the methodology could be evaluated from short time-scale to relative long-time scale (up to 10 years). Dedicated models for describing these experiments have been developed.
- ***Waste package scale*:** The key feature of the waste package scale is that several materials are present in a specific configuration and are interacting with each other under chemical and possible other gradients. The used configurations are representative for HLW and ILW disposal cells without interaction with host rocks or other waste packages. In HLW cells, the chemical evolution of the waste package is governed to a very high degree by the integrity of the canister – as long as it is intact, interactions between the glass with iron or with the backfill materials does not exist. Therefore, the studies in ACED related to HLW at the waste package scale assumes that the canister is breached without discussing the process or timing of breaching and concentrate on (i) the small-scale evolution of the system glass-iron corrosion products (ii) the interaction of glass and steel corrosion on theadjacent backfill material (typically clay/cement) and (iii)the evolution of the glass and cement alteration zones when the materials are separated by a permeable stainless steel barrier (representing the condition after breaching).
- ***Disposal cell scale***: The disposal cell scale – the target scale of ACED – consists of waste packages and their immediate surrounding being other waste packages or other near field components. A complex coupled reactive transport model has been built for each disposal cell with the integration of scientific knowledge into a single model consisting of all materials and their interfaces. The models are based on existing knowledge (as summarized in (Deissmann et al., 2020, Neeft et al., 2020, 2022) and integrated in narrative, conceptual and mathematical models as described in Samper et al. (2022). In addition, a number of approaches were evaluated in which the conceptual and mathematical models are simpler; a process called model abstraction (see below).

Two methodological routes have been applied in the numerical studies on the geochemical evolution in a disposal cell:

- ***Process integration:*** This concerns the integration of scientific knowledge, conceptual and mathematical models on individual or selected processes into an integrated conceptual and mathematical model. The integration serves for understanding system behaviour and evolution,

for identification of key processes or parameters, or for transfer of information from a more detailed scale to a larger scale. Illustration of these applications was performed for a number of cases with different materials and governing processes relevant for ILW and HLW disposal cells.

- ***Systematic abstraction:*** The aim is to reduce model complexity in a systematic way such that (i) an acceptable description of the chemical evolution is preserved during model abstraction, and/or (ii) differences in some key variables of the chemical evolution can be described qualitatively and/or quantitatively. This leads to a better representation of the expected evolution in safety or performance models, thus helping in reducing and quantifying conservatism and uncertainty and thus directly impact the definition of safety margins.

1.3 Structure of the report

The objective of this report is an update of the knowledge relevant to assess the geochemical evolution at the disposal cell scale gained within the ACED project. Therefore, the current report contains no systematic overview of knowledge that became available in the open literature (during the last five years) but highlights the main findings of the R&D activities performed in the framework of ACED. The reader is referred to the underlying reports to obtain additional detailed information of these R&D activities.

This reports is structured in following way:

- Chapter 2 focusses on the geochemical evolution in disposal cells for ILW and HLW waste. The generic disposal cells are introduced and their materials are described. Process understanding of interface processes are discussed based on the experimental program of ACED for the interfaces “glass – steel”, “steel – concrete”, “steel – clay”, and also for the degradation of cementitious materials. A narrative of the geochemical evolution is given. Finally, the main insights obtained from mathematical models to simulate the geochemical evolution are given; information on the conceptual, mathematical and numerical models are described in detail in Samper et al. (2022).
- Chapter 3 describes mainly coupled reactive transport models that describe geochemical changes at different spatial and temporal scales that are relevant for detailed insight in the geochemical evolution at disposal cell scale. A few other modelling approaches that give complementary information are described as well. Models are either based on integration of relevant process-based knowledge or on simplifying more complex models.
- Chapter 4 puts the work of ACED – assessing the geochemical evolution – in a somewhat broader context related to material degradation and radionuclide migration.

2. Chemical evolution in disposal cells

2.1 Main characteristics of the HLW and ILW disposal cells studied in ACED

The main characteristics of the generic vitrified HLW and cemented ILW disposal cells studied in ACED have been derived from the national programmes in Europe (Neeft et al., 2019). This derivation ensures that the studies performed, and information obtained within ACED are relevant for European radioactive waste disposal programs. Cemented ILW with cellulose (organic) and with steel (metallic) were chosen as type of waste in the generic ILW disposal cells in order to use the experimental results with their associated predictions obtained in ACED (De Windt et al., 2020; Havlova et al., 2021; Mladenovic et al., 2019) and the EURAD Work Package CORI e.g. Altmaier et al., (2021). The characteristics of the Callovo-Oxfordian claystone and Spanish Reference Granite were used in these studies (Samper et al., 2022).

The section starts with the characteristics of the waste and the engineered barriers. Construction and operation of the disposal facility can have an impact on the clayey and granitic host rocks and affect both ILW and HLW disposal cells. How these effects are considered in the studied disposal cells is described at the end of this section. The vitrified HLW is encapsulated in a carbon steel overpack. The buffer that surrounds this overpack is bentonite for granitic rock and a cementitious material for indurated clay (see Figure 2-1). For both host rocks, the void volume in cemented ILW is backfilled with a porous cementitious mortar (see Figure 2-2).

2.1.1 Waste form and other engineered barriers in HLW disposal cells

Vitrified HLW results from the reprocessing of spent fuel in which uranium and plutonium have been extracted. The High-Level Liquid Waste (HLLW) is poured with a melted glass frit into a stainless steel container. This waste processing ensures that the radionuclides are homogeneously distributed in a borosilicate glass matrix. The dimensions of the canister, thermal power as a function of time and parameters to conduct the generated heat as supplied by the waste producer (AREVA, 2007) have been used in the generic HLW disposal cell. Apart from the vitrified waste form, Figure 2-1 shows that each disposal cell has a steel overpack and a buffer either made from clay with a high swelling potential (bentonite) or a cementitious material (concrete). The thickness of the overpack is determined by the mechanical load provided by the host rock and additional load of an ice-sheet and the corrosion allowance for the period in which the waste heats the host rock. The thickness of steel is assumed to be 5 cm for the disposal cell studied in ACED. The steel has a low alloy content e.g. carbon steel (Samper et al., 2022). This thickness is a compromise between the larger considered thickness of 14 cm for bentonite based systems and smaller considered thickness of 3 cm for concrete-based systems (Neeft et al., 2022). The studied generic disposal cells are simplifications of the actual disposal cells. For example, gaps between the waste package and steel overpack as a result to manoeuvre this package in the overpack as well as the stainless steel canister are not included.

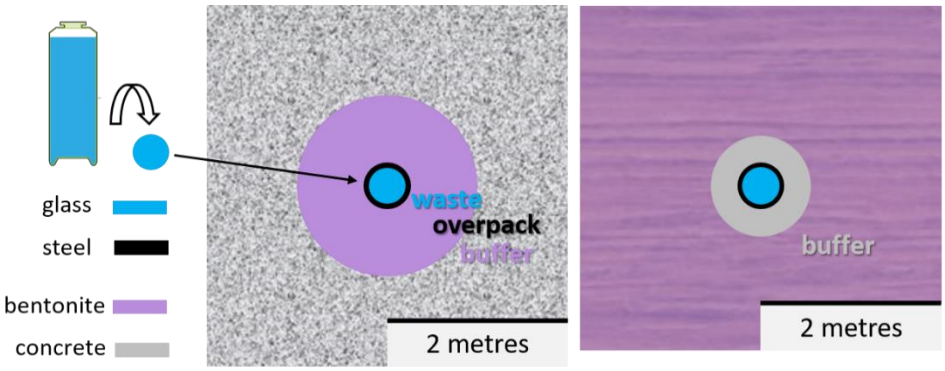

Figure 2-1: Waste package of vitrified HLW (left) and HLW disposal cells in granitic rock (middle) and indurated clay (right) adapted from Samper et al., (2022).

Bentonite as well as concrete buffers have very small connecting pore throats by which the microbial activity is limited and the transport of dissolved chemical species is dominated by diffusion. The bentonite buffer has limited mechanical strength and the mechanical load of the host rock will be transferred to the carbon steel overpack, especially when the swelling potential of the bentonite has been reduced by mineral transformations. The minimum in strength of the concrete buffer is at least 40 MPa (Van Humbeeck et al., 2007) which is higher than the indurated clay host rock with a value between 20-30 MPa (Delage, 2013). Transferral of the host rock mechanical load to the carbon steel overpack can only take place if the thickness of the concrete buffer with a particular strength is too small. Aggregates are primarily responsible for the strength of concrete and this feature of concrete is used in EURAD Work Package MAGIC for the selection of cementitious specimens (Neeft et al., 2021). In ACED, the impact of the mechanical properties of the materials on the chemical evolution of the disposal cell is not explicitly included. Contact between the waste form and pore water is assumed after the waste no longer heats the engineered barriers and host rock (Samper et al., 2022).

2.1.1.1 Bentonite buffer in HLW disposal cells

Mainly FEBEX bentonite as a clay buffer with a thickness of 75 cm (see Figure 2-1) is considered in ACED, MX bentonite with a thickness of 35 cm is used as a sensitivity case (see Table 2-1). FEBEX stands for ***F****ull-scale* ***e****ngineered* ***b****arriers* ***ex****periment in crystalline host rock* and was a research project that started in the 4th framework EURATOM programme and continued in the 5th programme. Almost 98% of the minerals in FEBEX bentonite is smectite (Samper et al., 2022). Smectite are clay minerals that are responsible for the swelling potential and thereby the self-healing capacity of induced fractures.

Table 2-1: Properties of bentonites (Samper et al, 2022)

Type of Bentonite	FEBEX	MX
Clay type: content	Smectite: 97.98 vol%	Montmorillonite: 75 wt%
CEC [meq/100 gram]	102	78.7
Hydraulic conductivity (saturated) [m/s]	6×10^{-14} (5×10^{-14})*	6×10^{-14} (1×10^{-13} to 2×10^{-12})*
Dry density [kg m^{-3}]	1600	1600
pH	6.46	8
Initial porosity [%]	40	39

*Values from EURAD Work Package GAS (Levasseur et al., 2021)

MX bentonite has a specific class of smectites i.e. montmorillonite. Clay minerals are cation exchangers due to their negatively charged surfaces. All cation sites are exchanged with sodium in case of MX bentonite by which it is usually phrased to be composed of Na-montmorillonite (Müller-Vonmoos and Kahr, 1983). This preparation allows all radionuclides that are dissolved as cations to be sorbed since all cations are more strongly sorbed than sodium, except for lithium (Helfferich, 1962; Stumm, 1992). The smectite content in MX bentonite as used in the Swiss programme is 75 wt% (Müller-Vonmoos and Kahr, 1983).

Accessory minerals in FEBEX as well as MX bentonite are quartz and carbonates. Their content is 1 vol% for both in FEBEX bentonite that also has a gypsum content of 0.08 vol%. MX bentonite has a quartz content of 10-14 vol% and carbonates and gypsum of 3-5 vol%. Other accessory minerals in MX bentonite are feldspars (5-9 vol%) and mica and chlorite (2-4 vol%) (Samper et al., 2022).

Bentonite is emplaced with a low saturation degree e.g. 58% for FEBEX (Samper et al., 2022). The pore water chemistry of this engineered barrier is therefore determined by the inflow of granitic water and establishment of equilibria between dissolved species present in this host rock water and minerals present in the bentonite buffer (Neeft et al., 2022). In ACED, it has been assumed that bentonite is saturated in the reactive transport modelling with the pore water chemistry as evolved by inflow and establishment of equilibria. (Samper et al., 2022). Experiments have been performed with carbon steel or iron interfacing bentonite as well as Boda clay stone (see section 2.2.3).

Another studied buffer also without aggregates in the modelling, is a cementitious buffer and contains also silica fume and CEM III/A which is a blended cement between clinker (35-65%), Blast Furnace Slag (BFS) (36-65%) (De Windt et al., 2020; Samper et al., 2022). The majority of the solid compounds in this buffer are cement and silica fume. Experimental results of this buffer as well as CEM I paste interfacing steel are described in section 2.2.2. Aggregates are the impermeable parts in a concrete buffer (Samper et al., 2022) and can therefore limit the transport of water to the steel interface.

2.1.1.2 Concrete buffer in HLW disposal cells

The concrete buffer considered in the modelling performed in ACED is made with Ordinary Portland Cement (OPC/CEM I). Steel interfacing CEM II/B grout has been experimentally investigated (De Windt

et al, 2020, see also section 2.2.2) which is defined in ACED as a blended cement 73.5% CEM I clinker and 24.5% blast furnace slag instead of a blended cement between clinker (65-79%), fly ash or puzzolans (21-35%) in the European standard EN 197-1. Hydrated cement acts as a glue holding the aggregates in concrete together. In the modelling, calcareous aggregates are considered for the concrete buffer. The cement minerals in concrete have no swelling potential to heal fractures. Only self-sealing of induced fractures can take place, for example with unreacted cement (Seymour et al., 2023). The thickness of the concrete buffer of 30 cm as drawn in Figure 2-1 is a compromise between disposal concepts considered in Belgium and the Netherlands with a thickness of 75 cm and the French disposal concept with a thickness of 5 cm (Samper et al., 2022).

Concrete is considered for both HLW and ILW disposal cells. Its characteristics are therefore described in section 2.1.3.

2.1.2 Waste form and other engineered barriers in ILW disposal cells

Organic waste arises as a result of purification of nuclear plant waste water, removal of contamination during handling of radioactive waste and research. Therefore, there is a large variety in organic waste forms. Cellulose as a type of organic waste form is studied in ACED (Mladenovic et al., 2024, see also section 2.2.4). The waste package is a 200 litre zinc coated carbon steel drum with four compacted 30 litre stainless steel drums. These compacted drums are contained in waste package mortar (Blanc et al., 2024, see also Figure 3-6). A reinforced concrete container with 12 of these 200 litre drums infilled with mortar is considered as the waste package of which nine are disposed of in the reference disposal cell.

Organic complexes that are released while degradation of organic waste are dissolved anionic complexes. The content of calcium in the concrete pore water (see Figure 2-3 **Erreur ! Source du renvoi introuvable.**) is therefore an important information, e.g. Altmaier et al., (2021). Figure 2-3 shows that CSH minerals are positively charged from a pH of 13 until 11.7 by which sorption of dissolved organic complexes by CSH minerals is possible. This sorption reduces the potential soluble content for complexation with radionuclides dissolved as cations or cationic complexes.

Metallic radioactive waste is mainly generated by activation of stable isotopes within these metals by neutron irradiation. Stainless steel and carbon steel arise from the maintenance and dismantling of nuclear reactors. Carbon steel as a metallic waste form is studied within ACED (Blanc et al., 2024). The waste package in ACED is a reinforced concrete container code L3 LC-84 in Stein (2014) with neutron irradiated steel conditioned in mortar. Figure 2-2 shows the reinforced concrete containers disposed of in granitic and indurated clay host rocks.

Metallic waste such as steel generates hydrogen and consumes water in an anaerobic corrosion process. Hydrogen gas is very insoluble and will be outgassed from the concrete pore water. The transport of hydrogen gas within concrete depends on the saturation degree. The saturation of concrete during the chemical evolution of the disposal cell is therefore important information to assess the potential perturbation in the host rock by generation of gas in the EBS, especially clay host rocks (e.g. Levasseur et al., 2021).

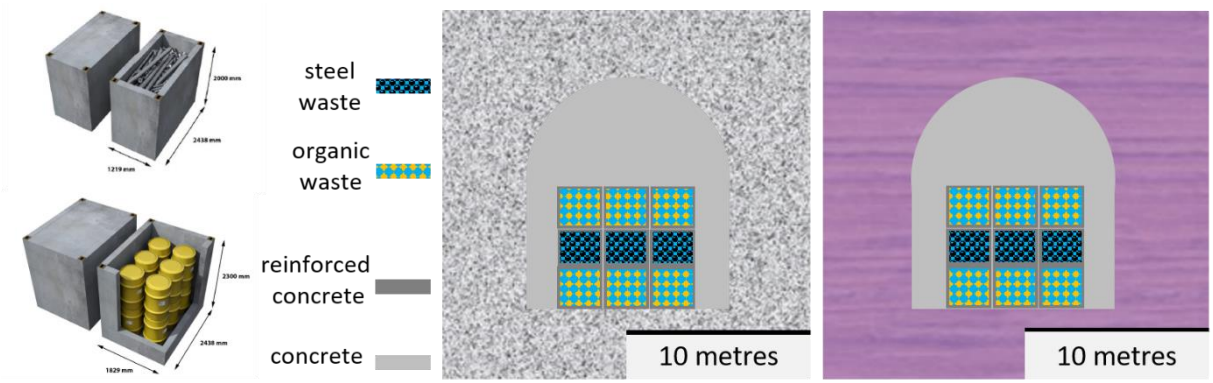

Figure 2-2: Packages for steel (L3 LC-84) and organic (L5 LC-86H) waste (Stein, 1984) (left) and ILW disposal cells in granitic rock (middle) and indurated clay (right) (adapted from Samper et al., 2022).

In ACED, the types of concrete in the generic disposal cell for ILW are the reinforced concrete (waste package) and concrete (mortar) used as a backfill. In the modelling, all types of concretes are assumed to be made with ordinary Portland Cement (OPC/CEM I). Calcareous aggregates are assumed to be present in reinforced concrete but the major type of aggregate in the mortar is siliceous. A sensitivity study was proposed with the Nirex Reference Vault Backfill (NVRB) that has finely grained calcareous aggregates instead of siliceous aggregates (Samper et al., 2022). Experimental results have been obtained for waste package concrete made with CEM III/B (see section 2.2.4) which is a blended cement between clinker (20-34%), Blast Furnace Slag (BFS) (66-80%).

2.1.3 Characteristics of concrete as an engineered barrier

2.1.3.1 Chemical properties

Like clay, concrete can also be an ion exchanger. The nature and type of ion exchange for cement minerals depends on the calcium concentration in concrete pore water (Pointeau et al., 2006). The calcium concentration in concrete pore water depends on the pH (Berner, 1992; van Eijk and Brouwers, 2000; Vehmas and Itälä, 2019). Figure 2-3shows the pH of concrete pore water, dissolved calcium concentration and at which stages there is a positive and negative surface potential of the CSH mineral.

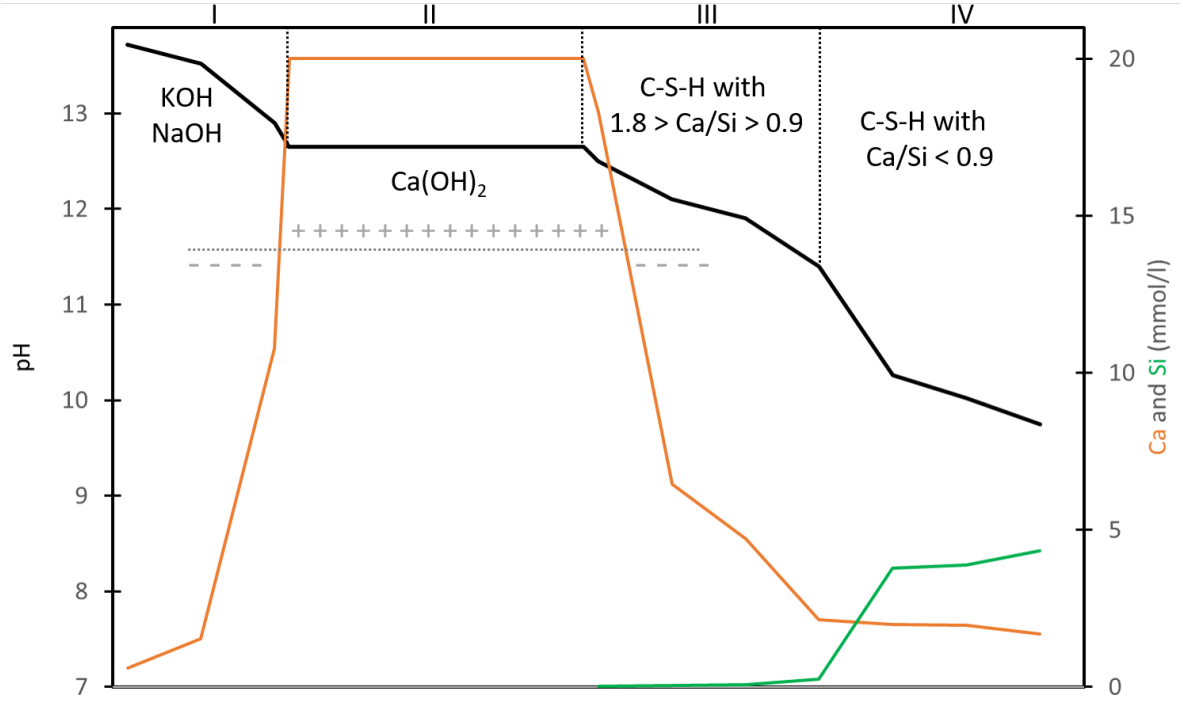

Figure 2-3: Concrete pore water in terms of pH (black line), dissolved calcium (orange line) and silicon (green line) at room temperature. Kind of surface potential of C-S-H mineral is indicated. Stages in pH by Atkinson et al. (1985) with added calcium and silicon by Berner (1992) at a pH < 12.65, dissolved calcium at a pH > 12.65 from van Eijk and Brouwers (2000) and nature of the surface potential of C-S-H mineral from Pointeau et al. (2006).

At a pH higher than 12.65 and room temperature, the pH of concrete pore water is determined by the excess of dissolved alkalis. At a pH lower than 12.65, the presence of cement minerals control the pH and dissolved calcium and silicon species. At room temperature, the pH of the concrete pore water will remain 12.6 as long as portlandite is present. C-S-H is the major hydration phase in cement paste and is positively charged between a pH of 11.7 and 13.0 with a maximum around 12.6 (Pointeau et al., 2006). The uptake of dissolved anions has amongst others been measured to increase with increasing charge of the anion or anionic complex and atomic number (Pointeau et al., 2008). With decreasing pH:

- the ratio between calcium and silicon in C-S-H minerals decreases (decalcification);
- the dissolved calcium concentration in equilibrium with the C-S-H mineral decreases;
- the dissolved silicon concentration in equilibrium with the C-S-H mineral increases.

2.1.3.2 Physical properties

The porosity in the cementitious materials is controlled according to their application. Aggregates are usually impermeable and have a negligible porosity. Provided there is a good bonding between the cement paste and aggregates, pores are only present in the hardened cement paste and the interfacial transition zone between the cement paste and aggregates (Zhang et al., 2021) also called reaction rims (Jackson et al., 2017). There is also some additional porosity at the interface between cemented paste and aggregate in case of too much air has been entrapped in the manufacturing process. The amounts of quartz (siliceous) or calcareous aggregates ranges between 1700 and 2000 kg m^{-3} (Neeft et al., 2022) i.e. about 70 vol% for concrete (Samper et al., 2022). The concrete buffer in Figure 2-1 is such a concrete and the porosity has been calculated to be 11.54% with capillary pores and gel pores. The ratio between water and binder (w/b) is 0.47 in the concrete buffer for HLW disposal cells and 0.45 for reinforced concrete in ILW disposal cells (see Figure 2-2) (Samper et al., 2022).

A higher ratio between water and binder results into higher porosities. For example a w/b ratio of 1.25 has been calculated to yield a porosity of 29% (Samper et al., 2022). Apart from capillary pores and gel pores, there can also be larger pores present without a capillary force. The values for water permeability of cementitious materials can be orders in magnitude larger with high w/b ratios, i.e., a permeability of 1.0×10^{-19} m^2 is assumed for reinforced (or functional) concrete (w/b=0.45) and 3.1×10^{-14} m^2 for backfill mortar (w/b=1.25) all made with OPC.

2.1.4 Granitic host rock

Granitic rocks are crystalline hard rocks with an unconfined compressive strength (UCS) of about 100 MPa. Drilling and blasting have therefore been used to excavate vaults for disposal of ILW in Sweden and Finland. The procedures to excavate granitic host rocks determine the size of the excavation damaged zone (EDZ) and the fracture density inside this zone. For HLW disposal cells other excavation procedures are used leading to smaller sizes of EDZs and fracture densities. Transport of pore water within granitic rock takes primarily place through the fractures. This transport is so fast that measures need to be taken to mitigate or prevent water inflow into the disposal tunnel. The redox conditions may be controlled by microbial activity and the groundwater composition is near neutral. The granitic pore waters in Sweden and Finland are brackish and in Czech and Spain fresh (Neeft et al., 2019).

The granitic Spanish or Czech pore water is used as a boundary for the EBS in the modelling because the transport of water is fast compared to transport in the bentonite buffer for HLW or concrete backfill for ILW disposal cells. Spanish reference granitic pore water has a dissolved calcium concentration of 0.152 mmol/L (Samper et al., 2022). Also Czech granitic pore water has a calcium concentration smaller than concrete pore water (see Figure 2-3) by which leaching of the concrete is expected.

2.1.5 Indurated clay host rock

The UCS of Callovo-Oxfordian clay is 20 to 30 MPa (Delage, 2013) i.e. much smaller than the one of granite. Road headers are used to excavate rock for disposal of ILW and tunnel boring machines are envisaged to make room to dispose of HLW in France. The transport of water is too slow in this clay host rock to have water inflow to the disposal facility in the operational phase. The induced fractures resulting from excavation enhances the drying of the clay host rock due to ventilation in the operational phase. Closure of the fractures is envisaged to take place by precipitation (Alcolea et al., 2014) i.e. a self-sealing process that consumes water. In the modelling, the clay pore water is assumed to be more slightly saline (Samper et al., 2022) than initially reported in ACED (Gaucher et al., 2009; Neeft et al., 2019). The redox conditions in Callovo-Oxfordian may just after sedimentation be controlled by microbes and minerals such as pyrite are formed by sulphate reducing bacteria. After the millions of years of the sedimentation process, the connecting pore throats of this virgin clay host rock have become too small for microbial activity. The presence of pyrite in the mineralogy of the clay host rock shows that reducing conditions are present. This pyrite can become oxidized during excavation and acidifies clay pore water in the oxidation process. The use of concrete limits this acidification.

Transport of solutes in the pore water in virgin clay host rock is dominated by diffusion. The transport of water in this host rock is slower than in the concrete used as an engineered barrier. A permeability of 4×10^{-20} m^2 is assumed for Callovo-Oxfordian clay host rock (Samper et al., 2022) while 1×10^{-19} m^2 was assumed in the modelling for the functional reinforced concrete (see section 2.1.3.2). The reference value of the permeability in this clay is 1×10^{-21} m^2 (Levasseur et al., 2021) i.e. 40 times smaller than assumed in ACED. Indurated clay host rock in the vicinity of the EBS for ILW disposal cells is estimated to be still unsaturated after 100.000 years (Leupin et al., 2016, Samper et al., 2022). The water permeability and diffusion decreases with decreasing degree of saturation. Modelling HLW disposal cells include the initial unsaturation and modelling ILW disposal cells included 20 meters of saturated clay host rock surrounding the EBS. The contribution of the dehydrated clay host rock in the vicinity of

the EBS leads initially to a smaller influx of water and ingress of dissolved species from the clay host rock into the engineered barriers. Degradation of metallic and organic waste is neglected in the modelling. The clay minerals in this host rock have - like the bentonite buffer - also an exchange capacity but much smaller i.e. 17.4 meq /100 gram. The dissolved calcium concentration is 7.6 mmol/L (Samper et al., 2022) slight smaller than the dissolved calcium concentration in equilibrium with a C-S-H high in calcium (see Figure 2-3). The impact of saturation degree is included for models at waste package scale.

2.2 Interfaces

Various studies on deep geological disposal of nuclear wastes showed that chemical and physical interactions will be focused on interfaces between the different barrier materials, due to the prevailing chemical and – under certain conditions – thermal gradients (e.g., Claret et al., 2018; Bildstein et al., 2019). In this context, the nature and the extent of the alteration within the different materials, the progress of the perturbations with time and the evolution of the material properties are essential to evaluate the impact on the overall performance of the disposal system.

Within ACED, we started from the knowledge available at the scale of interfaces between two materials (Deissmann et al., 2021; Neeft et al., 2022) to build models for assessing the chemical evolution at the disposal cell scale. This section updates the state-of-the-art on the phenomenological chemical processes occurring at the interface between two materials for the combinations relevant for European repository concepts (cf. section 2.1; see also Neeft et al., 2019) based on results of dedicated experiments performed within ACED. For each interface, a short description of the phenomenology encountered, and the knowledge gained is given together with references to ACED outcomes for interfacial processes relevant to the chemical evolution of the disposal cells to highlight the major conclusions of WP ACED.

Compared to the barrier interfaces addressed previously (cf. Deissmann et al., 2021; Neeft et al., 2022) the experimental work performed within ACED focussed in particular on the interfaces with steel (i.e., glass/steel/clay; steel/concrete, and steel/clay) as well as on long-term processes in cementitious materials. The major outcome with respect of each of these topics is provided in sections 2.2.1 to 2.2.4

2.2.1 Interface “glass – steel”

The interface glass – steel is related in particular to the disposal of vitrified HLW: vitrified wastes are contained in stainless steel canisters, which are placed usually in carbon steel overpacks prior to disposal (cf. Neeft et al., 2019). According to existing HLW concepts in Europe, experiments performed within ACED within this context focused on the study of three experimental systems, namely (i) glass/steel/clay, (ii) glass/steel/cement, and (iii) glass/steel/cement/clay (Gin et al., 2022). These systems allowed to study the different interfaces expected in HLW disposal cells with vitrified waste, metallic components, presence of cementitious material and a near-field clay-rich host rock.

Glass/steel/COx clay experiment at 50 °C

Within the context of the French basic concept for the CIGEO repository two long-term mock-up experiments in which glass interacts with iron and iron corrosion products in a core of Callovo-Oxfordian claystone (COx) at 50 °C were initiated in 2014 and analysed within ACED. The experimental setup is comprised a COx claystone cylinder, in which two coupons of SON68 glass (inactive surrogate of the French R7T7 glass) were inserted in the vicinity of an iron piece. One of the glass coupons was doped with ^{57}Fe and ^{29}Si to investigate their migration into the materials, while the second coupon remained undoped. The Callovo-Oxfordian claystone was saturated with synthetic pore water and the mock-up was placed in an oven at 50 °C under anoxic conditions. The experiments were carried out for 2.5 years (cf. Carriere et al., 2021) and 6.1 years, respectively. The chemical processes at the interfaces were evaluated by post-mortem analyses of a selection of solid samples employing, i.a., SEM-EDS, Raman spectroscopy, ToF-SIMS, HRTEM and STXM. LA-ICP-MS was used to determine ^{29}Si and ^{57}Fe migration into the surrounding claystone.

A glass alteration layer (GAL) was observed on the surface of the material with a thickness ranging from 6 to 10 µm after 2.5 years, and 15 to 25 µm after 6.1 years at the glass/iron interface. The GALs are composed of iron phyllosilicates (smectite/nontronite, serpentine) and minor SiO_2(am). In addition, on the 6.1 years sample, a homogeneous neoformed Fe-phyllosilicate layer (3 µm thickness) was identified on the GAL surface with a composition close to the GAL one. The glass alteration rate was estimated based on the GAL thickness and ranged from 1.8×10^{-2} to 3.0×10^{-2} g m^{-2} d^{-1} after 2.5 years and from 1.8×10^{-2} to 2.5×10^{-2} g $m^{-2}d^{-1}$ after 6.1 years, corresponding to $r_0/5$ to $r_0/3$, where r_0 represents the initial dissolution rate at 50°C in COx groundwater (maximum dissolution rate under these conditions $r_0 = 9.3 \times 10^{-2}$ g m^{-2} d^{-1}; Jollivet et al., 2012). These results strongly suggest that the GAL composed of iron phyllosilicates is not passivating since the interaction of dissolved Fe (from iron corrosion) and the Si released by glass corrosion leading to the formation of iron phyllosilicates in the GAL prevented the formation of a passivating amorphous silica gel. The thickness of iron corrosion products (ICP) formed at the expense of the iron coupon ranged from 5 µm to 100 µm after 2.5 years, and from 15 to 120 µm after 6.1 years. Two types of ICP were observed: (i) Si-free phases identified as iron carbonates, such as chukanovite ($Fe_2(OH)_2CO_3$) and siderite ($FeCO_3$), and (2) Si-bearing phases such as poorly crystallized iron smectites (nontronite, 22% Fe^{II} and 78% Fe^{III}) and potentially a serpentine-like phase. Furthermore, a 25 µm to 40 µm thick neo-formed precipitate composed of iron phyllosilicates was characterized on the ICP surface after 6.1 years. In this experiment a 1 µm thick discontinuous layer of a Fe^{III}-rich iron oxide (maghemite (γ-Fe_2O_3), magnetite (Fe_3O_4) or a maghemite/magnetite phase) was observed at the metallic iron/ICP interface. The fate of Fe and Si released from the glass was investigated by monitoring the distribution of ^{57}Fe and ^{29}Si, indicating that about 90% of the Fe in the phyllosilicates comes from iron corrosion of the iron and around 1/3 of the Si contained in the phyllosilicates comes from the glass, while the remaining 2/3 is supplied by the silicate minerals present in the COx. Overall, these results suggest that the GAL is formed by the dissolution of the glass triggered by the precipitation of phyllosilicates, instead of *in situ* reorganization of the glassy network. In this case, neoformation of Si-Fe bearing phases prevents the reorganisation of the silicate network and thus the formation of a passivating film.

Glass/steel/Boda claystone experiment at 80 °C

Related to the Hungarian HLW disposal concept, within ACED a series of glass/steel/clay experiments at 80 °C were launched with a powdered simplified 5 oxide glass, iron powder, crushed clay and synthetic clay pore water for durations ranging from 3 months to 1 year. The aim of this work was to study the chemical evolution of a borosilicate glass/steel/Boda claystone system for conditions similar to those in a deep geological repository (temperature, groundwater, etc.). The experimental set-up comprised an internal Teflon vessel containing a mixture of powdered glass, iron powder, and crushed Boda claystone, contained in an external vessel filled with synthetic Boda pore water – saturation of the material in the internal vessel was achieved by small holes in the internal vessel (cf. Gin et al., 2023). The three experiments were terminated after 3 months, 7 months and 12 months, respectively, and the solids were investigated using µXRF, SEM-EDS, FIB-SEM and XRD. No alteration layer was found on the borosilicate glass powder samples in any case, and no significant iron oxide formation was detected. The composition of the leaching solution was determined predominantly by the dissolution of glass and clay particles, leading to a distinct increase in the concentrations of Si, K, Na, and B and a decrease in Ca and Mg compared to the initial synthetic clay pore water. The glass dissolution rates calculated from the boron release were rather low and decreased from 0.0054 g m^{-2} d^{-1} in the first 7 months to 0.0011 g m^{-2} d^{-1} from months 7 to 12. The low rates were attributed to the fact that in the experimental set-up the glass does not come into direct contact with the bulk leaching fluid. The low B concentration in the leachate after 12 months (45.52 mg L^{-1}) suggested that there was no significant change in the structure of the glass during the experimental period. Based on the dissolved B concentration, the thickness of the glass alteration layer was estimated at about 0.5 µm, which was below the resolution limit of the SEM-EDS.

Glass/steel/cement-bentonite/COx clay experiment at 70 °C

In 2013-2014, the CIGEO reference disposal concept in France was modified regarding the disposal of HLW. A new material, a cement-based buffer, was planned to be placed in the gap between the disposal cell liner (steel) and the COx clay rock. The cementitious material should serve to reduce acidity induced by pyrite oxidation and buffer the pH, to maintain favourable conditions for low canister corrosion rates at least for the thermal phase of the repository. Thus, integrated experiments to study the impact of the cementitious buffer on the nuclear glass dissolution rate in a configuration reproducing all the interfaces were initiated in 2018. The experiments were conducted at 70 °C in static mode and lasted for 3 years, investigating two different glasses (SON68 glass, i.e. R7T7 surrogate, and AVM glass from vitrification campaigns at the Marcoule vitrification facility). Each reactor contained 3 types of samples: (i) glass powder inside a pierced steel canister, (ii) glass powder in a steel canister coated with magnetite to observe the impact of corrosion products, and (iii) two glass monoliths squeezed between a stainless steel plate on one side and a steel plate on the other ("sandwich"). Each setting was tested with and without a cementitious buffer between the different samples and the COx clay. The in total 16 parallel experiments were terminated after 6, 12, 24 and 36 months, respectively.

SEM observations showed the presence of a GAL on every sample of AVM glass after 6, 12, 24 and 36 months. In contrast, no alteration layer was observed on any of the SON68 glass powder samples, only on one of the monolith sandwich samples. Measurements of the thickness of the GAL revealed no clear effect of the cementitious buffer on the alteration layer thickness and on the dissolution rate. As expected, the AVM glass dissolves faster than SON68 and the measured initial and residual rates were in good agreement with the literature.

Glass/steel/cement experiment at 20-25 °C

Integrated tests on glass dissolution were performed in the context of the Belgian Supercontainer concept between 2009 and 2013 to quantify the effects of the presence of the concrete. These experiments were performed in mock-up cells with glass powder (SON68 glass or SM539 glass) either in contact with a hardened ordinary Portland cement plug or separated from the cement plug by a stainless steel filter, to study the effects of a spatial separation between the glass and the cementitious material. The cells were saturated with a young cementitious water (YCWCa, i.e., a cementitious water representative for the first degradation stage of concrete with a pore water pH exceeding 13 and an excess of dissolved alkalis, cf. Figure 2-3); leachate samples were abstracted at different times and analysed. The experiments were run for nearly 900 to 960 days and dismantled 1530 days after the last sampling (i.e., about 7 years after the start of the experiments). The whole cells were embedded in epoxy resin under vacuum to allow sampling of the solids and the interfaces which were investigated by SEM-EDS, XRD, TG-DSC, µRaman spectroscopy and LA-ICP-MS.

Based on the B concentration measured in the leachates in the glass compartment, bulk or overall glass dissolution rates of about 0.001 g m^{-2} d^{-1} were calculated for both glasses, similar to the dissolution rates determined in another experimental setup, where glass powder was confined between stainless steel filters and leached in a YCWCa without cement present. However, the rates were lower than the dissolution rates in cement water with dispersed glass particles without cement or with dispersed cement particles. This indicates that the dispersion of the glass and cement particles increases the reactive surface area and thus accelerates the interaction. This demonstrates that the presence of cementitious materials can increase the dissolution rate in YCWCa, but only if there is good contact between glass and cement. When a cement plug is used in the experiments, the small reactive surface area and transport processes slow down the interaction with the glass.

In the two cells, the alteration of the glass grains was found to be heterogeneous depending on their location, with grains located in the first 400 µm close to the stainless steel filter seemingly more altered. The SM539 glass grains close to the stainless steel filter showed a multilayer alteration with the core of some glass grains still protected from leaching, but a Na, Li, B, and Mo depletion in the GAL. In contrast, SON68 glass rather seemed to be leached up to the core of each grain, confirmed by the depletion of Li, B, Zn, Zr, Mo, Cs, Ce, La, and Mn. In this glass, an enrichment of Mg, K and S (from the cement and the leaching solution) was observed, indicating different processes of alteration and/or rate of dissolution

of the two glasses during the experiments. In the presence of SM539 and SON68 glass, the hardened cement pastes were altered over distances of approximately 80 µm and 200 µm, respectively. The altered layer was characterized by a porosity increase and by mineralogical and chemical changes including dissolution of portlandite and precipitation of C-S-H with low Ca/Si ratios. The C-S-H phases were enriched in alkalis (from the interstitial pore solution in the cement) and partly filled the porosity created by the portlandite dissolution. The interface was also characterised by a decrease in the content of unreacted cement clinker phases (i.e. C2S, C3S, C3A, C4AF). Even though the tests were conducted in CO_2-free atmosphere, the presence of distinct amounts of calcite at the interfaces revealed carbonation processes in both cases. In the test with SON68 glass, the formation of a dense poorly crystalline or amorphous phase with a very low Ca/Si ratio edging the cement paste was observed. This phase was found to be enriched in elements coming either from the glass (Li, Cs, B) or from the cement paste (K) or from both (Na). It was suggested to be either a C-S-H phase with a very low Ca/Si ratio that incorporated alkalis and B, or an alkali-silica gel similar to the one formed during alkali silica reaction (ASR). Minor amounts of monocarboaluminate that can incorporate B and sulphate, were found to be coexisting with this phase. In the test involving SM539 glass, secondary alteration products precipitated in much lower amounts at the edge of the cement paste. This Al-enriched phase showed a collomorphous texture and was assumed to be a mixture of glassy components with C-A-S-H or Al-containing alkali silica reaction gel; minor amounts of zeolites were also observed in this area.

2.2.2 Interface “steel – concrete”

Various concepts for the deep geological disposal of HLW, e.g. in France, Belgium, or Hungary have developed barrier systems implying large amounts of both metallic and cement-based materials that will come into contact. The heat produced by radioactive decay would induce an increase in the temperature in the disposal cell. Such a thermal phase may impact the corrosion processes affecting carbon steel elements thermodynamically and kinetically through the evolution of geochemical, mineralogical, and microstructural properties of the cementitious material induced by temperature increase. In this context, within ACED key information on interactions occurring at interfaces between steel and cementitious materials at 80 °C were obtained to provide basic data for the up-scaling to waste package and disposal cell scale modelling (Wittebroodt et al., 2024).

The pH effect on anoxic corrosion processes was investigated by performing *in situ* and laboratory mock-up experiments involving classic CEM I and CEM II cements (pH>12) as well as a low-pH cement grout (10<pH<11). The geochemical evolution of such carbon steel/cementitious material systems was characterized for both perfect and imperfect interfaces (i.e., presence of spatial heterogeneity between steel and cement). Corrosion processes, the evolution of cementitious materials and porewater composition were monitored over periods ranging from one to two years of interaction. SEM, XRD and µ-Raman spectroscopy analyses supported by geochemical modelling allowed a full characterization of the corrosion mechanism. The corrosion rates were estimated by continuous monitoring by electrochemical techniques and electrical corrosion sensors as well as by post mortem analyses (weight loss and optical measurements).

In the presence of highly alkaline cementitious material (CEM I/CEM II), generalized corrosion was observed, and very low corrosion rates were obtained confirming previous literature data. Corrosion rates of low carbon-steel in the presence of CEM I followed an exponential decay law with corrosion rates dropping to less than 0.1 µm/year within 100 days of interaction. Magnetite and Si-hydrogarnet were the only corrosion products observed in these highly alkaline experiments. Si-hydrogarnet can form at the expense of magnetite providing a source of silicon and calcium is available. In a tightly closed system, favouring very reducing conditions and limiting ingress of elements from the cementitious materials, magnetite will be the predominant corrosion product.

For all steel/low-pH grout interaction tests (mock-up and *in situ*) performed in presence of solid grout, localized corrosion was observed, highlighted the role of cementitious materials in steel corrosion processes. The low-pH grout favoured the formation of corrosion cells that induced localized corrosion primarily due to the presence of sulphides in both CEM III-A and the bentonite component. Moreover,

also the amount of residual oxygen able to easily migrate through such highly porous grout materials was found to be important. The corrosion sequence showed that iron sulphides and/or hydroxides are first formed locally in the anodic zone of the corrosion cell. Depending on the remaining amount of oxygen in the system, the depletion of sulphides led to the formation of either a dense magnetite layer or of a porous layer consisting of iron hydroxides. Finally, the transformation of magnetite (or iron hydroxides) to iron silicates (e.g., greenalite, cronstedtite) mixed with iron sulphides was observed in the corrosion sequence. This transformation was facilitated by the dissolution of hydrated silica fume occurring in the vicinity of the cathodic area where hydroxyl ions are produced, in combination with the release of a second source of sulphides (probably included in blast furnace slag particles).

In mock-up tests, it was observed that magnetite transformation into iron sulphides/silicates was slow due to the stability of the very dense magnetite layer acting as a diffusion barrier. For *in situ* experiments, the transformation of the more porous hydroxides was faster and generated larger amounts of iron silicates in the corrosion product sequence. Corrosion rate measured for mock-up experiments exhibited initial values around 10 µm/year that seemed to stabilize or decrease over time. Several pits with depth ranging from 10 to 100 µm were detected and optical measurements clearly indicated an increase of the number of damaged zones with time, rather than an increase of the pit depth. This observation suggests that the coalescence of these pits would eventually lead to a generalized corrosion process,

This suggestion was supported by results from *in situ* experiments lasting for more than two years. SEM observations performed on *in situ* test steel samples revealed a uniform corrosion product layer of around 230 µm thickness that formed over a period of about two years. The high corrosion rate (115 µm/year) associated to this observation was confirmed by electrical resistance sensor monitoring. This corrosion rate would be more than ten times higher than the corrosion rates obtained after one year of interaction in the corresponding mock-up tests. It was proposed that these differences could be explained either by the higher amount of residual oxygen trapped in the porosity of the grout or by the *in situ* heating conditions that enhanced the renewal of porewater at the interface and thus favoured sulphide and oxygen ingress at the carbon steel surface or finally by the formation of a galvanic coupling between steel/argillite and steel/grout contact zones. The discrepancies between *in situ* and mock-up laboratory tests highlight the impact of the experimental design on corrosion processes (i.e., corrosion products and rates) and emphasize the need to perform experimental investigations at different scales to gain relevant information regarding mass transfer and geochemical interactions.

Only few information on the nature and density of the microbial population were obtained, limiting the interpretation of the results associated with experiments studying the impacts of microbial activity on anoxic carbon steel corrosion processes when exposed to low pH grout material at ambient temperatures. However, some particular corrosion features were observed, such as the formation of homogeneous iron sulphide layers in mock-up tests which can be attributed to bacterial activity, since these tests did not involve solid grout or argillite materials and no sulphide had been added to the synthetic solution. Thus, the formation of the iron sulphides could only originate from a biocatalysed sulphate reduction reaction.

Carbonation of cementitious materials and the associated decrease in pore water pH can have deleterious effects on reinforcing steel, resulting in increasing corrosion due to the loss of passivation. Steel corrosion in partially water saturated carbonated cementitious materials has been investigated for decades; however, the mechanisms governing the corrosion rates under these conditions are not fully understood and debated. This lacking consensus on the mechanistic process understanding is seen as the main reason for the general lack of reliable quantitative models for prediction of steel corrosion rates in carbonated concrete (Stefanoni et al., 2018). In this context, recently, Stefanoni et al. (2018) designed an experimental setup which allowed studying relevant electrical/ electrochemical parameters of steel corrosion in carbonated cementitious material under well-defined conditions, permitting fast equilibration with exposure conditions (i.e. CO_2 and relative humidity (RH)).

Various mortar samples with embedded steel were prepared from two different cement types (CEM I 52,5 R and CEM II/B-M (T-LL) 42,5) with a sand to binder ratio of 2, using three different water/cement

(w/c) ratios ranging between 0.4 and 0.6. The samples were cured at 95% RH and carbonated in a carbonation chamber at 20 °C, at 57% RH and a CO_2 concentration of 4%. The mortars were carbonated for two (CEM II mortars) and three weeks (CEM I mortars), respectively, to ensure complete carbonation of the samples. After the pre carbonation, the steel corrosion was studied at different RH (between 50 and 99%) at a constant temperature of 20 °C by means of various electrochemical measurement techniques. It was found that the steel corrosion rates in the carbonated mortar increased drastically with increasing RH, i.e. the increase of RH from 50% to 99% enhanced the corrosion rate by up to two orders of magnitude. In contrast, the cement type and the water/cement ratio were found to have only minor influence, affecting the corrosion rate generally by a factor of 2–3 at maximum. The results indicate that the availability of oxygen at the steel surface was not a limiting factor for the corrosion rate in these experiments, contradicting the assumption that corrosion is hindered by higher pore water saturation states (higher RH) as a consequence of limited oxygen to diffusion through water filled pores. According to Stefanoni et al. (2018) the high variations of corrosion rates with changing RH cannot be explained by the electrochemistry of the corroding system, or by kinetic limitations arising from the ohmic resistivity of the pore system, or by limited oxygen availability. The authors demonstrated that the most dominant factor influencing the corrosion rate in carbonated concrete is the moisture state and suggested that capillary condensation in the pore structure controls the electrochemically active steel surface, whose variability upon changes in RH is accountable for the orders of magnitude variation in the measured corrosion rates.

2.2.3 Interface “steel – clay”

In various European repository concepts (e.g., Switzerland, Czech Republic), interfaces between steel and clays/clay rocks or bentonites exist (cf. Neeft et al., 2019), for example, between carbon steel waste canisters and bentonite buffer/backfill. Within ACED, experimental studies were performed to inform geochemical and coupled reactive transport models for assessing the geochemical evolution at steel/clay material interfaces in terms of corrosion rates, geochemical and physical alterations to increase confidence and decrease uncertainty of simulations at the disposal cell scale (cf. Turrero et al., 2024). These studies comprised the dismantling and investigation of long-term (up to 15 years) experiments on bentonite-iron interfaces using FEBEX bentonite, the investigation of the interaction of Fe^{2+} with montmorillonite under anaerobic conditions, and experiments addressing carbon steel corrosion in Boda claystone.

Iron-bentonite interfaces

The objective of the investigations of the iron-bentonite interface investigation was to obtain information on chemical variables and alteration in the composition of the solid phase at a the µm to cm scale. The investigations focused on several aspects considered representative of the transient phase of a deep geological repository: (i) estimation of corrosion rates, (ii) analysis of chemical gradients, (iii) identification of mineralogical changes, and (iv) examination of the microstructural modifications. The first set of experiments, started in the context of the past European NF-PRO project, consisted of columnar cells (FB5 and FB6) containing a layer of iron powder (13 mm) in contact with compacted FEBEX bentonite block (87 mm) that were heated to 100 °C from the iron side and hydrated with a Ca-Na-HCO_3- granite-type water from the bentonite side. The cells were dismantled after 14 years (FB5) and 15 years (FB6), respectively, and analysed within ACED, with respect to various mineralogical, geochemical, and microstructural properties. Further in the context of the NF-PRO project, a single iron-bentonite interaction experiment (FeMo) was initiated aiming at the evaluation of the mobility of iron and the alteration of bentonite (FEBEX) under saturated (Ca-Na-HCO_3-granite-type water) and initially aerobic conditions at room temperature. The FeMo experiment was terminated after 15 years of operation and analysed in the context of ACED.

The results of the long-term FB and FeMo experiments showed that water content gradients were related to the thermal gradient and the hydration front. Advective movement of salts towards the heater occurred and salts precipitated right at the Fe/bentonite interface. Chloride was found on the surface of the Fe powder and may play a relevant role in the initiation of corrosion. Near the heater, the Fe particles

retained their metallic luster and showed no signs of corrosion. Iron corrosion was limited to areas close to the interface (≈ 2 mm) with calculated corrosion rates less than 0.5 µm/y. Corrosion products consisted of iron oxides, mainly hematite (predominant), and magnetite – maghemite (FB) as well as goethite (FeMo). These results are similar to the *in situ* FEBEX test at the Grimsel Test Site where the Fe(III) oxides also prevail under non-saturated conditions close to the heater (cf. Wersin and Kober, 2017). After 15 years of interaction, the maximum thickness of corrosion products formed around the iron grains was about 10 µm; the maximum thickness of bentonite interface material affected by iron mineral formation was about 200 µm. There was no evidence of expansion or pressure increase potentially produced by the increased molar volumes of oxides compared to elemental iron. Unsaturated conditions appeared to locally favour potential oxidizing environments. On the other hand, the dry conditions greatly limited the extent of the formation of newly formed minerals.

Interaction of dissolved Fe^{2+} with montmorillonite

After repository closure, anaerobic corrosion will eventually occur on canister surfaces in contact with the bentonite, releasing Fe^{2+} into the bentonite, which can potentially alter its sealing properties (e.g., swelling pressure, redox properties). Thus, the interaction of Fe^{2+} with purified SWy-3 montmorillonite was investigated in anaerobic batch and diffusion experiments. The objective of these experiments was to understand the effects of iron corrosion on bentonite stability under anaerobic conditions in the long-term, focussing on the interaction of Fe(II) with smectite without complicating factors from the transient phase (e.g., variable saturation, variable redox conditions). This included the understanding and quantification of the electron transfer of sorbed Fe(II) to structural Fe(III) (Fe_{str}) in the octahedral montmorillonite structure and of Fe migration (i.e., retention and diffusion) in compacted bentonite. Analyses carried out included determination of Fe concentrations and redox speciation in solution and solids by UV-Vis spectrometry and Fe redox speciation in the montmorillonite by ^{57}Fe Mössbauer spectrometry. For the diffusion experiments and a part of the batch experiments, isotopically purified $^{56}Fe^{2+}$ (transparent to Mössbauer spectrometry) was used to assess the extent of possible electron transfer between sorbed Fe (Fe_{sor}) and Fe structurally incorporated in the montmorillonite (Fe_{str}). In addition, the swelling pressure was also recorded during the diffusion experiments.

It was found that the Fe^{2+} uptake by the clay depends on multiple factors, especially on the pH and on the relative concentrations of dissolved Fe and Fe_{str}. At low pH, cation exchange largely dominates the interaction whereas at higher pH sorption to edge sites and interaction with Fe_{str} becomes more important (see also below in the section on modelling, section 3.1.1 and Figure 3-1). In batch experiments at high Fe(II) equilibrium concentrations, edge sorption accounts only for a minor portion of the Fe uptake. A major part of the Fe uptake observed at pH between 6 and 7 could be described by a pH dependent complexation reaction linked to Fe_{str} sites. Mössbauer spectroscopy of selected experiments performed with ^{56}Fe demonstrated that this process involves an electron transfer to Fe_{str}. At higher Fe uptake, this process presumably extends to the stepwise surface precipitation of tiny green rust like Fe hydroxide domains at the vicinity of the reduced Fe_{str} sites scattered on the clay surfaces. Thus, a very high Fe uptake by the clay can be reached exceeding the initial CEC and Fe_{str} capacity by up to a factor of at least two. However, it has to be taken into account that such high Fe uptake was only observed in case of extremely high Fe concentrations in solution (>25 mmol/L) or very high liquid to solid ratios in the batch experiments.

In compacted conditions in the Fe(II) diffusion experiments, processes involving electron-transfer were limited to the close vicinity of the filters (< 1 mm) and suppressed within the bulk core material. Fe diffusion and retention in the anaerobic bulk of the core could be therefore modelled by a classical 2-site non-electrostatic surface complexation and cation exchange model only (section 3.1.1). So far, the reason for this significant difference between observations from batch and diffusion experiments with respect to the redox interaction of dissolved Fe^{2+} and Fe_{str} is not yet entirely understood. The batch experiments indicated that the pH has a major control on this process and low pH (below 5) could largely supress the redox interaction. It was thus hypothesized that, due to ion exclusion and interaction with Fe^{2+}, the pH at the surface and in the interlayer of the montmorillonite may have been distinctly lower in the compacted clay core than in the reservoirs (pH 7.2).

Carbon steel corrosion in Boda claystone

The interface between carbon steel and clay is a key issue in the design of a disposal cell for vitrified HLW in argillaceous rock formations for the Hungarian national waste disposal program. The design relies on steel-containers encased in a prefabricated cylindrical clay buffer material originating from the Boda Claystone Formation (BCF), the host rock considered for the disposal program in Hungary. To gain information on chemical-physical processes at the steel/clay interface for different environmental conditions (e.g. temperature, groundwater composition), within ACED, laboratory-scale experiments were performed in triplicate under water-saturated (synthetic clay pore water) and anaerobic conditions at 80 °C, lasting for 3 (CSC-M3), 7 (CSC-M7) and 12 months (CSC-M12), respectively. Besides monitoring the corrosion potential, a set of complementary characterisation methods were applied to the synthetic clay pore water (e.g. ICOP-OES, IC) and solid phases (e.g., SEM/EDS and µRaman analyses) with support of geochemical modelling. To exclude leakage and ensure saturation, the mass of each experimental setup was checked monthly.

During experiments CSC-M3 and CSC-M7 fluctuations of the corrosion potential were observed (between -900 and -400 mV) indicating local corrosion processes; in experiment CSC-M12 the corrosion potential reached a nearly constant value of about -650 mV after six months. The corrosion of the carbon steel corrosion under simulated geological disposal conditions resulted in the formation of a variety of corrosion products in varying proportions with exposure time. Microstructural characterization by SEM and µRaman showed that at short time (3 and 7 month) exposure a corrosion layer comprising magnetite and hematite were formed as the main corrosion product, while at longer time (12 month) magnetite and ferrihydrite were formed, indicating oxic conditions in this experiment at some point. Besides the Fe(II)- and Fe(III)-(hydr)oxide phases, other Fe-based phases such as Fe-silicates or Fe-sulphides were not detected in the experiments.

2.2.4 Degradation of cementitious materials

Cementitious materials are used for waste conditioning and backfilling void space as they provide a stable encapsulant for waste storage, transport, and disposal. In addition, the highly alkaline conditions provide a favourable environment for retarding most radionuclides, minimize other chemical reactions like corrosion of iron/steel, and reduce microbiological activity. The long-term chemical evolution of such waste packages in deep geological repositories depends to a large degree on waste package design, waste content and conditioning, and on boundary conditions imposed by the repository design and evolution.

Within ACED long-term concrete degradation and its implications on waste degradation were addressed at the waste package scale (Mladenovic et al., 2024), focussing on the analysis of long-term experiments on chemical processes, corrosion and gas generation in waste containers, the degradation of concretes in contact with clay pore water, and on the study of aggregate-cement reactions in concretes. These systems allowed to study different aspects of long-term degradation of concrete and waste-concrete interactions. Experimental work conducted and analysed in this context comprised (i) long-term experiments on waste stability and gas generation (Gas Generation Experiment – GGE), (ii) exposure of waste package concrete and foamed concrete to air at defined relative humidities and submersion in clay pore water, and (iii) investigations of alkali aggregate interactions in concrete from old hydroelectric power plant dams.

Gas generation experiment

A large-scale *in situ* Gas Generation Experiment (GGE) was established in 1997 in Olkiluoto, Finland, to simulate the gas generation and chemical changes from LLW under geological repository conditions. The GGE comprised carbon steel drums containing operating waste LLW from nuclear power plants including cellulose (paper, cardboard, cotton), polyethylene, polyvinylchloride, polycarbonate, natural rubber, metal wastes, glass fibre and electrical components, placed within a concrete box enclosed in a stainless steel gas tight reaction vessel filled with natural river water. The evolution of water chemistry in the waste drums and the tank as well as gas evolution was monitored.

A significant observation from the GGE was that the pH conditions were heterogeneous (pH 6 to 11), providing optimal neutral pH niches for microbial activity from the outset of the experiment. Over the extended time scale of the experiment, chemical conditions were stabilized and differences in the microbial abundances and community structure in various GGE compartments became less significant. The results demonstrate that organic matter in LLW is converted to methane and carbon dioxide by a succession of anaerobic processes within a complex microbial consortium. From gas generation rates it could be estimated that between 4% and 6.5% of the potentially degradable materials was disintegrated in 16 years of experiment, indicating that these chemical processes will continue for a long time. Mass balance calculations suggested that carbonation fronts in the cementitious materials proceeded with about 0.07 mm per year, indicating that after disintegration of all organic cellulose and hemicellulose the totally carbonated layer is between 17 mm and 27 mm and thus still lot of noncarbonated concrete left.

In ILW the amounts of organic degradable materials are much lower than in the GGE resulting in less concrete degradation. This could be taken into account by reducing the CO_2 generation rate in modelling approaches. It could be assumed that degradation itself is happening at the same rate (%/a), but due to lower amount of material, the CO_2 release would be lower. It was suggested that in the future modelling approaches it could be assumed that 0.3% of cellulose and hemicellulose will be consumed by microbial activity annually. Thus, each kg of degradable material would release 20 mM CO_2 annually for 300 years according to the GGE. However, the GGE is totally closed system with no diffusion or convection of gases out of the system. In contrast, in real waste disposal packages there is gas diffusion and convection out and into the waste packages, which has to be taken into account when modelling a whole disposal cell. Moreover, the GGE revealed that the porosity and as consequence also permeability of the cementitious materials increased due to chemical reactions including Ca leaching. However, the experiment suggested that at complete destruction of concrete is not expected due to the examined chemical reactions (Mladenovic et al., 2024).

Experiments with waste package concrete and foamed concrete

Waste package concrete and foamed concrete made of blended cement containing Ordinary Portland cement and blast furnace slag were exposed to air at different relative humidities to provide quantitative data to study the ingress of gases such as carbon dioxide, but also oxygen. Ingress of oxygen can be important in the operational phase during the implementation of geological disposal of radioactive waste for reinforced concrete or other interfaces between concrete and steel. Moreover, concrete samples were exposed to synthetic clay pore water around room temperature for several years.

The elemental concentration of the concrete and the solutions to which they have been exposed were determined. The cementitious materials were not completely carbonated, i.e. there was still some acid neutralisation capacity in the samples, for waste package concrete more than foamed concrete. The clay water was enriched in dissolved alkalis that may result from the leaching of concrete though leaching of Ca has not been observed for both types of concrete. The investigated waste package concrete is impermeable in engineering terms. However, the effect of temperature and relative humidity after exposure to air for 1000 days could clearly be observed in the reaction fronts in which trace amounts of iron-sulphides had reacted while carbonation profiles could hardly be observed. Also, a chemical effect by exposure to a solution as saline as seawater for $4^1/_3$ years, could not been deduced. The investigated foamed concrete had a higher porosity than the waste package concrete, which had a high impact: trace amounts of iron-sulphides uniformly reacted at almost any relative humidity. After exposure to air for 1000 days, carbonation profiles were clearly visible but a relation with the relative humidity could not been observed.

The predictive capabilities of models simulating the chemical evolution of cementitious materials in a disposal cell depend on the accuracy of input parameters such as reaction rates, diffusivity and permeability and their changes as the distribution in pore size evolves due to chemical interactions. The relative humidity and temperature dependent oxygen and carbonation profiles determined at 5°C and 20°C for concretes with the same cement content but different porosity allowed the determination of

accurate reaction rates. The van Genuchten parameters and characteristic pore radii obtained from the water retention curves were used to determine the water saturated permeabilities of the concretes with the equation of Millington and Quirk. As the water saturation is higher at lower relative humidities for concrete compared to cement paste, it was tentatively proposed that reaction rims between quartz aggregates and cementitious fluid made upon hardening of concrete result into a finer refined pore structure. Consequently, the cementitious phase within hardened concrete is less permeable than solely hardened cement paste.

Alkali silica reactions in old concrete materials

In order to get insights into the long-term aggregate reactivity in concrete structures and trying to overcome the difficulties in simulating long term alkali-aggregate reaction (AAR) damage in cementitious materials with short term laboratory tests and the translation/extrapolation of the results, core samples were taken out of three hydroelectric power plant dams on the Drava River. The oldest one is 120 years old. The alkali content of the cements and the types of cements used in structures are unknown. The samples were investigated by SEM-EDS and micro-XRF/XAS. The presence of alkali silica reactions (ASR) was confirmed in all samples, regardless of their sampling position with the extent of damage depending on the porosity of the samples. It was found that the main driver of ASR was siliceous aggregate (deformed quartz, quartzite, gneiss, sandstone), which is slowly reacting due to its mineralogical characteristics. Damage manifests itself as cracks around the aggregate grains and in the aggregates themselves, dissolution of grains and formation of reaction products, both gels and crystalline products.

It was concluded that the most important input data for high-quality ASR modeling are: (i) knowledge of the aggregate in terms of their petrographic composition and proportions of individual potentially reactive components, (ii) speed, extent and mechanism of the reaction in alkaline media (iii) potential “pessimistic content” of the aggregate and the risk of alkali release from of the aggregate itself, (iv) the composition of the cement, especially with regard to the proportion of water-soluble alkalis and mineral/chemical additives, in the function of inhibiting the reaction, and (v) the quality of the concrete and the environmental conditions during its lifetime (Mladenovic et al., 2024).

2.3 Narrative of the evolution at disposal cell scale

2.3.1 HLW disposal cells

There can be three phases identified in the post-closure phase. In the first phase (I in Figure 2-4 and Figure 2-5), the heat generated by the waste raises the temperature of the host rock in the vicinity of the Engineered Barriers System (EBS). There is transport of water from the host rock into the engineered barriers and full saturation will be achieved since any disposal cell is designed in such a way that the temperature in the engineered barriers will never exceed 100°C. The period in which the host rock is heated depends on the waste characteristics and design. This period has been calculated to be several thousands of years with the thermal power as a function of time for vitrified HLW (Neeft et al., 2022), an assumed interim storage period to prevent a temperature of 100°C in the buffers and the size of the engineered barriers shown in Figure 2-1, their thermal properties as a function of the saturation degree and the properties of the rocks. The thickness of the bentonite buffer in granitic rock is much larger than the thickness of the concrete buffer in clay rock. Consequently, there is more thermal dissipation of heat in the EBS embedded within granitic rock than for the EBS embedded within clay rock. The period in which the waste can raise the temperature of the host rock has been estimated to be about 4000 years for the granitic rock (see Figure 2-4) and 7000 years for the clay rock (see Figure 2-5).

Any oxygen incorporated during the manufacturing of these barriers is consumed by corrosion of steel in the first phase. Anaerobic corrosion of steel occurs in which water is consumed after oxygen is depleted. This corrosion process produces also hydroxyl ions by which the pH of pore water near steel is locally increased. A pH larger than 9 to 10 in order to form the low soluble corrosion product magnetite, is achieved for concrete as well as bentonite interfacing steel. Magnetite passivates the steel corrosion process by which the corrosion rate is controlled by the low solubility of magnetite and dissipation of dissolved iron from the magnetite. The hydrogen generated in this anaerobic corrosion process is dissipated through the buffers into the host rocks.

2.3.1.1 Specific features for the HLW disposal cell in granitic rock

In the second phase (II in Figure 2-4), alteration of the engineered barriers continues. The anaerobic corrosion of steel further consumes water. The clay minerals are negatively charged and reduce concentration of dissolved positively charged iron by sorption (fixation) in the vicinity of steel. The corrosion rate becomes controlled by the sorption rate of dissolved iron by the clay minerals in the bentonite buffer. This iron-sorption changes the hydraulic and chemical properties of the bentonite buffer. By design, there is always a fraction of unaffected bentonite left since the potential extent in iron affecting the bentonite buffer can be well predicted. The dimension of the deposition hole in granitic rock may be stable on a human time scale due to the high UCS of granitic rock but eventually some mechanical load is transferred to the engineered barrier system, especially during glaciation by which the mechanical load is determined by the initial depth of the facility and thickness of the ice sheet. This load is directly transferred to the steel overpack since the bentonite buffer may have too limited strength and the potential swelling pressure is reduced. The iron-affected buffer is more brittle than the unaffected buffer. If a fracture in the buffer is generated, the closure process of this fracture in the buffer has been changed from self-healing by swelling of montmorillonite in the virgin buffer into sealing by precipitation in the iron-affected buffer. The hydraulic conductivity of the clay increases due to the alteration of montmorillonite into non-swelling sheet silicates (Savage, 2014).

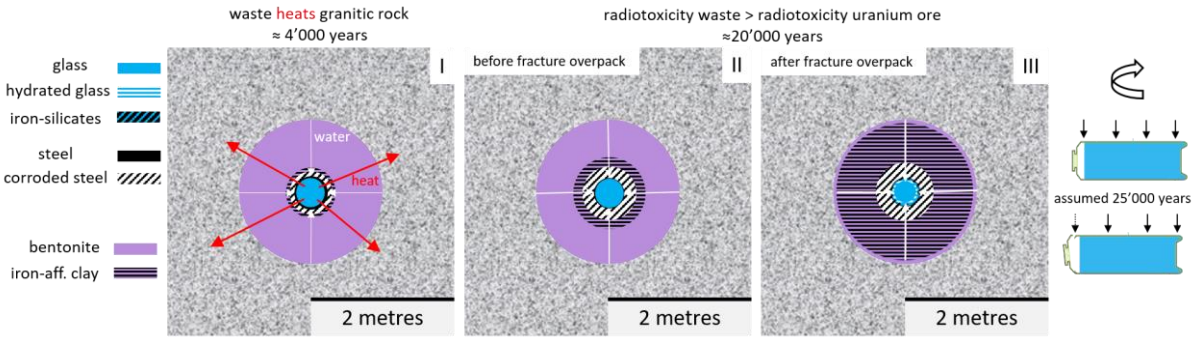

Figure 2-4: Illustrations of the disposal cell in granitic rock for the three different phases. The increase in extent of iron-affected buffer allows more transport of water from the granitic rock towards the steel overpack (visualised with an increase in thickness of the white arrows).

In the third phase (III in Figure 2-4), the steel overpack can no longer provide sufficient support against the mechanical load. After 20'000 years, the radionuclides in the vitrified waste have decayed to such an extent that the radiotoxicity of the vitrified waste has become smaller than that of uranium ore (Gruppelaar et al., 1998; Neeft et al., 2022). There is an empty volume on top of the vitrified waste form in the stainless steel canister. This is the weakest part of the canister and the steel will fracture there. There will be some helium gas present in this empty volume due to decay of actinides since helium diffuses very fast through the vitrified waste form at disposal representative temperatures (Chamssedine et al., 2010). This helium gas is - like hydrogen gas - dissipated through the buffer into the granitic rock. In the modelling performed in ACED, it is assumed that there is contact between pore water and the

vitrified waste form after 25'000 years in order to include the transferral of the mechanical load. The impact of helium gas collected in the empty volume in this period, is considered to be negligible.

Ingress of water in the canister is possible by the fracture in the stainless steel canister. The generated contact between pore water and the vitrified waste form allows hydration of glass. The glass alteration rate depends on its solubility and dissipation rate of dissolved silicon from the glass. The dissolved iron generated during steel corrosion leads to the formation of iron phyllosilicates that reduces the dissolved silicon concentration thus enhancing the glass alteration rate. Consequently, in the vicinity of steel, the glass alteration rate can be larger.

2.3.1.2 Specific features for the HLW disposal cell in clay rock

The alteration of the engineered barriers embedded in clay rock that started in phase I, continues in phase II. Unlike the granitic rock, the clay rock minimizes the transport of water towards the EBS. However, ingress of CO_2 and bicarbonate ions from clay rock pore water can lead to reactions with cementitious minerals in the concrete buffer and produce water, especially for concrete made with CEM I due to its high portlandite content. Overall smaller anaerobic steel corrosion rates are found for steel interfacing concrete than steel interfacing clay probably because the sorption rate of positively charged dissolved iron by the CSH minerals (also positively charged in a wide range in pH of concrete pore water) is negligible (see Figure 2-3).

The dissolved alkalis from concrete pore water react with the clay minerals in clay rock. Illite is the major clay mineral in COX. Zeolites are envisaged to be formed when illite reacts with cementitious fluid as described in the (documents for the) initial SOTA (Deissmann et al., 2021; Neeft et al., 2022).

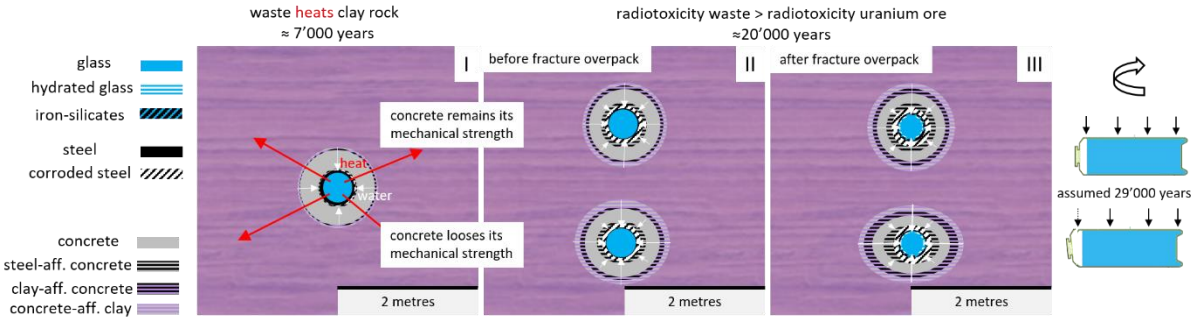

Figure 2-5: Illustrations of the disposal cell in clay rock for the three different phases. Reduction in mechanical strength of the concrete buffer is associated with a larger diffusion value for water and allows more transport of water from the clay rock towards the steel overpack (visualised with an increase in thickness of the white arrows i.e. neglecting self-sealing). The concrete buffer may produce water with ingress of dissolved CO_2 and bicarbonate.

COX has a much smaller UCS than granitic rock. The dimension of the deposition hole in this clay rock requires some support already on a human time scale. Consequently, for the disposal cells in Figure 2-1, it depends on the strength of the concrete buffer whether the lithostatic load is transferred to the carbon steel overpack and whether the dimension of the tunnel changes. In ACED, two cementitious buffers are investigated, one with aggregates and one without aggregates.

The buffer without aggregates mechanically acts like the bentonite buffer, except that this cementitious buffer does not have a swelling pressure so the mechanical load is directly transferred to the carbon steel overpack. The dimension of the tunnel is envisaged to change since the UCS of the clay rock is so much smaller than the UCS of granite. In Figure 2-5, for simplicity no compaction of the concrete buffer is assumed but compaction would occur if the buffer is also very porous by which the dimension

of the tunnel changes even more than currently drawn. Like described in the narrative for the granitic rock, fracturing of the carbon steel overpack occurs when the corroded thickness is too large.

The buffer with aggregates may provide support by which the mechanical load is not transferred to the carbon steel overpack. The dimension of the tunnel does not change as long as concrete retains its strength. The uptake of iron in concrete has been shown in archaeological analogues (e.g., Chitty et al., 2005). Based on the observations from third framework programme that the concrete interfacing steel is loosely bound (Atkins et al., 1991), it was assumed that uptake of iron reduces the strength of concrete in the vicinity of steel in the initial SOTA (Neeft et al., 2022). Steel-affected concrete may therefore assumed to have a smaller strength than manufactured concrete. In the long-term, pH of the concrete buffer will decrease and the charge of the CSH minerals become negative at a pH below 11.7 (Pointeau et al., 2006) for concrete interfacing steel. The altered buffer can like the bentonite buffer then start uptaking dissolved iron by sorption. As the negative charge becomes larger with decreasing pH, the sorption rate of iron may increase until the concrete is completely carbonated. The oxidation state of iron is therefore crucial (see section 3.1.2). In the corrosion process, Fe^{2+} (Fe(II)) is formed while $Fe(OH)_4^-$ (Fe(III)) is present at very high pH (Neeft et al., 2022).

In the modelling performed in ACED, the impact of the changing charge of the CSH minerals is not explicitly addressed but a faster iron corrosion rate at lower pH is used. For clay-affected concrete, it may highly depend on the clay pore water composition interfacing the concrete buffer how the strength of the concrete buffer evolves. Leaching occurs if the calcium concentration in the clay pore water is small compared to the calcium concentration of concrete pore water indicated in Figure 2-3. Leaching may increase the porosity and the size of the pores. This increase in porosity and size of pores reduces the strength of concrete by which the concrete buffer may compact when reducing the pore volume.

For the start of phase III in the modelling performed in ACED, it is assumed that there is contact between pore water and the vitrified waste form after 29’000 years in order to include the transferral of the mechanical load leading to fracturing of the overpack. The diameter of the tunnel was assumed to remain stable. The generated contact between pore water and the vitrified waste form allows hydration of glass. Like earlier stated for the granitic rock, the glass alteration rate depends on its solubility and dissipation of dissolved silicon from the reacting glass surface. The dissolved silicon in equilibrium with CSH minerals increases with decreasing pH (see Figure 2-3) but on the other hand the solubility of silicon increases with increasing pH. Apart from the vitrified waste form, there is therefore another source of dissolved silicon to react with dissolved iron from the steel corrosion process to form iron-silicates. Consequently, in the vicinity of steel and altering concrete, the glass alteration rate may be smaller than within the bentonite buffer. So far, as explained in section 2.2.1, smaller glass alteration rates have been found for the glass/steel/cement systems than for the glass/steel/clay systems. The cation exchange capacity for bentonite is around 100 meq/100 gram (see section 2.1.1.1) and 17.4 meq/100 gram for COX (see section 2.1.5). A higher cation exchange capacity may allow sorption rates of iron by which larger corrosion rates may be possible.

2.3.2 ILW disposal cells

The radiotoxicity of ILW is small compared to the radiotoxicity of HLW at the start of disposal. It would be sensible to compare the radiotoxicity of the waste with a radioactive material that is used in ordinary life in order to put the hazard potential of the waste in perspective. In ACED, we use a lot of concrete in the disposal cells. Concrete has therefore been used to compare the radiotoxicity of radioactive waste.

Concrete contains traces of uranium, thorium and radioactive potassium. These radionuclides have very large half-lives and any decay is insignificant compared to the decay of radionuclides in ILW. These traces are so small in concrete by which it is safe to handle concrete without special precautions. Consequently, concrete is a radioactive material but concrete is not considered to be radioactive waste.

The contribution of radioactive cobalt to the radiotoxicity of metallic waste is large but its half-life is just slightly more than 5 years. The decrease in the radiotoxicity of this waste as a function of time is

therefore envisaged to be fast, perhaps within 100 years its radiotoxicity is similar to concrete. Usually, radioactive caesium and strontium are the second and third contributors to the radiotoxicity of metallic waste. Their half-lives, 30.08 years for caesium-137 and 28.91 years for strontium-90 are larger by which a larger period may be required in order achieve a similar radiotoxicity as concrete. Nevertheless, metallic waste is frequently considered short-lived ILW for which disposal depths of tens of meters to some 100 metres are required. The necessary disposal depth for short-lived ILW is therefore smaller than for HLW since short-lived ILW requires a smaller period for isolation and containment than HLW.

The variety of radionuclides contributing to the radiotoxicity or organic waste is much larger than for metallic waste. It is therefore more difficult to determine the necessary period for isolation and containment with the current information available. In the case of a large amount of actinides in organic waste, the required period for containment and isolation may be larger. For spent fuel, it takes about 200'000 years to achieve a similar radiotoxicity as uranium ore (Gruppelaar et al., 1998) due to its presence of plutonium. A similar period is therefore currently considered as a maximum for organic waste.

Freshly manufactured concrete is unsaturated and all organic and metallic waste degradation mechanism require water. The transport of water in the disposal cells is therefore an essential feature to assess potential waste degradation rates. Gaseous carbon dioxide and organic complexes may be formed during degradation of organic waste. Gaseous hydrogen is formed during anaerobic corrosion of steel. The access of water during dry storage of waste may be too limited for detectable degradation of waste. This access in the disposal cell depends on the transport properties of water in the engineered barriers and host rocks.

2.3.2.1 Specific features for the ILW disposal cell in granitic rock

The ILW disposal cells within granitic rock are envisaged to have a larger thickness in EDZ with a larger fracture density than HLW disposal cells due to different excavation procedures. Common practice shows that some support is already necessary in the operational phase of the disposal facility as explained in (the documents for) the initial SOTA (Neeft et al., 2022; Neeft et al., 2019). The granitic rock would converge in the case that the disposal cell is backfilled with a porous mortar with negligible strength. This may be the case for the chosen vault backfill mortar in ACED by which the mortar will compact when reducing pore volume since its strength may be too small to stop convergence of the granitic rock (see Figure 2-6). This compaction reduces the porosity by which lower transport (diffusion, permeability) values for water may be assumed. In the modelling performed in ACED, the transport properties and dimension of the vault is assumed not to change.

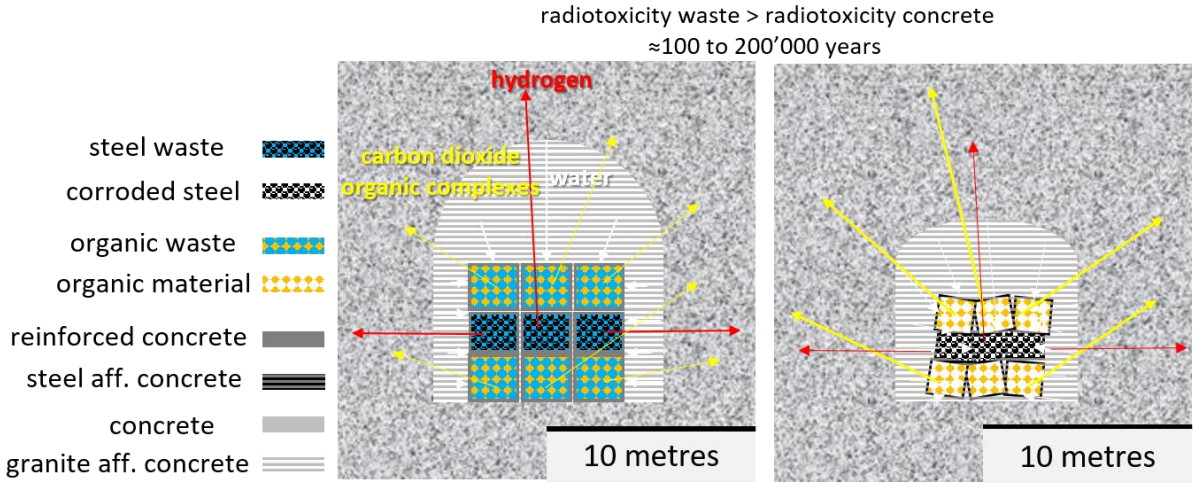

Figure 2-6: Illustrations of the disposal cell in granitic rock. Compaction of the backfill may allow less transport of water from the granitic towards the waste packages (visualised with a decrease in thickness of the white arrows). The backfill may produce water with ingress of dissolved CO_2 and bicarbonate.

The potential flux of water available for the degradation of waste is entirely determined by the (changing) hydraulic properties of (reinforced) concrete since the transport of water in granitic rock is so fast. There can also be water produced by carbonation of cement minerals since the concrete is assumed to be made with CEM I. The necessary saturation degree in concrete for corrosion of steel has been estimated to be at least 20% (Stefanoni et al., 2018). Organic degradation rates are usually obtained from experiments in which organic matter is put in a (cementitious) solution. Microbial organic degradation in these experiments cannot be excluded since there is no restriction in space for microbial life. These microbial organic degradation rates can be (much) larger than chemical organic degradation rates and require much higher saturation degrees, for example in bentonite more than 96% saturation is necessary for microbial life (Stroes-Gascoyne and West, 1997). In Figure 2-6, it is therefore assumed that primarily first anaerobic corrosion of steel takes place followed by organic degradation of waste. It depends on the dissipation of generated gases whether high pressures of gas within concrete are formed that might change the transport of water towards the waste. In any case, the perturbation of the granitic rock by the generated gases is not expected since the dissipation of gases through the cracks in granitic rock is so fast. Concrete affected granite is not indicated since it may be rather the minerals in the fractures in the granitic rock that may alter by egress of dissolved species from concrete.

2.3.2.2 Specific features for the ILW disposal cell in clay rock

Also for the ILW disposal cells within clay rock, a larger thickness of the EDZ with a larger fracture density needs to be assumed than for HLW disposal cells due to different excavation procedures. Like granitic rock, the clay rock may also converge in the case that the disposal cell is backfilled with a porous mortar with negligible strength and backfill can be compacted by which the volume of this cementitious material decreases (see Figure 2-7). In the modelling performed in ACED, the transport properties and dimension of the vault are assumed not to change.

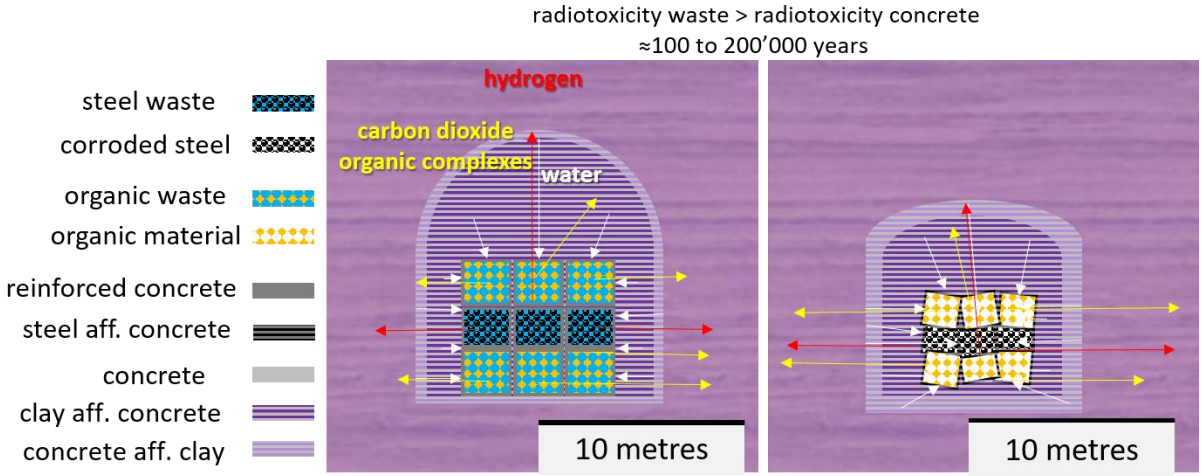

Figure 2-7: Illustrations of the disposal cell in clay rock. Compaction of the backfill may have no impact on the transport of water in the EBS towards the waste packages since that may be controlled by the clay rock. The backfill may produce water with ingress of dissolved CO_2 and bicarbonate.

Unlike granitic rock, the potential flux of water available for the degradation of waste is entirely determined by the (changing) hydraulic properties of the clay rock and the evolution of its saturation degree in the vicinity of the EBS. Like granitic rock, there may be water produced by carbonation of cement minerals since the concrete is assumed to be made with CEM I, but the ingress of CO_2 and bicarbonate ions from the clay pore water is much slower compared to granitic rock. All processes earlier described for granitic rock also take place in the clay rock, except that the organic and metallic degradation rates are much slower. Whether high pressures of gas within concrete are formed that might change the transport of water towards the waste may be questioned with a very low degradation rate of waste. More important is that the gas entry pressure in concrete is several times larger than the gas entry pressure of clay rock. What needs to be assessed is whether the gas entry pressure of the clay host rock is exceeded at low waste degradation rates in order to assess whether there is perturbation in the clay host rock. In any case of perturbation, the anisotropy of the clay host rock will contribute to minimize eventual gas enhanced transport to the overburden and living environment since preferential gas pathways will be along the layered structure of this rock as shown in Figure 2-7.

2.4 Modelled chemical evolution at disposal cell scale

Modelling of the chemical evolution of a disposal cell is a key point assessing the evolution of that system at relevant spatial and temporal scales and gives insight in the durability of the different near-field components but as well in the chemical background for modelling the speciation and migration of radionuclides. As such, these models are potential inputs in performance (durability) and safety (chemical background) assessments. Reactive transport models (RTM) have been central to understanding and assessing how thermal, hydrological, and geochemical processes are coupled in these containment barriers, which are expected to experience a range of temperatures and geochemical conditions, yet, must maintain their integrity for more than 100,000 years. This section summarizes the modelled geochemical evolution of the four disposal cells. The conceptual and mathematical models were based on the narrative evolution discussed in section 2.3 and details were provided in Samper et al. (2022).

2.4.1 HLW

Details on the evolutions were given in section 2.3. Three systems will be discussed (more details on the conceptual, mathematical and numerical models are available in Samper et al. (2022) and on results and discussion in De Windt et al. (2024): (i) a HLW disposal cell in granite covering Period II and III, (ii) a HLW disposal cell in clay considering transient water saturation and temperature conditions related to Period I, and (iii) a HLW disposal cell in clay covering Period II and III. In these models, the vitrified waste is represented by a simplified composition referred to the international simple glass (ISG) throughout this report.

2.4.1.1 HLW disposal cell in granite – Periods II and III

The reactive transport model for HLW disposal in granite includes the vitrified waste – steel overpack – FEBEX bentonite buffer – Spanish reference granite host rock multibarrier system in a 1D radial transport domain (Montenegro et al., 2023). The non-isothermal water-saturated model that considered kinetic glass dissolution, kinetic steel corrosion, kinetic smectite dissolution and thermodynamic equilibrium models for aqueous speciation, mineral dissolution/precipitation, cation exchange and surface complexation reactions was implemented in CORE^{2D} V5 (Samper et al., 2009; Fernández, 2017; Águila et al., 2020). The constant steel corrosion rate was fixed such that the canister fails when 70% of the canister is corroded after 25,000 years where after the dissolution of the glass starts.

In Period II, the pH near the steel/bentonite interface increases due to steel corrosion. Magnetite forms mainly in the canister (represented as a porous medium in the reactive transport model, see section

3.2.1), siderite at both sides of the steel/bentontite interface, and greenalite mainly at the bentonite side. Smectite dissolution is larger near the steel/bentonite interface. A general trend of decreasing porosity is simulated in the regions of secondary phase precipitation. Fe(II) sorption occurs on the exchanger but also on strong and weak surface complexation sites in the bentonite. Period III starts after 25,000 years with progressive glass dissolution leading to a pH increase in the glass. Steel corrosion proceeds for another 10,000 years in Period III with magnetite precipitation in the canister. When all steel is corroded, magnetite redissolves at the glass/steel interface and forms greenalite driven by the Si flux provided by glass dissolution; siderite precipitates at the canister/bentonite interface. Smectite dissolution continues most intensively at the canister side with the formation of Mg-saponite. Also Fe(II) further interacts with bentonite with an increasing thickness of the bentonite zone enriched with Fe. Cl and major cation concentrations in the bentonite pore water decrease with time but are relative uniform throughout the bentonite.

2.4.1.2 HLW disposal cell in clay – Period I with transient water saturation and temperature conditions

The transient thermal and water resaturation stage has been investigated on a subsystem consisting of magnetite (corroded steel) – CEM I concrete buffer – COx rock with the focus on the durability of the cementitious buffer. The model has been implemented in iCP (Nardi et al., 2014). The evolution of temperature in space and time (higher temperature closer to the canister and earlier in time) modified the effective diffusion coefficient and the solubility of the minerals for about 1,000 years. Specifically in a cement system, temperature has an influence on the stability of (S,Al)-bearing minerals. Ettringite and monocarboaluminate are progressively dissolved at higher temperature, but secondary ettringite precipitated once the temperature decreases again. In terms of quantitative indicators of cement degradation (complete portlandite dissolution and C-S-H decalcification to a Ca/Si ratio of 0.8), accounting for the temperature transient result in faster degradation of concrete for both indicators and is more significant for thinner buffers. In a thicker buffer, only a part of the cement buffer is degraded in the time frame of transient temperatures; the remaining buffer degrades under similar temperature conditions as in a case without transient temperatures. The partial water saturation modified the effective diffusion coefficients through, e.g., a Millington and Quirk type model with slower diffusion in case of a lower saturation degree. Consequently, the influence of the desaturation tends globally to slow down the decalcification sequence. For thin buffers (5 cm was considered in the simulation), the temperature effect is more important than saturation (e.g., portlandite dissolution in a 5 cm thick buffer took 300, 100 and 150 y for, respectively, constant conditions, variable temperature and variable temperature and saturation). For thicker buffers (30 cm was considered in the simulation), the thermal transient is too short in comparison to the mineral sequence and the influence of the desaturation tends globally to slow down the decalcification sequence (e.g., portlandite dissolution in a 30 cm thick buffer took 8000, 6500 and 10,250 years for, respectively, constant conditions, variable temperature and variable temperature and saturation).

2.4.1.3 HLW disposal cell in clay – Periods II and III

Within ACED, for the first time, a reactive transport model was developed to assess the chemical evolution of a full HLW disposal cell system in clay, i.e., including in a common model the multi-barrier components “vitrified waste – steel overpack – concrete buffer – clay host rock” such that different types of chemical processes for the entire multibarrier systems of the HLW disposal cell in clay host rock were coupled within one model. The geochemical model included kinetic dissolution of the glass matrix, kinetic corrosion of the canister, kinetic alteration of the host rock minerals, equilibrium cement degradation and formation of secondary minerals or corrosion products. The rate constants were pH dependent - the lower the pH, the slower the chemical degradation of the host rock (and IS glass) but, on the opposite, the faster the corrosion rate of steel. The 1D radial model was implemented in HYTEC (van der Lee et al., 2003).

Figure 3-7 illustrates the key steps in geochemical evolution of the HLW disposal cell in clay including the initial state (Figure 3-7a). In a first stage in Period II, the cement degrades driven by the strong chemical gradient that exists with the host rock pore water (Figure 3-7b). The perturbation and

degradation (decalcification, sulphate attack, carbonation) slowly propagated by diffusion towards the steel overpack with a pH decrease. Perturbation in the host rock led to changes in the cation exchange occupancy, dissolution of primary minerals, and precipitation of secondary phases (e.g. saponite), limited to a few dozen of centimetres after 40,000 years. Steel corrosion is very slow (passivation at high pH) with magnetite as the main corrosion product. Phase 2 in Period II is characterized by lower pH values (advanced state of cement degradation when C-S-H reaches lower Ca/Si ratios) at the steel-cement interface leading to faster corrosion of steel and formation of corrosion products (greenalite) at the steel-cement interface. After about 29,000 y (Figure 3-7c), the canister breaches (assumed to occur once only 1.5 cm of steel remained uncorroded) and glass alteration starts (Period III, Figure 3-7d). Greenalite remains the main corrosion product with Si originating from dissolution of the glass precipitating at the glass-steel interface (in phase 2, Si originates from cement). Consequently, glass dissolution rate is strongly coupled with steel corrosion and greenalite precipitation acting as a silica sink as long as some Fe(0) still remained and was corroding. Once all Fe(0) was fully dissolved (after approximately 34,000 years), the ISG glass dissolution is under residual kinetic control only and slowed down considerably. Diffusion-driven transfer leads to a protective effect of the inner zone of the glass by the external ones.

(*a*) Initial state of the cell component

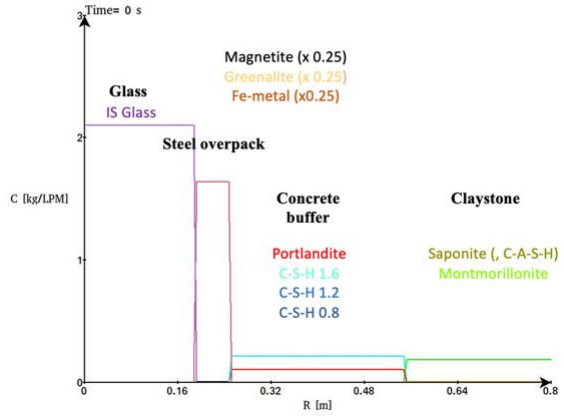

(b) 7,000 y –cement alteration driven by the clay host rock

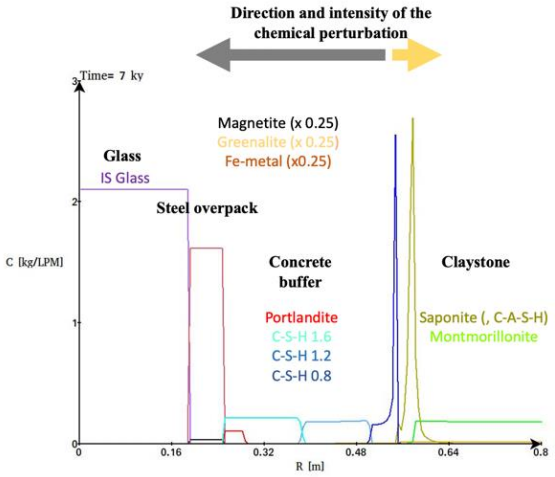

(*c*) 25,000 y – steel corrosion enhanced in the advanced state of cement alteration

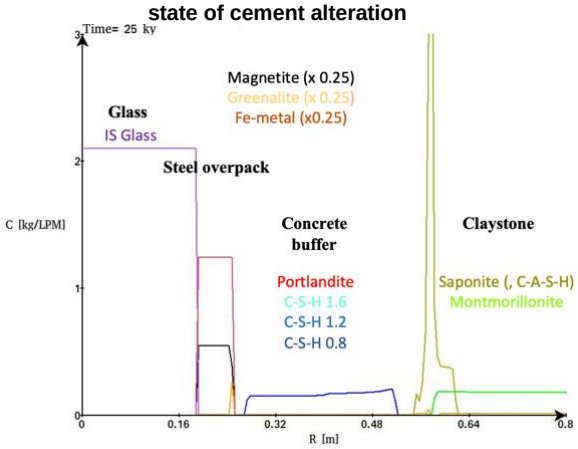

(*d*) 31,000 y – nuclear glass dissolution sustained by steel corrosion

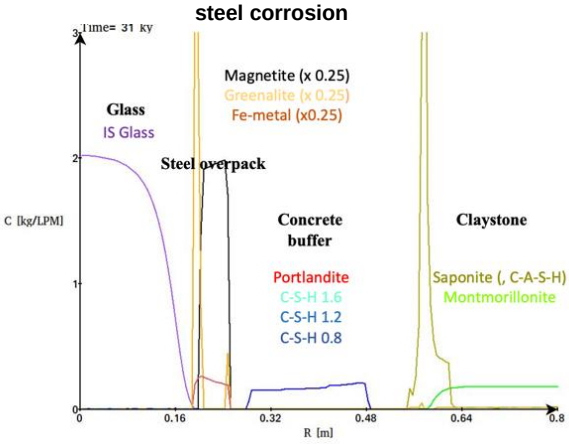

(e) 37,000 y – slow glass dissolution after full corrosion of steel

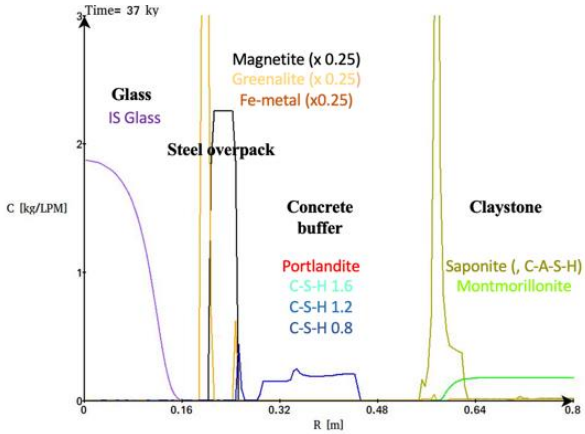

*Figure 2-8. M*odelling of the *chemical evolution of the HLW disposal cell with time with a selection of the key "disruptive" processes (HYTEC simulations, see de Windt et al., 2024).*

2.4.2 ILW

The detailed geometry of the disposal cells for ILW is shown in Figure 2-9. Degradation of organic waste or steel waste is not included in the model – these aspects are covered in chapter 3 both at the waste package scale and with a multiphase modelling approach for the disposal cell scale in clay. The main consequences of not taking this into account are: (i) no waste-induced carbonation reactions of the cementitious materials because there is no production of CO_2; (ii) no internal water consumption by degradation of organic waste and steel corrosion, and (iii) no production of gases (e.g., CO_2, CH_4, H_2) by degradation of organic waste and steel corrosion. The latter may lead to unsaturated conditions, gas pressure build up and gas flow depending on waste and host rock properties (see also chapter 3). The model also ignores a potential initial unsaturated state of the disposal system and considers thus saturated conditions during the complete simulation period of 100,000 years. Models for the clay and granite host rock are implemented in OpenGeoSys-6 (Naumov et al., 2018; Bilke et al., 2019). For computational reasons, relatively large grid sizes and time steps are required to solve the system in a reasonable amount of time. As 2D maps of output variables are not easy to interpret, the evolution of the system was also simulated and interpreted along one or more 1D profiles (Figure 2-9).

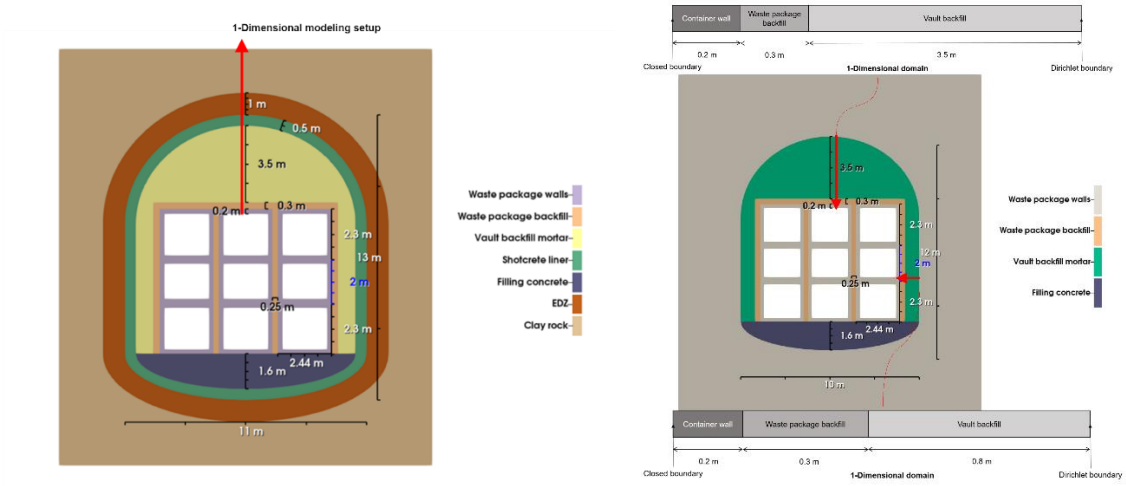

Figure 2-9. (Left) Dimensions and layout configuration of the ILW disposal cell concept in clay, and (Right) in granite. Red lines indicate the studied 1D profiles.

2.4.2.1 ILW disposal cell in granite

For the disposal cell model in granite, it is assumed that water is flowing longitudinal along the disposal gallery. The granite is not included in the simulation domain, but the granite pore water composition is imposed as a constant concentration condition (Dirichlet) at the boundaries of the engineered barrier system. The geochemical evolution is driven by the chemical gradients that exist between the pore water composition of the granite and the cementitious materials. Consequently, typical leaching patterns develop with time: fast leaching of alkali's obtaining a relative uniform pH controlled by portlandite throughout the engineered barrier system, subsequent dissolution of portlandite, and conversion of C-S-H with a high Ca/Si ratio to a low Ca/Si variant and precipitation of calcite (see Figure 2-10 (left) for the vertical 1D profile after 100,000 years; similar sequence for the horizontal profile, but much faster alteration). Leaching fronts progress from outside to inside in the 2D model, but a specific spatial-temporal pattern develops because of the geometry and the location of different materials. Figure 2-11 shows the 2D map of the pH after 100,000 years. The cement is in a further degradation state (lower pH) at the two sides and the bottom; the larger volume of cement above the waste containers is still at values above 11. Importantly, the pH inside the waste packages is still very alkaline keeping advantageous conditions (e.g., low steel corrosion rates) for a long time – at least when there is no

internal pH decreasing processes such as carbonation induced by CO_2 from organic waste degradation or reactive aggregate reactions (see section 3.3.2).

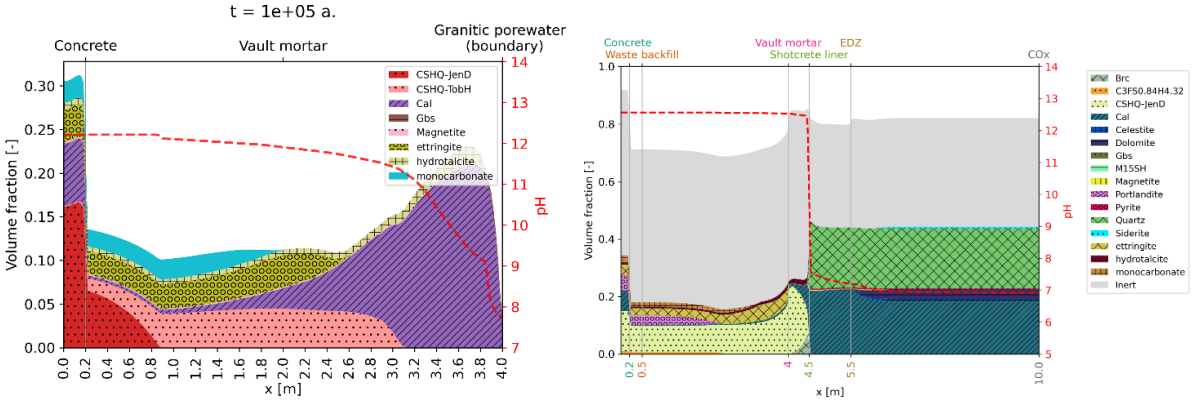

Figure 2-10 – 1D profiles of mineral distribution and pH after 100,000 years in ILW disposal cells in granite (left, vertical profile) and clay (right)

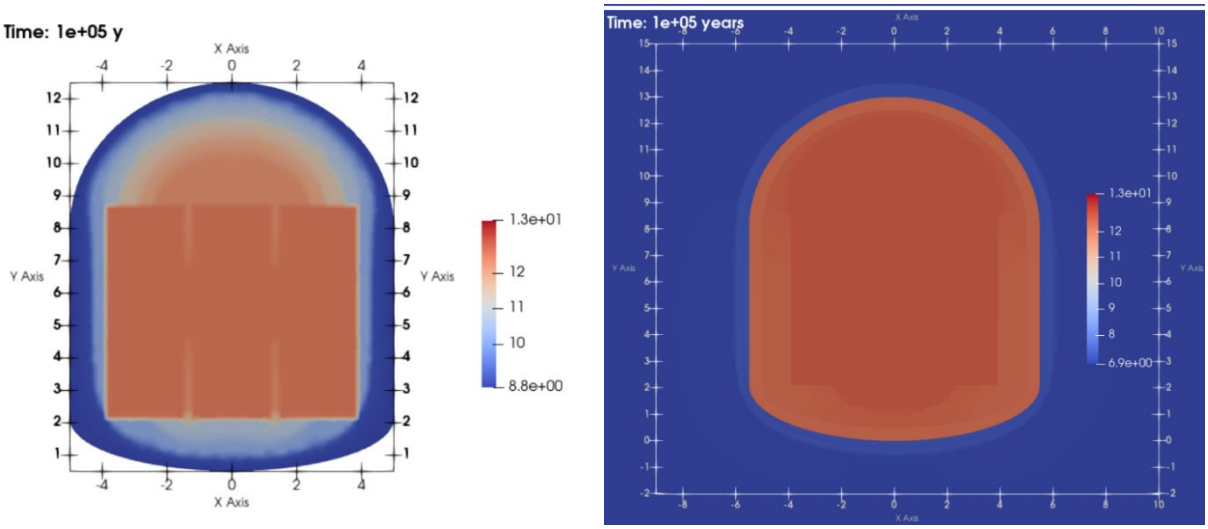

Figure 2-11 – 2D map of pH of the ILW disposal cell in granite (left) and clay (right) after 100,000 years.

2.4.2.2 ILW disposal cell in clay

The main difference to the disposal cell in granite is that, for the disposal cell in clay, transport in the host rock is by diffusion only. A constant concentration boundary at the interface between the engineered barrier and the host rock is not a good representation; therefore the host rock should be included in the model (an extent of about 20 m was sufficient to have no artefact of boundaries on the simulation in this set up; note that, for symmetry reasons, only half of the disposal cell was modelled). The detailed mineralogical sequence after 100,000 years along the 1D profile is shown in Figure 2-10 (right). The chemical gradients that exists between the engineered barrier system and the host rock result in (i) complete portlandite dissolution in parts of the EBS, (ii) formation of a high Ca/Si C-S-H in the liner (replacing a low Ca/Si C-S-H phase), (iii) complex cement phase dissolution/precipitation (ettringite, straetlingite, hydrotalcite, monocarbonate, CSFH, and ferrihydrite) upon interaction with clay water, and (iv) calcite precipitation at the cement-clay interface both in the cement and in the clay. Dolomite dissolves in the host rock. Porosity changes are relatively small. The pH alteration in the clay

caused by the alkaline plume of the cement materials pore water extends to about 1.5 m from the interface. In the cement-based materials, the pH stabilizes at around 12.5 after 50,000 years.

The 2D model indicates that calcite precipitation, dolomite dissolution and changes in the high Ca/Si phase occur relatively uniform around the cement/clay interface. These two mineralogical changes in the host rock occurred quite uniformly around the engineered barrier system. Portlandite and also ettringite showed strong space-dependency. The pH just outside the EBS is increased slightly quite uniformly around the complete interface (Figure 2-11 (right)). In the EBS, pH values are still quite alkaline with small gradients – the high Ca/Si C-S-H phase is still present in the complete domain buffering the pH at a high value.

3. Integration of process-knowledge in reactive transport models for assessing the chemical evolution at disposal cell scale

This chapter discusses mathematical models that are dealing with different aspects that influences the geochemical evolution in the disposal cell. Some applications and modelling from these results are also discussed within the framework of ACED, thus related to the generic disposal cells defined above and to the specific work in which a steel-cement or steel-clay interface is present. From that point of view, beside the disposal cell scale that was discussed in section 2.1, following aspects are addressed: (i) Fe fate in the two types of material (section 3.1), (ii) alteration of materials at interfaces with steel (including glass, clay and cement), formation of corrosion products and migration of elements including Fe (section 3.2), (iii) Modelling evolution at the waste package scale, i.e. mainly without the influence of the host formation (section 3.3), and (iv) overview of model abstraction methods and application to the generic cases for the disposal cell scale (section 3.4).

3.1 Fe fate in buffer and construction materials based on clay or cementitious materials

A relevant source of Fe in disposal cells is the release from steel corrosion. Apart from precipitation in corrosion products, Fe will also diffuse in the buffer material and will interact by sorption, incorporation in existing phases or additional secondary phases. This section describes the fate of Fe in clay (section 3.1.1) and in cementitious (section 3.1.2) materials.

3.1.1 Fe in clay

Fe released from steel corrosion at a Fe-clay interface will diffuse and being retained in the clay material being either bentonite as buffer, filler or seal, or host rock. A starting point for modelling the retention of Fe is an iron sorption model based on the 2-site protolysis non-electrostatic surface complexation and cation exchange model (2SPNESC/CE) models developed by Bradbury and Baeyens to model sorption on illite and montmorillonite (Bradbury and Baeyens, 1997) – cation exchange as a result of isomorphic substitution in the interlayer and basal plane surfaces, surface complexation on sorption active sites being surface hydroxyl groups at edge or broken bonds. In order to model sorption, two types of these sites were assumed, namely, strong sites, Ss, with higher abundance and strong complexation, and weak sites, Sw, with lower abundance and weaker complexation; these sites were identified as distinct sites with spectroscopic differences for Zn sorption on montmorillonite (Dähn et al., 2011). Soltermann et al. (Soltermann et al., 2014) added surface complexation reactions and cation exchange reactions for Fe(II). Similarly, and more recently, Chen et al. (2022) proposed reactions and thermodynamic constants for Fe sorption on illite; this model contains also a variant with oxidation of Fe(II) surface complexes or surface precipitation.

Geochemical modelling of Fe(II) sorption on purified SWy-3 montmorillonite with the model of (Soltermann et al., 2014) which was extended by an additional surface complexation reaction accounting for the interaction of Fe(II) with structural Fe (redox sorption) provides insights into the main sorption mechanisms, and the importance of the electron transfer process. The model was validated with experimental anaerobic batch studies (discussed in section 2.2.3). In experimental series with constant initial Fe concentrations, the absolute amount of exchanged Fe decreases with increasing pH. In parallel, the uptake of Fe by the redox sorption process at the sites of Fe in the structure increases (Figure 3-1-left)[1]. The relevance of the cation exchange processes decreases also with increasing Na concentrations (>0.25 M, not shown). Surface complexation at the clay edge sites (pH dependent process, strong and weak surface complexes indicated by, respectively, Ss and Sw in Figure 3-1 2SPNE) contributes only to a minor degree to the total sequestered Fe due to the limited site capacity.

[1] Fe concentrations at a pH higher than 7 are likely to remain below those studied in the batch experiments due to solubility constraints

The redox sorption process – Fe_{str} at isolated sites in the octahedral sheet of montmorillonites is reduced by aqueous Fe(II) - successfully describes the increasing additional Fe sorption/sequestration over a pH range from 4.3 to 7 (Figure 3-1-left). Because the redox sorption process represents an additional Fe uptake process at the Fe_{str} sites, the total Fe uptake may exceed the sorption capacity inferred from the cation exchange and edge site capacity. At very high Fe concentrations, the observed Fe uptake was even higher than predicted by the model and partly exceeded the overall uptake capacity (CEC, Sw and Ss sites, Fe_{str}) pointing to some additional process (stepwise surface precipitation of Fe hydroxides at the vicinity of the reduced Fe_{str} sites scattered on clay surfaces) (Figure 3-1-right). Note that sorption also decreased at high Cl concentrations because of the occurrence of Fe-Cl complexes. The model applied for batch experiments seems to capture different factors that influence Fe(II) uptake on montmorillonite being the pH, the relative Fe_{aq} and Fe_{str} concentrations and the Fe/Na ratio (or of other competing cations).

A RTM for diffusive transport with the model for sorption of Fe(II) in montmorillonite together with an adequate parameterization for the transport parameters reflected Fe accumulation profiles in diffusion experiments. Compared with the model for the batch experiments, it required however a slightly decreased cation exchange and edge site capacity and the deactivation of the Fe_{str} sites in the bulk of the clay core. Such RTM provides again insight into the contributions of the different sorption mechanisms. Of course, these contributions depend on the prevailing conditions (pH, Fe(II) amount, redox state, etc.) but are elucidated by the RTM implementation. In the study reported in Wittebroodt et al. (2024a), it was noticeable that the redox sorption played only a minor role in the diffusion experiments compared to its role in the batch experiments, which may be due to clay compaction or different geochemical conditions at the surface of the clay sheets (e.g., pH conditions) and might be limited to direct interfaces. The Fe diffusion and retention in the anaerobic bulk of the core could be therefore modelled by a classical 2-site non-electrostatic surface complexation and cation exchange model only. A supplementary Fe uptake process (analogous to redox sorption in the batch experiments) had only to be invoked at the vicinity of the filter based on experimental observations. Note also that cations involved in cation exchange are known to exert a specific mobility whereas Fe sorbed by surface complexation reactions may be considered rather immobile. Increasing retention of Fe(II) by cation exchange may thus increase Fe diffusivity which could be accounted for by an increasing effective diffusion coefficient.

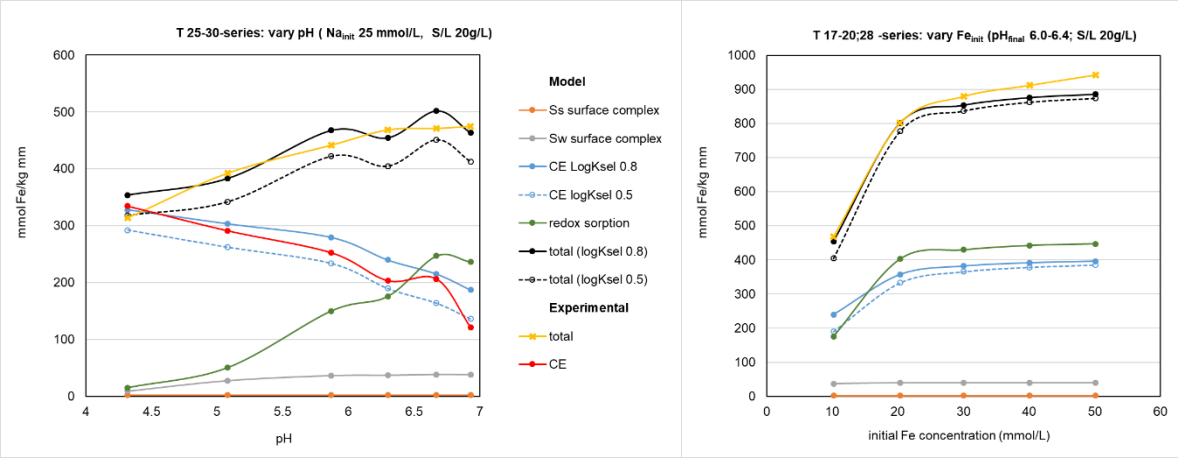

Figure 3-1 – Modelling Fe sorption on SWy-3 montmorillonite under batch conditions for varying pH conditions (left) or initial Fe concentrations (right) (Ss and Sw indicate respectively strong and weak sites, CE indicates cation exchange) (Wittebroodt et al, 2024a).

3.1.2 Fe in cementitious materials

A review of Fe-containing cement hydrates can be found in De Windt et al. (2020) and Wieland et al. (2023). The stability of these phases depends on the composition of the system, including pH, concentrations of Al, Si, Fe, C, and S, as well as temperature. In the presence of silica, which is typical

in cement systems, (Al, Fe)Si-hydrogarnet is the most thermodynamically stable hydrate, forming at ambient to elevated temperatures (~110 °C) (Dilnesa et al., 2014a; Dilnesa et al., 2014b; Pally et al., 2020; Wieland et al., 2023). Stabilizing hydrogarnet requires a pH of around 12 or higher, while at low pH values, magnetite and iron oxy/hydroxides (e.g., ferrihydrite, lepidocrocite, goethite) become more stable (Wieland et al., 2023). The stability of (Al, Fe)Si-hydrogarnet increases with temperature but decreases with pH. Outside the stability conditions of (Al, Fe)Si-hydrogarnet, magnetite, oxy/hydroxides, and iron-bearing phyllosilicates may also form, depending on the concentrations of Fe, Si, Al, and the redox conditions,. These conditions are typical for low pH cement or in late stages of cement degradation.

(Al,Fe)Si-hydrogarnet phases are represented by an ideal solid-solution model in thermodynamic model (C3AS0.84H4.32 and C3FS0.84H4.32). Thermodynamic properties, in particular their temperature dependency in the range of 0-100 °C, are reassessed for different end members using the additive method or volume-based thermodynamics (Wittebroodt et al., 2023). In addition, calculations have been done for Fe-hemicarbonate, Fe-monocarbonate, Fe-monosulfate and Fe Friedel's salt to be consistent with those of (Al,Fe)Si-hydrogarnet. The updated thermodynamic data gave results in qualitative agreement with the experimental observations and with the iron silicious hydrogarnet being the dominant phase at elevated pH both in reduced and oxidized conditions. An example of the Pourbaix diagram at 80 °C with the revised thermodynamic data is shown in Figure 3-2.

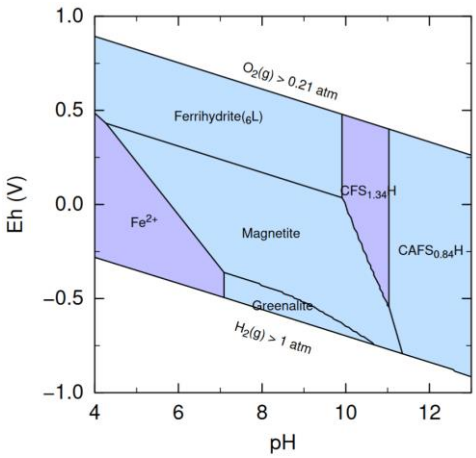

Figure 3-2 - Pourbaix diagram at 80 °C calculated using hydrogarnet properties as reported in (Wittebroodt et al., 2024b).

Calcium silicate hydrates, the main solid phase in hardened CEM I paste, also take up Fe(II) and Fe(III). The thermodynamic model CASH+ (Miron et al., 2022a; Miron et al., 2022b) was extended for the uptake of Fe(II) and Fe(III) (De Windt et al., 2020). The experimental data showed that Fe(III) uptake in C-S-H is not affected by the Ca/Si ratio (0.8, 1.2 and 1.5) with an average K_d Fe(III) of 700'000 ± 1.5E05 L/kg which is higher than that of Al. Fe(II) showed a roughly 3 orders of magnitude smaller uptake, K_d Fe(II) 100 ± 20 L/kg, similar to other bivalent cations. However, as in the case of Al that is incorporated in C-S-H but with time stabilizes in the more favourable hydrogarnet phase, also Fe will stabilize in hydrogarnet. Evidence in literature and modelling with the CASH+ model (Wittebroodt et al., 2023) suggest that (Al, Fe)Si-hydrogarnet is the main Fe bearing phase and that in its presence the uptake of Fe in C-S-H is insignificant. Thus, in real systems, over some periods of time, iron may be incorporated into C-S-H initially but with time the amount of Fe in C-S-H will decrease, forming other phases such as (Al,Fe)Si-hydrogarnet. Due to kinetic constraints and metastability, the formation of (Al,Fe)Si-hydrogarnet may not be observed in experiments.

To increase the usability of the CASH+ model in codes that do not have the implementation of multisite solid solution formulations, it can be represented by a set of discrete solid phases. Therefore, a script to produce discrete C-S-H phases with associated log K of reaction and its temperature dependence was

developed; the user can decide - based on the compositional space – on the degree of discretization that is relevant to the system that needs to be modelled. The script is available at the following link to be downloaded and used https://github.com/thermohub/thermofun-jupyter/tree/master/applications and it can be directly used in the browser here:

https://mybinder.org/v2/gh/thermohub/thermofun-jupyter/master?urlpath=lab/tree/applications/ (using the ChemicalFun and ThermoFun libraries (Miron et al., 2023)).

3.2 Modelling the corrosion of steel in contact with different materials

This section discusses conceptual and mathematical models describing the geochemical evolution at interfaces where steel is present. A first section describes how corrosion of steel could be conceptualized in a pragmatic way in coupled reactive transport models. Further, model concepts, implementations and results are discussed for interfaces with either clay or cement in absence or presence of glass. The model describes several experimental set-ups and conditions with data ranging from a few months to several years.

3.2.1 Treatment of steel in reactive transport models

During the corrosion of steel in the repository environment, an initial aerobic corrosion phase is followed by an anaerobic corrosion phase. Iron corrosion during the aerobic phase is written as:

$$Fe^0 + 0.5O_2(aq) + 2H^+ \rightarrow Fe^{2+} + H_2O \quad (1)$$

Whereas for the anaerobic phase, it is:

$$Fe^0 + H_2O \rightarrow Fe^{2+} + 2OH^- + H_2 \quad (2)$$

In the aerobic corrosion phase, the ferrous iron (Fe(II)) is rapidly oxidized to ferric iron (Fe(III)) and precipitates as a corrosion product (e.g. goethite). The ferrous iron formed in the anaerobic corrosion phase may precipitate as a corrosion product (including potentially Fe-rich silicate minerals as cronstedite or greenalite) or migrate into e.g. the bentonite and react with montmorillonite (e.g. by sorption, surface precipitation, or by formation of Fe-bearing clay minerals).

The rate of the corrosion during the aerobic phase can be described with a constant rate constant and a first-order kinetic rate with respect to oxygen.

For the anaerobic phase, the most simplified rate equation used for steel corrosion is a zero-order rate equation with a constant rate parameter. Based on measurements, a constant rate (mol/m^2/s) is assumed that is related to the steel corrosion rate r_c (µm/year) via:

$$k = \frac{r_c \rho}{M_{Fe} t_{conv}} \quad (3)$$

where r_c is the steel corrosion rate (µm/year), ρ is the steel density (g/cm^3), M_{Fe} is the molecular weight of Fe (55.85 g/mol) and t_{conv} is a constant to convert from year to second (86400*365).

When used in reactive transport models, different approaches are possible:

- Flux boundary model – the steel is not explicitly present in the transport domain, but implicitly at a boundary with a kinetic Fe-flux towards the domain. Based on the solution chemistry of the contacting node (of the backfill material in contact with the steel), the steel corrosion rate is calculated and the calculated amount of Fe is added to the solution (and, if relevant, reactants are removed). The formation of corrosion products can thus only occur in the backfill material, diffusion is not possible from backfill into the steel as in the other two approach in which (part of) the steel is represented as a porous medium;

- Porous medium representation – the steel is represented as a porous medium with a (low initial) porosity. Corrosion occurs throughout the complete steel cross-section releasing Fe in the aqueous phase in the steel and subsequent diffusion towards the surrounding materials.
- Layer-by-layer corrosion (Figure 3-3) – the cross-section of the steel is divided into a number of small layers. Corrosion only occurs in the outermost layer (the superficial layer); corrosion in deeper layers cannot start if iron remains in the superficial layer. Thus, the steel is represented as a porous medium only in the superficial layer; deeper layers are not porous and are impermeable.

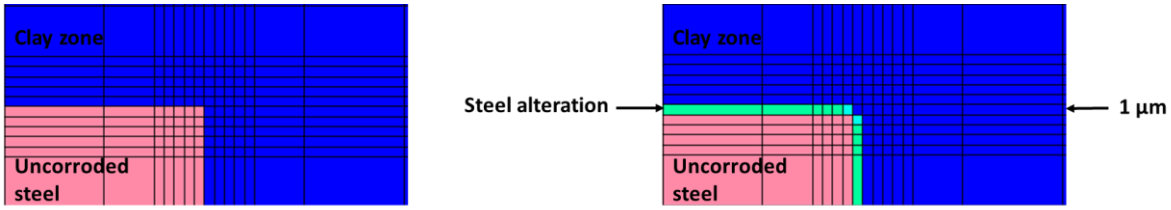

Figure 3-3 – Representation of the layer-by-layer approach (after Lemmens et al. (2024)) in which only the outer (superficial) layer of steel is a porous medium and can corrode.

3.2.2 Modelling Steel-Clay interfaces

Significant progress has been made by modelling steel-bentonite interfaces, specifically with FEBEX bentonite (see section 2.2.3). The overall goal of this model development is to improve and evaluate the modelling approaches of complex coupled Fe corrosion and Fe-clay interaction processes with coupled reactive transport codes. Advancements have been made with respect to:

- Initial unsaturated conditions in the bentonite with resaturation (under a temperature gradient) and swelling taken into account
- Initial aerobic conditions in bentonite with subsequent transition to anaerobic conditions
- Modelling the Fe fate in the steel-bentonite system including:
  - Precipitation in the steel corrosion zone
  - Sorption by cation exchange and surface complexation
  - Electron transfer from Fe(II) to structural Fe(III) in bentonite

Oxygen available near the bentonite-steel interface at the start or diffused towards the bentonite-steel interface at later times resulted in a zone with goethite precipitation close to the bentonite-steel interface. A high diffusive flux of ferrous iron (Fe(II)) into the bentonite is maintained due to goethite precipitation. When goethite precipitation becomes limited by the oxygen flux towards the ferrous iron front, ferrous iron starts to sorb on bentonite. Because of the counter-diffusion of Fe and oxygen (respectively from steel to bentonite and from bentonite to steel), at a given distance, oxygen concentrations are too low to result in goethite precipitation. The model accounting for this transient stage from aerobic to anaerobic corrosion resulted in a concave shape of the Fe accumulation front (Figure 3-4). Experimental studies of Hadi et al. (2019) also showed this characteristic profile shape with a high accumulation of Fe at the interface dominated by goethite, whereas sorbed Fe dominates further in the bentonite (characteristic coloured halo formation observed in the FEBEX in-situ experiment, top photo in Figure 3-4). The width of the goethite precipitation zone is extending with a higher degree of water saturation at the time when the O_2 influx stops, a lower diffusion coefficient in the gas phase, or a higher diffusion coefficient in the aqueous phase. These processes correspond also with a smaller Fe sorption front. When the retention capacity in the clay is increased (e.g., assuming increased accessibility of sorption sites or including an additional retention process by electron transfer to structural Fe(III)), the goethite precipitation zone steepens and shortens, but also the Fe-sorption zone shortens, although the fraction of Fe diffusing from the corrosion layer to the bentonite increases. Also, higher temperatures reduce the extent of the Fe-bentonite interaction zone.

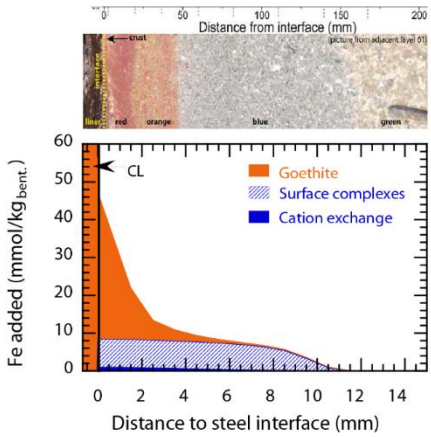

Figure 3-4 - Final profile of Fe accumulation in the bentonite as calculated for a base case model taking into account the transient aerobic-anaerobic phase (section 4.2 in (Wittebroodt, 2024)). Top photograph with scale from (Hadi et al., 2019) showing the visual colour zonation in the sample with extreme Fe-bentonite interaction.

In the models for experiments with Fe powder in contact with bentonite (FB and FeMo tests, see section 2.1 in Wittebroodt et al. (2024a) and section 2.2.3), magnetite precipitation was predicted mainly in the Fe powder zone with a limited amount precipitating also in the first millimeters of the bentonite. The latter was not observed in the experiments except some precipitation at the interface itself. The model did not predict any other corrosion product in case of the FB test, but predicted siderite, greenalite and saponite-Mg precipitates at the Fe powder/ bentonite interface in the model for the FeMo experiment.

The models for FEBEX bentonite – steel interactions described in general the experimental data well; however, uncertainties still remain related to e.g. time varying corrosion rates depending on pH and saturation index, kinetic processes related to corrosion product formation and/or dissolution of primary minerals in the bentontite, and changes in porosity and permeability. The use of Fe-powder adds also uncertainty related to migration through the Fe-powder layer with some particles being more exposed to the oxidizing agent than others.

3.2.3 Modelling Steel-Cement interfaces

<u>High temperature modelling at 80 °C</u>

The evolution of cementitious materials interacting both with free water (in reservoirs in the experimental set up) and steel at a high temperature was modelled for 3 types of materials (Wittebroodt et al., 2023):

- **CEM-I material** – Thermodynamic models indicates that the stability domain of stable Fe-Al-siliceous hydrogarnets (CAFSH) significantly enlarges in the cement pH range while temperature increases from 20°C to 80°C. Beside temperature, a second critical factor is the availability of Si; without sufficiently high amounts of dissolved silicium, magnetite rather than hydrogarnet will be formed. A higher temperature also promotes the dissolution of cement hydrates such as ettringite. The experimental formation of CAFSH and water chemistry are correctly reproduced by RTM taking into account the specific geometry in the experiments with part of the steel only in contact with water and another part with hardened CEM I paste. In particular, gaps filled by water at the steel/cement interface increase the diffusive flux of Ca, Al and Si from both the solution cell and the cement matrix.
- **CEM II/B-S based material** - Modelling was done for the concrete representative within the Hungarian disposal program; the cement component consisting of 73.5% CEM I clinker and 24.5% blast furnace slag (Fabian et al., 2023; Wittebroodt et al., 2023). After hydration (50% of slag) at 80 °C, the typical cement hydrates are formed (portlandite, C-A-S-H, monocarboaluminate, hydrotalcite) but ettringite is transformed into monosulfoaluminate. RTM

that takes into account the specific geometry in the experiments could reproduce fairly well the pore water geochemistry evolution of one year experimental period which brings some confidence in the modelling.

- **CEM III/A based material** with silica fume and mixed with bentonite (Bentonic grout cement (BGC)) – Modelling of the hydration of BGC at 80 °C was a first of a kind. In this system, portlandite is not formed, a low Ca/Si C-S-H form is present and either a crystalline or amorphous C-A-S-H phase (depending on which of the two is included in the model). However, some important processes were not considered yet: (i) hydration of silica fume and its evolution which may influence the stability of the C-A-S-H phases, and (ii) neglecting carbonate in the material present due to the fast carbonation of slag-rich cement which may decalcify the C-A-S-H phases. Note also that upon hydration, the cation occupancy changes and may alter the Na-montmorillonite partly into a Ca/Mg-montmorillonite (Bonnet et al., 2022). Modelling of interaction of BGC with pore water at 80 °C (no steel corrosion products) showed in general a good agreement with experimental data although some systematic overpredictions (Na, K, S) of concentrations was observed; Mg and Al concentrations were predicted to be fairly low; Si concentrations were less well captured. A reaction path model was developed to simulate the alterations when $Fe(OH)_2$ reacts with BCG (Goethals et al., 2023). In a first stage, available pyrite is transformed into mackinawite and cronstedtite (an experimentally observed Fe-silicate[2] (Goethals et al., 2023) formed in the presence of metallic iron at neutral or alkaline pH and a temperature between 50 and 120 °C (Lanson et al., 2012)); in the second stage, the unhydrated silica fume particles dissolved to from cronstedtite; magnetite precipitates in the thirds stage when the silica source is exhausted. This model indicates that cronstedtite can form at the expense of magnetite in the presence of additional silica sources, provided a $Fe(OH)_2$ source is supplied by steel corrosion. This is in agreement with the observed corrosion product sequence in the layer with corrosion products and it suggests that the magnetite layer would not be totally destabilized by Fe-silicates from the drop in the corrosion rate (Wittebroodt et al., 2023b).

3.2.4 Modelling Glass-Steel-Cement/Clay systems

3.2.4.1 Glass dissolution models

Models used for dissolution kinetics of glass depend on the prevailing geochemical conditions:

- More neutral pH conditions – the GRAAL model (Frugier et al., 2018) is used which has been implemented in geochemical models as PHREEQC (Debure et al., 2019).
- Alkaline conditions – two different models are used:
  - A diffusion driven glass dissolution model assuming isovolumetric dissolution/reprecipitation: Congruent dissolution of glass constituents followed by precipitation of some elements in a glass alteration layer with an increase of the glass alteration layer thickness proportional to the square root of time (Liu et al., 2019); no stabilization occurs due to the very high SiO_2 solubility at high pH. All kinetic and affinity processes are captured by an apparent diffusion coefficient in the glass phase.
  - the GRAAL model: concentrations of glass constituents in solution determine the glass dissolution rate via the formation of a passivating SiAl gel. In this model, the glass dissolution kinetics depend directly on the selection of secondary phases. Note however that pH conditions were out of the validity domain of GRAAL (i.e. pH > 11)

For the disposal cell scale, an affinity driven glass dissolution model was used with a simplified selection of secondary phases and with parameter values for the pH range 7 – 10, even for the cement systems. Indeed, in this complete system, glass dissolution only starts when the steel is breached; at that time, the pH of the cement has already been decreased to values smaller than 10.

[2] Goethals et al.(2023) identified greenalite and/or cronstedtite

As for the steel (section 3.2.1), the glass matrix can be represented as a porous medium or glass dissolution can be simulated by a layer-by-layer approach (Lemmens et al., 2024).

3.2.4.2 Interaction Glass-Steel-Clay and Glass-Steel-Cement

Modelling Glass – Steel – Callovo-Oxfordian claystone

Experiments of glass-steel-COx interaction (at 70°C, section 2.2.1) were modelled with mixed kinetic-equilibrium models to describe the different processes: (i) kinetic dissolution of glass (GRAAL) with equilibrium precipitation of end members in glass, (ii) kinetic corrosion of steel with a constant corrosion rate, kinetic precipitation of magnetite in iron (and equilibrium in other materials) and equilibrium of some other secondary phases, and (iii) mixed equilibrium and kinetic dissolution of primary minerals and equilibrium of selected secondary minerals (Lemmens et al., 2024). Depending on the experimental geometry of the set-up, steel and glass were represented by a layer-by-layer approach (glass monolith, steel coupon) or porous media (glass powder and perforated steel). The selection of the secondary phases is a critical process but resulted in a model that captured the main mechanisms (pH increase due to steel corrosion, and Si consumption due to the formation of Fe-bearing silicates) that drive the glass alteration. Regarding the glass-steel interface, this modelling approach led to a glass alteration layer thickness in the same range as in the experiments within the uncertainty bounds. The spatial aspect of larger glass alteration layers closer to the glass-steel interface is captured by the model. Moreover, the formation of a passivating gel was in competition with the precipitation of cronstedtite, leading to an increase of glass alteration with the increase in corrosion rate. Fe-Si bearing minerals (cronstedtite, but also saponite) were also modelled in the COx where Si came from (limited) clay alteration (e.g. montmorillonite dissolution), but in a smaller amount compared to the glass side. In addition, some Fe-Si bearing minerals were only found at the COx side (berthierine).

Modelling Glass – Steel – Cement

Experiments of glass-steel-cement systems were modelled with the glass dissolution model for high pH conditions, a kinetic hydration model for cement clinkers, an equilibrium model for cement hydrates and sorption of Na, K, Li and B on cement hydrates. The steel was treated as an inert material due to passivation at high pH. Modelling results are available for SON68 and SM539. In contrast to the approach for glass-steel-COx, the model here was not conceived to describe the difference in alteration of the glass particles depending on their location. The glass dissolution model here is used rather as a high-level source term model that describes the total release of glass components to the cement component. The pH did not change significantly during the experiment which was also reproduced by the model. The reactive transport model with the diffusion-controlled glass dissolution model can well reproduce the B solution concentration in the glass compartment, and the LA-ICP-MS and mineralogical profiles in the cement, including sorption of alkali cations on newly formed C-S-H with low Ca/Si ratio. The model required diffusion coefficients for boron in the altered young cement paste that are 100 to 1000 times smaller than the values usually assumed for cement. It is not clear if the low D_e values are due to the boron and silicon speciation, or to a lower diffusivity of the altered cement paste. The penetration depths in the cement for different elements from the glass are different, indicative of complex interactions between elements from the glass and cement, for example, the diffusion length for B in the cement is about 2 mm whereas the diffusion length for Si is less than 0.5 mm. The formation of a porous layer depleted in portlandite is well reproduced, but the exact porosity (gel versus open porosity) is not clear.

Overall conclusion

The two models could reproduce the main observations from the experiments using mixed equilibrium-kinetic models. However, some model assumptions or parameters were adapted based on the available data such as choice of secondary minerals or diffusion coefficients in different materials. However, it is fair to state that, given the complexity of these systems with a multitude of simultaneous processes, the developed and evaluated models provide a valid basis for extrapolation to more generic systems or

longer time frames for assessing the geochemical evolution at larger scales such as the waste package scale (see section 3.3.1).

3.3 Modelling the evolution at waste package scale

When the geochemical evolution of the waste form and container/package is not influenced significantly by the geochemistry of the host rock and the focus is on interfaces in the waste package, so-called waste package scale models can be used to assess the geochemical evolution. For HLW waste packages (section 3.3.1), a somewhat different definition applies because during Periods I and II there is no contact between the glass and the buffer material as the steel canister is intact. Therefore, the focus is on Period III with materials already influenced by the host rock (specifically, a low pH in the concrete is required for increased corrosion rates). For ILW (section 3.3.2), two types of waste are considered: organic waste and steel waste.

3.3.1 HLW waste packages

HLW glass/steel/Cox

The model for the waste package scale considers a fully saturated system at 70 °C consisting of SON68 glass, a 5 cm thick steel overpack represented as a porous medium, and 75 cm thick COx material. The upscaling from the interface scale (section 3.2.4.2) was done only by an increase of the grid size from 1 µm to 5 mm. In essence, the same type of corrosion and reaction products were obtained, i.e. cronstedtite in the glass, magnetite and chukavonite (the latter at the steel/COx interface) as main corrosion products in the steel, and siderite, saponite and berthierine in the COx after 1000 years. After 10,000 years, cronstedtite also appeared at the COx side which might be also a consequence of treating steel as a porous medium – note that cronstedtite was not observed in the models of the interface experiments.

HLW glass/steel/cement/clay system

The model for the waste package scale considers a fully saturated system at 25 °C consisting of ISG glass, a 5 cm thick steel overpack represented as porous medium, and a 5 or 100 cm thick cementitious layer (CEM I material; young with pH 13.5 or evolved with pH 10.5) and the COx host rock matrix. Because of a significant different pH at the glass and cement side of the steel, different corrosion rates were used with a lower rate at the cement interface. Following mineralogical changes are obtained:

- At the cement-clay interface – formation of calcite, and a decalcification of the cement phases;
- At the cement-steel interface – precipitation of magnetite as a corrosion product, also in the cementitious material due to the high pH. Also chukanovite is formed as a corrosion product in the steel, and saponite in the cement
- At the steel-glass interface – beside the above mentioned corrosion products in the steel, cronstedtite is formed in the glass.

The qualitative profiles of minerals are relatively insensitive to the conditions (buffer of 5 or 100 cm, young or evolved concrete), but the amounts of phases and thus rates of both glass and steel alteration depend strongly on the prevailing geochemical conditions. Figure 3-5 shows the calculated alteration rates of ISG and steel as a function of time for different geochemical conditions. A large buffer of cement (top in Figure 3-5) keeps the steel corrosion rates low for a long time, but glass dissolution rates increase due to the high pH (predicted rates are higher than observed experimentally although conditions in the small scale experiments and the large scale model were not exactly the same (Lemmens et al., 2024)). With a smaller cement buffer (middle in Figure 3-5), the glass dissolute rate decreased fast because the cement buffer evolved fast to evolved cement with a lower pH. Consequently, steel corrosion rates increase. With an aged concrete (bottom in Figure 3-5), the glass dissolution rate is low from the start

of the simulation; steel corrosion rates are higher. However, keep in mind that contact with young concrete water is not expected unless in a scenario with (very) early canister failure.

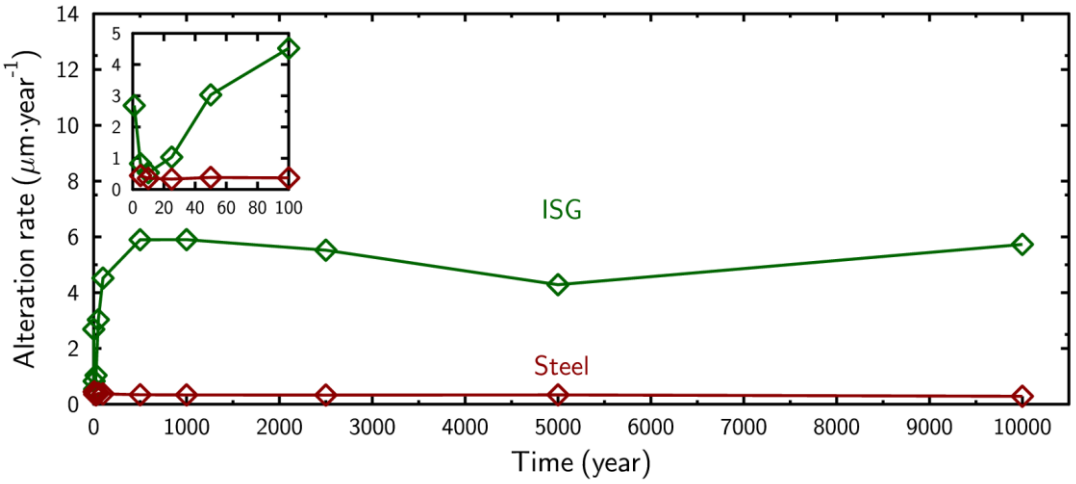

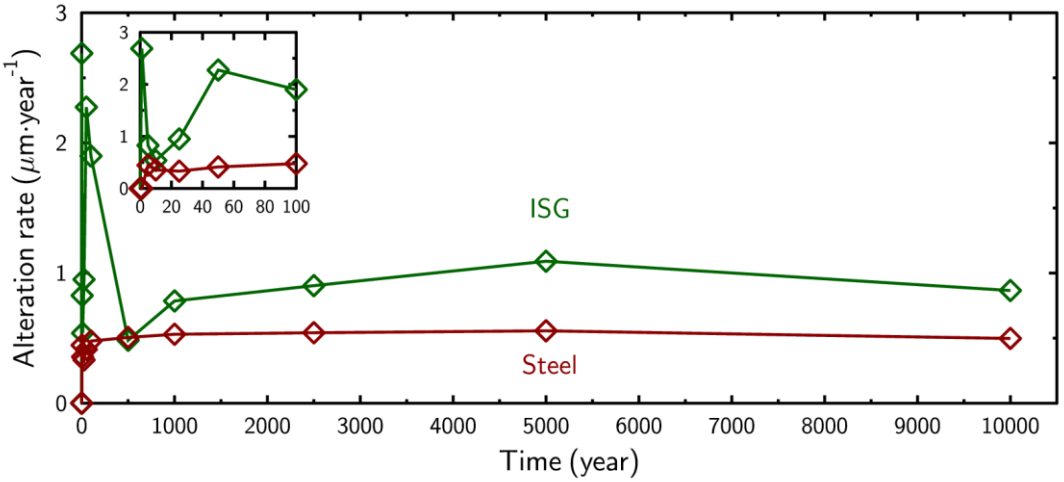

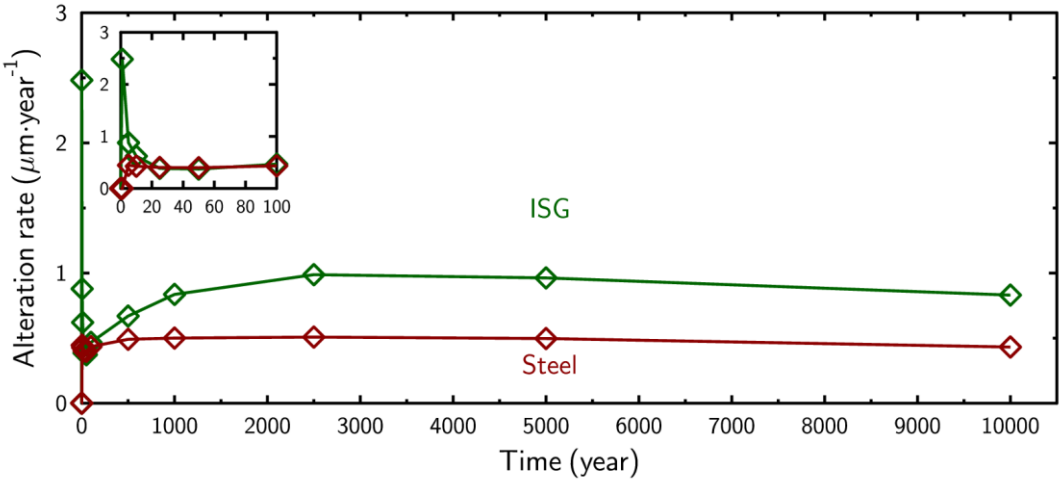

Figure 3-5 - Alteration rates calculated at the waste package scale: (Top) steel interface with a young concrete for a cement buffer of 100 cm thickness at 25 °C, (Middle) steel interface with a young concrete for a cement buffer of 5 cm thickness at 25 °C, (Bottom) steel interface, calculated with the BRGM model for an aged concrete at the waste package scale at 25 °C.

Conclusion

The modelling work has contributed to a better understanding of the coupled dissolution, corrosion and transport processes expected in a HLW disposal system. Upscaling from experimental spatial and time scales to waste package spatial and time scales is straightforward and mostly required only a coarser grid discretization. In systems with clay, the glass dissolution is triggered by the formation of iron silicates. The nature of the iron phyllosilicates affects the glass dissolution kinetics in the modelling as long as the iron is corroding – however, the modelled cases do not allow to evaluate how important the selection of iron corrosion products (magnetite, siderite, chukanovite, …) and iron silicates (greenalite, berthierine, cronstedite, …) is for the long-term glass dissolution kinetics. The experiments (see section 2.2.1) and modelling show that perforation of the overpack is delayed by using a high pH buffer (using cementitious materials) that decreases the overpack corrosion rate or by increasing the thickness of the overpack. Using a thicker cement buffer provides a longer protection, but once the overpack is perforated, the formation of iron-silicate phases is expected to trigger the glass dissolution. There is thus a trade-off between the short term advantage and long-term disadvantage of using a thicker overpack. However, some important questions remain to be solved: (i) identification of (under relevant disposal conditions) and/or thermodynamic data for secondary phases during the alteration of the glass, steel, clay or cement experiments (Fe-silicates), (ii) the glass dissolution behaviour and models in the pH range 10 – 12.5 requires further investigation and validation, (iii) although the set of experiments that were used in this report were very valuable for system understanding and model development and validation, a further parametric study is needed to validate reactive transport models under relevant conditions with relevant materials, (iv) further studies on the low diffusion coefficients of B (and possible Si) in glass-cement systems, and (v) studies on some aspects related to long time aspects (e.g. experiments of several decades) with further evolution of alteration products, evolution of fractures in the glass, evolution of rates depending on geochemical conditions (vi) mechanical coupling with the chemical evolution, as long as the concrete has a high strength, the carbon steel overpack cannot be fractured.

3.3.2 ILW waste packages

(LLW/)ILW waste forms originate from many sources and are therefore less well uniform in terms of physical, chemical and radiological characteristics. The focus in this state-of-the-art report is on two generic waste forms, one for activated steel and one for organic wastes because they are present in large quantities. These two types of waste also influence the long-term geochemical evolution of surrounding materials when they are degrading, specifically when immobilized or conditioned in cementitious materials as considered in the ACED project.

Organic waste

Organic wastes themselves are also extremely diverse but can be subdivided into (Wieland et al., 2020):

- slowly decomposable organic materials (high molecular weight (HMW) organic materials (bitumen, polystyrene (ion exchange resins), plastics, and rubber), and
- rapidly decomposable organic materials (cellulose, low molecular weight organics and cement additives).

The decomposition of organic materials in the waste may take place both through abiotic (both radiolysis and hydrolysis) and biotic processes (Uras et al., 2021). Radiolytic degradation of plastic polymers (Altmaier et al., 2021) produces gases as H_2, CO_2, CO, and CH_4; halogenated polymers also produce HCl or HF. H_2 would be produced in all scenarios while CO and CO_2 require oxidizing conditions. Cellulose degradation under highly alkaline conditions (pH > 11) is controlled by abiotic hydrolysis processes producing mainly isosaccharinic acid and minor quantities of other organic acids. Biotic

degradation leads also to the production of CO_2 – however, bacterial growth could also be hindered by ionizing radiation (Brown et al., 2014). A major consequence of CO_2 release due to organic matter degradation is the potential for carbonation of the surrounding materials.

Metal waste

Anoxic corrosion of steel (expected conditions after repository backfilling and closure) results, via the Schikorr reaction, in formation of magnetite and hydrogen gas evolution. If bicarbonate ions are present in solution, they can also lead towards formation of more stable carbonate phases such as iron carbonate (siderite, $FeCO_3$), or iron(II) hydroxycarbonate ($Fe_2(OH)_2(CO_3)$. However, many other iron oxide phases can be present in corrosion product films and oxide rusts (Furcas et al., 2022; Wieland et al., 2023).

Cement degradation state

ILW waste forms and packages contain typically large amounts of cementitious materials that will geochemically evolve, due to pore water and pore solutes exchange with the surroundings, reactions of the concrete constituents themselves, and alterations induces by degradation or corrosion products from the waste – see sections 2.2.4 and 2.3. The most crucial factor is a decrease in pH resulting from processes such as carbonation, leaching or alkali-aggregate reactions. This pH change influences the rate of degradation of both waste types:

- **Organic material –** Under extremely high pH solutions or high porous mortars, biotic degradation might be slow, whereas it is faster under more neutral conditions since the concentration of H^+ is at neutral pH sufficiently high to keep a neutral cellular life.
- **Steel corrosion** – Corrosion rates are pH dependent and will be very low for pore water pH >12 and 50-100 times higher at pH < 10.5.

Water availability

A crucial factor for the degradation/corrosion of these two waste types is the presence of water – both processes consumes water. Furthermore, water availability influences the geochemical reactivity (Blanc et al., 2024). According to Warthmann et al. (2013) the availability of water in the cementitious near field and specifically in waste packages is a limiting factor for microbial activity – one aspect for unsaturated porous media discussed by Tecon and Or (2017) is that water films might be too thin to support microbial activity. To account for reduced rates at lower water content or relative humidity (RH), rate equations include a term to scale the chemical reactivity with water content or RH of the gas phase (e.g., Trotignon et al. (2011)).

Therefore, the evolution of the surrounding near field in terms of water saturation is one of the most influencing external processes that drives organic material degradation and metal corrosion. After storage under dry conditions and venting during operational phase, cementitious materials of waste packages might be unsaturated. Water consumption by waste degradation or corrosion processes will further dry the waste zone. Water will move first from the cementitious materials into the waste packages, and later from the other cementitious materials in the near field and the surrounding host rock. The process is further complicated by the gas production and the potential expulsion of water by gas and by water production due to carbonation of cementitious materials. The amount of water moving from the host rock into the engineered barriers strongly depends on the type of rock: granitic rock types are assumed to provide sufficient transport pathways for water and gas, whereas a low permeable clay host rock may limit water inflow and gas efflux reaching full water saturation conditions only after very long times (see section 2.1),

3.3.2.1 Modelling water consumption, gas generation and transport

Degradation of organic waste

ILW organic wastes (PVC, cellulose) undergo degradation due to i) the radioactive elements included in the packages (radiolysis) and ii) the highly alkaline characteristics of pore waters packages generated

by the cement materials in the vicinity of organics in waste packages (hydrolysis). Organic waste degradation models were developed that include both aspects based on existing literature data and data collected in the WP CORI (EURAD, e.g., Ben Zeineb et al. (2021)).

- **PVC degradation modelling** includes the production of gaseous species HCl(g) and H_2(g) and the production of aqueous species (acetate, formate, oxalate and phthalates). For pure PVC, HCl(g) release strongly decreases the pH of the solution; for industrial PVC, the pH drop is buffered first by the dissolution of calcium carbonate filler with a release of Ca in solution.
- **Cellulose degradation modelling** considers only isosaccharinic acid (ISA) with the parameterisation of Glaus and Van Loon (2008). The model was able to reproduce correctly both the cellulose degradation rate and the modification in the solution (pH, Ca^{2+}).

It can be stated that gas generation due to radiolysis needs very high doses in order to become significant, and that, compared to metal corrosion and (a)biotic degradation of organic matter, gas generation is small.

Gas generation due to organic waste degradation

The model was developed based on the long-term investigation of gas generation and associated chemical changes in 200-liter carbon steel drums filled with organic waste materials under repository conditions from the in situ Gas Generation Experiment established in Olkiluoto, Finland since 1997 (details given in Mladenovic (2024); Mladenovic et al. (2019)). The biogeochemical model of Small et al. (2017) was used to calculate gas generation up to 2021 (~25 years) and showed that gas generation rates increase over time due to metal corrosion and organic matter degradation. CH_4 and CO_2 are the main generated gases, showing increasing gas generation rates ranging from 0.0301 to 0.1098 mol/kg/y and from 0.0003 to 0.0114 mol/kg/y, respectively. Combination of gas generation rates with a cement carbonation model indicates that the thickness of the carbonated layer of the cement is between 17 mm and 27 mm with a carbonation front velocity of about 0.07 mm/y; a significant amount of uncarbonated cement is still present. In addition, mass balance calculations are made to estimate the amount of calcium leached form the concrete and the resulting porosity change in the concrete. Total solid volume is reduced with about 10%. Note that also potassium and sodium have been leached from the concrete.

Transport of water and reactive gasses in partially saturated concrete

Unsaturated conditions of cementitious materials occur under different conditions: (i), during storage, (ii) during the operational phase when there is ventilation, and (iii) during part of the period after closure depending on the specific properties of the host rock, the cementitious materials and the waste. A key point for ILW waste packages is thus the transport of water through unsaturated cementitious materials. Experimental results of concrete samples with blended cement exposed to a range in relative humidity from 6% till 100% for about 1000 days at two temperatures (Mladenovic, 2024) is used to validate a model for water and reactive gas transport through concrete. The water flow is simulated with the diffusivity form of Richards' equation with a permeability model according to Millington and Quirk (1961). Such model formulations allowed to simulate the desaturation of cubic concrete samples under various conditions, although a correction factor (constant for all conditions) was required. The model was extended with diffusion of reactive gasses and a chemical reaction approach that links mineral dissolution rates to the size of spherical minerals grains and to pore sizes to model oxidation and carbonation fronts. It could be confirmed that the progress of carbonation fronts is slowed down if relative humidity is below a certain threshold value. This indicates that some chemical reactions are suppressed if relative humidity is lowered, although there should be still enough water available to drive the reaction. It can be speculated that water bound in relatively small nanometre sized pores, in cements these are typical "gel pores", is not available for reactions, or that those reactions do not happen in nano-meter sized pores.

3.3.2.2 Waste packages – Organic material

In an ILW waste package containing organic materials, different process will take place simultaneously. Figure 3-6 illustrates the waste drum geometry and materials that form the basis for the models developed in ACED together with the most relevant geochemical processes.

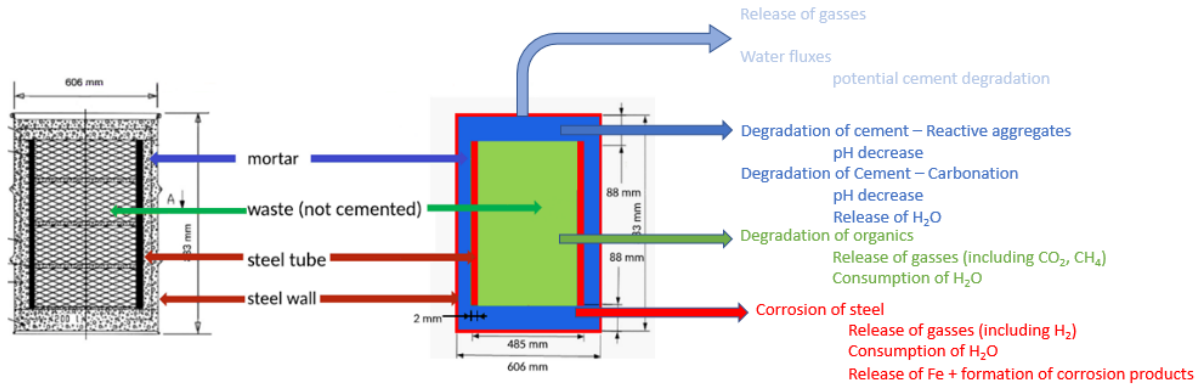

Figure 3-6 – 200-l waste drum geometry and materials (modified after Huang et al. (2021)) together with the most relevant geochemical processes

Three types of models were developed to assess the geochemical evolution at the waste package scale:

- **Mixing tank approach** – This approach accounts for the geochemical processes in the waste drums or package but neglects any spatial aspect or transport process (Kosakowski et al., 2020; Wieland et al., 2020; Wieland et al., 2018). It is a fast and simple method to assess mass balances and gives some indications on impact of material (e.g. carbonate vs. siliceous aggregates) and modelling choices (e.g. kinetic parameters). The approach includes both thermodynamic equilibrium reactions (cement carbonation processes) and time-dependent degradation processes (corrosion, organic material degradation, aggregate reactions). At each time step, the kinetic materials evolve and successively equilibrate all "reactive" materials of the waste package. An important aspect of this model approach is that the system is closed (no release of gases, no ingress of water).

  For this waste type, reactive materials for a 200-l waste drum (Figure 3-6) are taken as initial material with cementitious materials as unhydrated cement clinkers. After initial equilibration (cement hydration), still some free water is present but large parts of the porosity are not water-filled. As an illustration, the evolution of the phases for a waste package in which the aggregates are assumed to be reactive is shown in Figure 3-7. For this specific composition of the waste drum:

  - The temporal mineralogical evolution, available free water and amounts of gases are driven by the degradation of cellulose and the corrosion of steel.
  - Corrosion of steel and degradation of organic waste are completed in about, 300 and 3000 years, respectively, with sufficient water available via initial water in the system and production of water by carbonation. When the iron corrosion rate increases (under lower pH conditions), the net water balance is negative with larger water consumption than production; when all iron is corroded, water amounts increase due to further carbonation of the cement minerals.
  - There is a general pH decrease of the system by degradation of organic matter and cement carbonation. Consequently, the rate of iron corrosion increases but the rate of the aggregate reactivity decreases. Note that it was assumed here that the degradation of organic waste was pH independent.
  - Conditions are reducing, so steel/iron is transformed into magnetite.
  - It is to be expected that the balance of available water for the reaction is strongly dependent on the relative amounts of fast degrading organic waste (water production

by cement carbonation) and steel (water consumption). Reactivity of aggregates has only a minor effect.

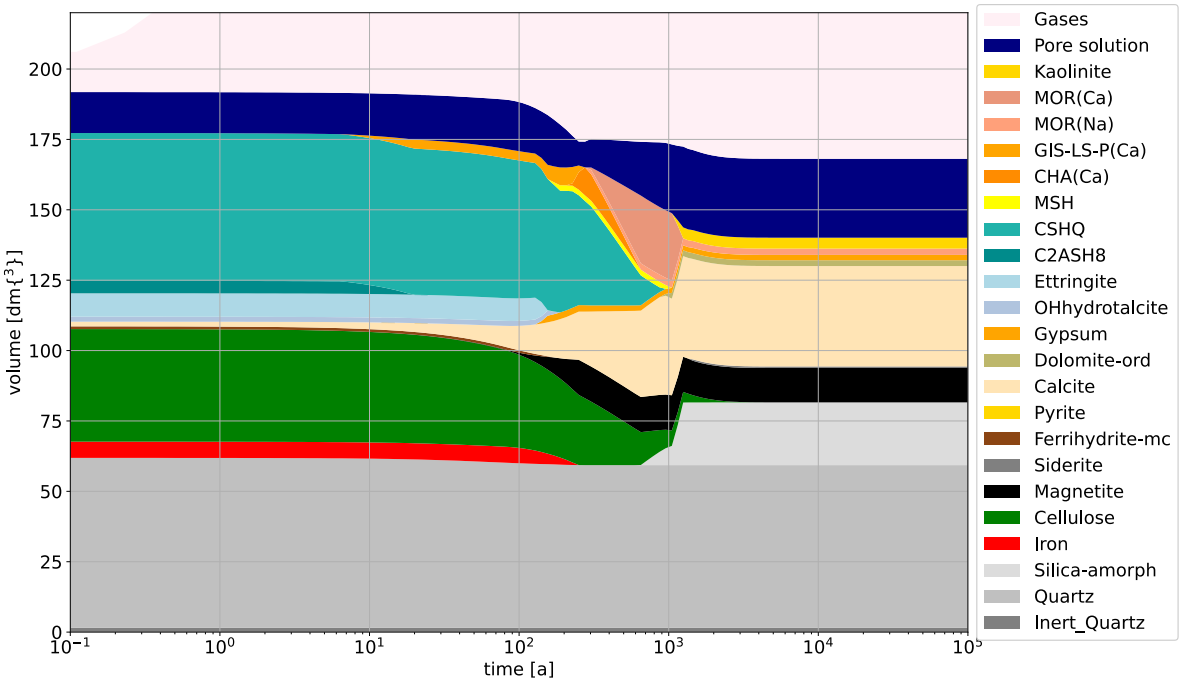

Figure 3-7 – Illustration of time evolution of phases in a 200-l organic waste drum calculated with the mixing tank approach (from Blanc et al. (2024))

- **Models focussed on water and gas flow** – The close interaction between water consumption, production and ingress, and gas production, pressure and flow at the waste package scale (multiple waste drums in a container) is simulated with a multiphase reactive transport model with look-up tables for geochemical processes (following the approach described in Huang et al. (2018) and Huang et al. (2021)). The model accounts for the precise geometry and material distribution of each waste drum and of the complete waste package. Four stages in the hydrological evolution of the multiple-drum container setup have been identified and characterized. In the first stage, an initial (gas) pressure build-up due to metal corrosion and drying of the waste compartment of the drum is observed. In the second stage the metal corrosion and associated gas production is controlled by water fluxes inside the drum towards metal surfaces. In the third stage the water potentials in the waste drums are so low, that water from outside is sucked into the drum. The fourth stage is characterized by an equilibrium between gas generation and water supply from outside the drum. The counter-flow of gas (leaving the drum) and liquid leads to an increase in gas saturation within the entire outer mortar area.
- **Coupled reactive transport models** – The last type of model links detailed geochemical calculations performed with a geochemical solver with transport calculations with a transport solver. Because the codes used here do not allow for multiphase calculations, the simplifying assumption of fully saturated conditions was taken. Two model geometries were implemented: (i) a 1D radial model containing waste, inner steel (represented as porous material) and infill mortar, and (ii) a 2D model of the exact geometry of a single drum with surroundings containing infill mortar (the steel parts are impermeable and nonreactive). A more complete organic matter degradation model was used in the 1D radial model accounting for hydrolysis and radiolysis of both PVC and cellulose. The pH in the waste zone decreased with high saturation indices for $CO_{2(g)}$ due to HCl(g) generation from PVC and $CO_{2(g)}$ generation from cellulose that is not buffered fully by cementitious materials. In the cementitious part, pH is buffered as long as portlandite and C-S-H with high a Ca/Si ratio are present. The 2D representation showed

strongly carbonated zones at the top and bottom of the drum with a small precipitated calcite shell. Midway from top and bottom, the infill mortar in the drum is still at a pH of 12 after a few hundreds of years of simulation. For the 1D model, the difference in pH between the waste/steel and the steel/infill mortar zones causes a faster steel corrosion at the former (lower pH) and the precipitation of siderite (presence of CO_2 from organic waste degradation) in addition to magnetite found at both sides.

3.3.2.1 Waste packages – steel waste

The waste package for metallic (steel) waste is a concrete container with 15 cm thick walls and an outer volume of close to 6 m^3 filled with carbon steel waste (~6.6 ton) and backfilled with infill mortar. For the waste package, it is not possible to have a precise geometry (of the inner part of the concrete) as for the organic waste. Following types of models were developed to assess the geochemical evolution at the waste package scale:

- **Mixing tank approach** – The same approach as described in section 3.3.2.2 was used for the waste package with steel waste – main reactions are steel corrosion and aggregate reactivity. Because both reactions consume water, the initial free water will be consumed in a few hundreds of years and all reactions stop if no water is added from outside. Steel corrosion resulted in magnetite precipitation and hydrogen production. The dissolution of reactive aggregate will cause the transformation of C-S-H with high Ca/Si ratio into C-S-H with lower Ca/Si ratio. When the free water amount is kept constant (mimicking a situation where water consumed by metal corrosion and aggregate-cement reactions is quickly replenished by influx of water into the waste package), complete steel corrosion is possible but, for the specific inventory in these calculations, more than ~ 3 m^3 of water is needed, most of it should thus come from outside the waste packages. Additionally, the more advanced aggregate-cement interaction will lower the pHwith replacement of cement phases by zeolites which will increase the rate of metal corrosion as well as resulting in two orders of magnitude faster complete steel corrosion compared to non-reactive aggregates.

  The evolution of waste packages, the consumption of external water and the release of gases from the waste package is highly dependent on waste inventory, the amount of cement present and the assumptions on kinetics of reactions. Mixing tank approaches allow relatively fast parametric studies on these aspects.

- **Models focussed on water and gas flow** – Because an exact geometrical representation of (bulk) steel waste and infill mortar is not possible, the inner part of the waste package is abstracted by a consumption rate of water induced by steel corrosion. A first model considers only the waste container wall with a Neumann boundary condition as the inner boundary representing a water flux leaving the concrete, simulating the consumption of water by anaerobic corrosion of ILW steel; the outer boundary has a Dirichlet boundary condition with a constant water content (i.e., the surrounding near field is able to provide sufficient water). This model approach allows to estimate (maximum) water consumption rates which will result in a steady-state saturation degree of the container wall (larger water consumption rates lead to a saturation degree of 0 or negative). In a second model, also the near field (cementitious materials and, in the specific calculation cases, indurated clay) is taken into account having still a flux boundary condition at the inner side of the waste containers. In this system, water transport through the host rock and cementitious near field towards the inner side of the waste containers is clearly the limiting factor for continuous steel corrosion inside the container.

3.4 Model upscaling, abstraction and sensitivity

The disposal cell scale models presented in section 2.4 are relatively computationally intensive and rather complex. Therefore, they might be difficult to interpret and to handle in sensitivity or uncertainty analyses. Model abstraction approaches strive to simply complex models without influencing too much

the key output variables. Section 3.4.1 presents the rationale of model abstraction and a systematic overview of approaches that could be apply with coupled reactive transport models. Some applications of these approaches are discussed for HLW and ILW disposal cells in the subsequent sections.

3.4.1 Model abstraction – rationale and approaches

Model abstraction (MA) is defined as the methodology for reducing the complexity or the computational burden of a simulation model while maintaining the validity of the simulation results with respect to the question that the simulation is being used to address (Frantz, 1995). Model abstraction reduces the simulated system to its essential components and processes through a simplification of conceptual (sub)models, selection of significant processes and appropriate time and spatial scales or more computationally efficient implementations (of specific model components and processes).

In the WP ACED, as discussed in this report, one of the main modelling tools are coupled reactive transport models which tend to become increasingly complex due to advancements in understanding and quantifying of (geo)chemical and transport-processes in the engineered barrier systems and surrounding geological layers – the result of a combination of the large number and intricacies of the simulated processes, differences in scales at which the interactions occur and amount of feedbacks to simulate and the long timescales (>10^4 years) and large spatial scales (up to several tens of m). Model abstraction can contribute (i) to cope with stochastic uncertainty and sensitivity analyses for which tens if not hundreds of simulations would have to be executed to perform a decent analysis, (ii) to obtain a more plain and uncomplicated form of a model, for instance to permit a more thorough analysis for a given analysis budget, and (iii) to allow for an increased model complexity for one or more processes by reducing the complexity in one or more other processes.

A distinction is made between two broad families under the large umbrella of model abstraction techniques: (1) lower-fidelity physically-based modelling and (2) response surface surrogates (or meta-modelling). The classification of MA techniques is based on a combination of the classifications proposed by Pachepsky et al. (2006) and Razavi et al. (2012).

The construction of **lower fidelity (reactive flow and transport) numerical models** with model abstraction can be done by one or more of the following strategies:

- using *pre-defined hierarchies of models* that contain a series of progressively simpler conceptual and corresponding mathematical representations of flow and (reactive) transport and geochemical reactions in porous media
- *delimiting the input domain* utilises the fact that some features, events, or processes may be not relevant for a given set of scenarios or for a given set of model outputs
- *scale change* provides transitions between different operational scales. Model abstraction with scale change alters model equations, variables and parameters with two classes of methods: upscaling and aggregation
- *reducing numerical accuracy* (e.g., larger time steps, coarser grids, less stringent convergence criteria) results in lower-fidelity models which are fundamentally the same as the original models

Response surface surrogates or Metamodeling seek to simulate the input-output relationships of the complex model with a statistical relationship without taking the underlying physics into account (i.e. black box models). Meta-models can be used to emulate the full reactive transport model, to replace the solver of the geochemical step in reactive transport codes and to replace computationally expensive process models. This approach potentially introduces errors in the model prediction because of the statistical models for the input-output relations; these errors cannot be solved by increasing numerical accuracy, but requires seeking of improving the statistical models. For the model describing the disposal cell scales, the most promising route here is to replace the geochemical solver in the coupled reactive transport model by a surrogate model – an approach that also is explored for more simplified geochemical systems in the DONUT work package in EURAD (e.g., Laloy and Jacques (2022), Prasianakis et al. (2024), Claret et al. (2024)).

Govaerts et al. (2022) presented a few recent examples of these abstractions related to the field of (reactive) transport for radioactive waste management, or other related fields.

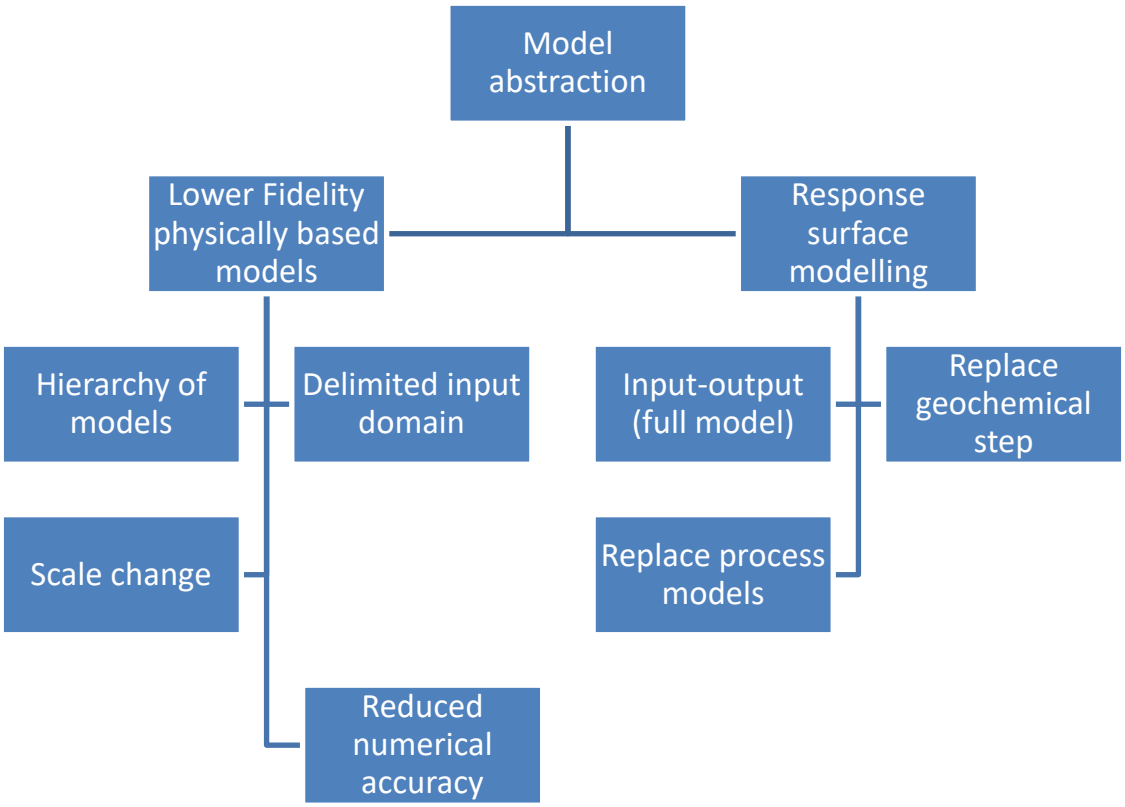

Figure 3-8: Model abstraction methods – classification (Govaerts et al., 2022)

Note that model abstraction approaches often started from the most complex case; in the analyses within ACED, the analyses were started from a fairly complex case based on available processes knowledge and expected numerical challenges. After numerical calculations and analysis, some processes could be added or made more complex.

3.4.2 HLW disposal cell scale

As base (reference) case for HLW disposal cell scale, the modelled evolution as discussed in section 2.4.1 was used. From a model abstraction point of view, the most relevant conclusions are:

- *Hierarchy of models*
  - The model complexity was increased by including porosity changes due to mineral dissolution/precipitation and consequences for transport parameters.
    - (disposal cell in granite) Including porosity update highlighted the potential of strong porosity decrease in the canister due to precipitation of corrosion products. In the used model set-up, this leads to porosity decrease up to a given threshold value with a sharp decrease in dissolution of the glass.
    - (disposal cell in clay) Fast clogging occurred due to precipitation of saponite, C-A-S-H phases and calcite in the cement buffer, and possible also due to corrosion products with larger molar volumes than dense metallic Fe(0). Thus, diffusion might be lower near the interface of the steel/cement due to a decreased porosity.
- *Delimited input space*

  - (disposal cell in granite) An increased model complexity was made by accounting for a varying steel corrosion rate depending on temperature and saturation index of dissolved iron (Samper et al., 2016) – pH in the disposal cell in granite remains at values around 8-8.5 at the bentonite-steel interface thus excluding significant pH effects on the corrosion rate. Including temperature dependence of the corrosion rate did not significantly affect the simulation results because of the relative short heat pulse. On the other hand, dependency on saturation index significantly decreases the corrosion rates of the steel.
  - (disposal cell in granite) The geochemical model for the bentonite buffer was simplified by considering smectite as an unreactive mineral phase. The general trends of the computed concentrations of dissolved, exchanged and sorbed species and mineral volume fractions are generally similar to the base case where only 0.5 % of the smectite is dissolved.
  - (disposal in clay) A complexity in many reactive transport models is the representation of the C-S-H model, specifically when the code cannot handle (non)ideal solid solution models. In that case, C-S-H is represented by a number of discrete phases. In the framework of this study, it has been shown that a set of 3 discrete phases gives similar results than a set of 9 discrete phases.
- *Reduced numerical accuracy*
  - (disposal cell in granite) Not refining the grid size near an interface led to a similar behaviour as a decreased grid size near the interface although the latter provides a more detailed profile near the interface at a significant increase in computational time.
  - (disposal cell in granite) Increase the numerical convergence tolerance – also no qualitative differences were observed although numerical values are different within acceptable limits. A smaller convergence tolerance significantly increases the computational time.
- *Surrogate Modelling*
  - (disposal cell in granite) For the first time, a surrogate model for a system with steel and bentonite including precipitation of corrosion products was constructed. Based on a Latin Hypercube sampling in the expected range of Fe, O_2 and H(1) concentrations (range based on base case simulations presented in section 2.4.1), Gaussian process was used to train the surrogate model. The surrogate model provides excellent results for most of the output variables with a log scale of some variables and by defining two groups, one for pH $\leq$ 10 and another for pH > 10. For predictive purposes the groups are defined by using random forests.

Some of the most relevant results from the different sensitivity studies are:

- (disposal cell in granite) A decrease in the silica saturation threshold in the glass dissolution model leads to a decrease in the glass dissolution rate, but has no effect on the pH.
- (disposal cell in granite) Having a faster breaching of the steel (shorted Period II duration) has a significant effect on the glass dissolution front; less magnetite and siderite is formed in favour of greenalite precipitation.
- (disposal cell in granite) Predictions are not sensitive to the increase of Cl^- concentration in the granite boundary water. Neither green rust nor akaganeite precipitate.
- (disposal cell in granite) Simulation with MX80 bentonite (35 cm) instead of FEBEX (75 cm) showed that the evolution is sensitive to the choice of buffer material: some variables are higher (e.g. pH), other lower (precipitation of siderite and greenalite, glass dissolution) with MX80 bentonite.
- (disposal cell in granite) Considering an EDZ and a larger conductivity in the host rock led to an increase of groundwater flow through the granite. This higher flux resulted in a larger decrease of solute concentrations in the bentonite. The precipitation of corrosion products is slightly sensitive to the increase in water flux through the granite.

- (disposal in granite) Chemical evolution is not sensitive to the choice of ground water composition when Reference Czech crystalline rock water (Červinka et al., 2018) is used.
- (disposal cell in clay) The effect of thickness and nature of the buffer were investigated. A thicker buffer of the same material (CEM I) led to the same sequence of phase alterations but of course with a shift in time and space. Using time to complete portlandite dissolution or time to a Ca/Si ratio in C-S-H of 0.8 in the cement as durability indicators with respect to steel corrosion, values for a buffer of 5, 30 or 100 cm are, respectively, ~300, 8,500, 82,000 years for portlandite depletion and ~1000, 25,000 and more than 100,000 years for C-S-H decalcification. Consequently, for a 100 cm thick buffer, steel corrosion remains in a passivated stage for 100,000 years; the steel overpack remained watertight and the IS glass was never altered. For the case with low-pH cement/bentonite grout (with a thickness of 5 cm), the grout was subjected to hydrolysis and magnesium attack, resulting in the formation of magnesium silicate hydrates M-S-H at the expense of the initial C-S-H 0.8 phase. The alteration of the claystone was much weaker and thinner than in the CEM I case. Steel corrosion was fast from the start due to the low pH conditions, but also for CEM-I with a thickness of 5 cm, the high pH conditions disappeared very fast. Therefore, there was no significant difference on the long term with respect to the effect of the buffer nature on the corrosion of steel and the dissolution of the IS glass.
- (disposal cell in clay) In a very first approach, the effects of potential (interconnected) crack (network) formation can be implicitly estimated in reactive transport models by assuming a larger effective diffusion coefficient. This approach led to a similar sequence of chemical alterations of the cementitious buffer as in the other cases without cracks: in the concrete, moving fronts of decalcification of the cement phases, another front of secondary ettringite formation at the expense of monocarboaluminate, dissolution of montmorillonite, in the host-rock partial illitization and neoformation of saponite and calcite. But cracking might significantly decrease the buffer lifetime.

3.4.3 ILW disposal cell scale

3.4.3.1 Disposal in clay

Two types of analyses were done for this system: (i) 1D profiles in a sensitivity analysis, and (ii) a 2D multiphase model to account for degradation reactions in the waste packages.

1D profile analysis

A comparison between the 1D and 2D simulations discussed in section 2.4.2.2 indicates qualitative and/or quantitative differences between the two models keeping in mind that the 1D model used a finer grid discretization. Figure 3-9 shows that the calcite precipitation and dolomite dissolution in the clay gives similar values with a slightly different pattern. Larger quantitative differences are observed in the cement side, although some fronts are captured quite well (ettringite dissolution front). The differences between the 1D profile, and the profile based on the 2D model is caused by different discretization and some 2D effects that might play a role.

Nevertheless, the overall picture allows to perform a sensitivity study on the effect of water saturation degree based on the 1D profile. Cases with 50% and 10% water saturation resulted in lower diffusion coefficients that reduced the spatial extent of the alteration, specifically in the case with 10% water saturation. Resulting porosity profiles differed quite significantly in the cement domain but were quite similar in the clay domain. Neglecting a feedback of porosity changes on transport properties did not lead to a significant change because porosity change was limited, specifically no significant decrease in porosity was simulated.

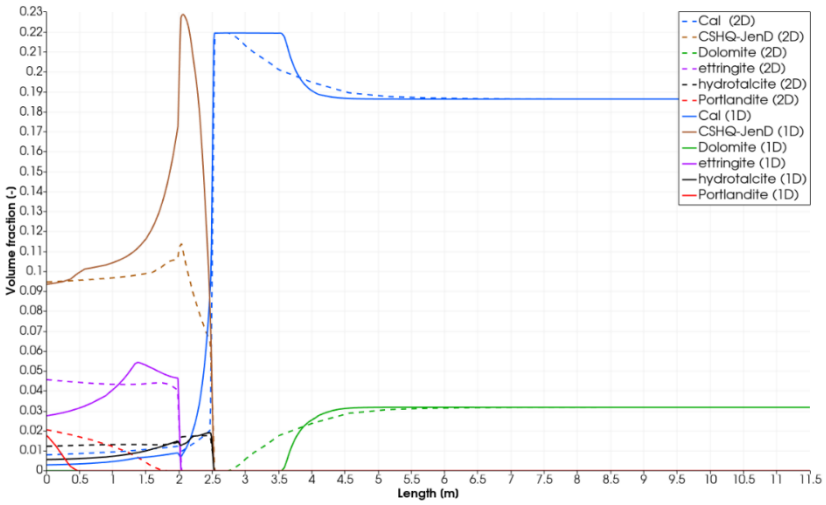

Figure 3-9. Comparison of the main minerals between the 2D and 1D ILW disposal cell in clay (cement/Clay interface at 2.5 m, clay extends at the right side).

2D multiphase flow model

The approach followed was to simplify the geochemical modelling approach by a look-up table approach (see section 3.3.2.2) on the one hand and considering (i) a more complex geometry (details on waste packages, compared to Figure 2-9 in section 2.4.2) and (ii) more complex processes for the flow and transport processes (gas production and multiphase flow) on the other hand, including a mixture of waste containers with organic material and steel (Figure 3-10). To move from the waste package scale to the disposal cell scale, the inner steel tube (Figure 3-6) is not accounted for in the disposal cell model. A time scale of 500 years was modelled.

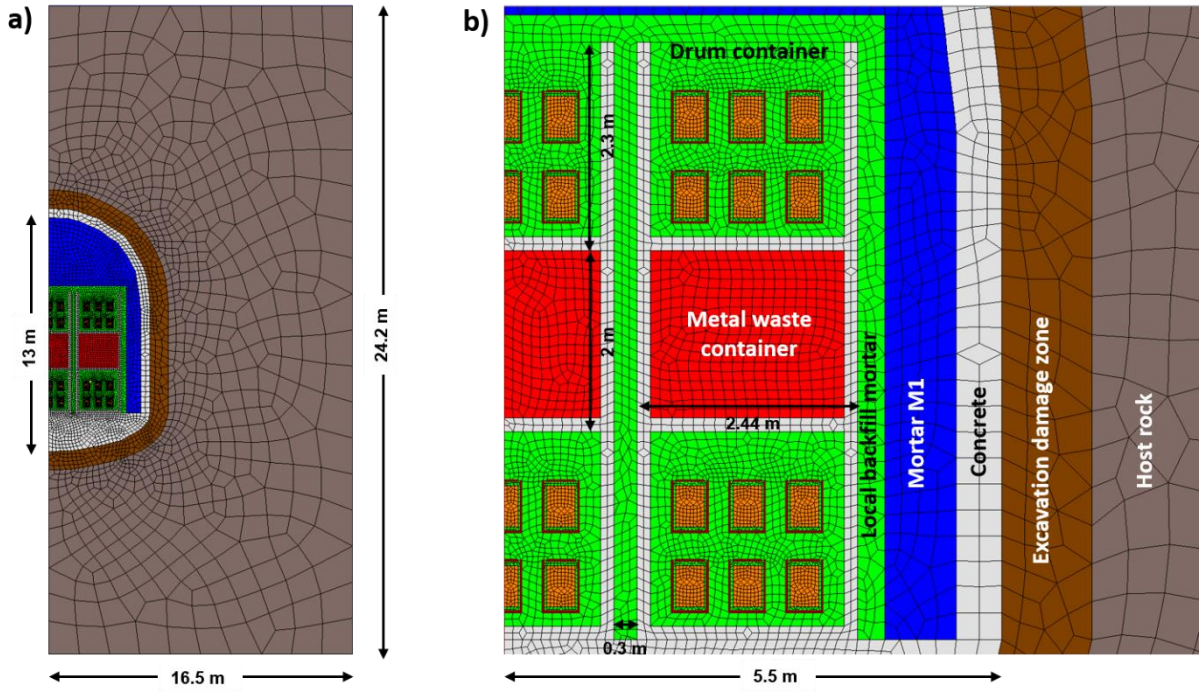

Figure 3-10: a) General geometry, material distribution (and discretization) of the ILW disposal cell in clay; b) Zoom-in view on the cross section of the gallery model. Brown lines show the metal hull of the drums and waste areas are shown in orange (Samper et al., 2024).

Importantly, a distinct difference between the behavior of the metal and organic material waste packages is modelled with lower gas generation rates in the former. The pH of the cement in the metal waste packages remains high (and thus iron corrosion rates low) because no CO_2 is produced in these containers, the reactivity of the aggregates is too low to induce a pH decrease and CO_2 of the organic material waste packages does not reach the metal waste packages. The water consumption rates in the organic material waste packages are smaller in the disposal cell scale model compared to the waste package scale model (section 3.3.2.2) because the fast corrosion of the metal within the drums is prohibited. The total gas flux out of a drum is a bit lower because the additional CO_2 (from more organic mass in the waste package) is consumed by the cement carbonation reaction of the backfill mortar within the drum. From the lower and middle containers, the produced gases are mostly transported horizontally into the high permeable M1 mortar (Figure 3-10). Here the gases can easily move upwards into the gallery roof, where the M1 mortar is designed as intermediate gas storage.

3.4.3.2 Disposal in granite

As base (reference) case for the ILW disposal cell scale in granite, the modelled evolution as discussed in section 2.4.2.1 was used for a time scale of 100,000 years. For constructing **physically-based lower fidelity models**, two sets of model abstractions were performed: (i) 1D transects not containing any waste container, and (ii) models with homogenized waste zones.

Models without the waste containers

For computational reasons, relatively large grid sizes and time steps were required in the 2D model (section 2.4.2.1) to solve the system in a reasonable amount of time. In a strict model abstraction approach, one has to start from smaller grid sizes and time steps and increase them to evaluate if the information is still sufficiently accurate. Instead, two 1D profiles (vertical and horizontal, see Figure 3-11) were defined with finer discretization. In the Y-direction, qualitatively the same mineralogical sequence was simulated, although quantitatively there were significant differences (Figure 3-11). In the X direction, the coarser grid in the 2D model probable led to too much smoothing with also qualitative differences between the 1D and 2D models. Decreasing dimensionality and decreasing grid sizes provide for this system probable a more detailed view on the phase profiles; the 2D model provides more insights into the general spatial-temporal evolution of the system.

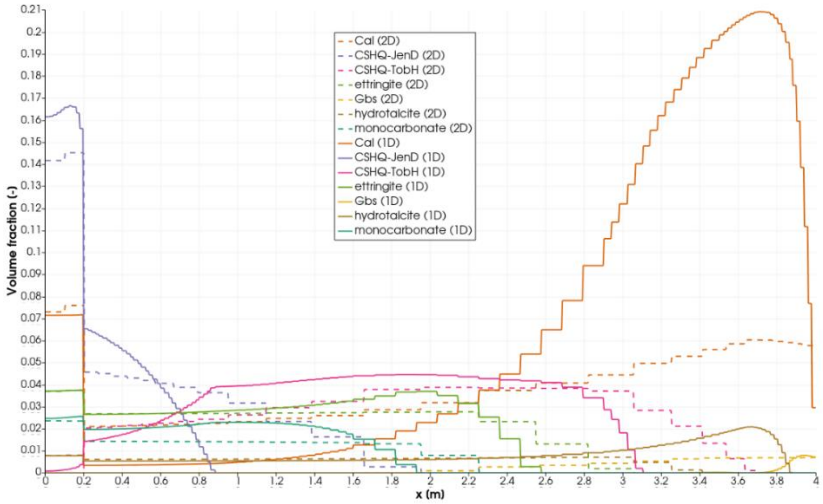

Figure 3-11 –Comparison between the volume fraction of different minerals obtained with the vertical 1D profile (full lines) and the 2D model (dashed lines) after 100 000 y.

Models with homogenized waste zones.

A set of different models was developed in which the waste zone was always homogenized, i.e. averaged properties for backfill mortar, infill mortar, container walls and waste zone. Then, several abstractions were performed, but mainly due to computational reasons, several aspects were combined:

- Model 1: A two-dimensional model with full chemistry but with coarser grid discretization compared to model 2
- Model 2: A one-dimensional model with full chemistry
- Model 3: A one-dimensional model neglecting reactions in the granite (delimited input domain compared to model 1 and 2) but including porosity changes (model 2 – model 3: hierarchy of models).
- Model 4: A one-dimensional model with full chemistry but coarser grid (reduced numerical accuracy compared to model 2)

Models 1 and 2 show consistent pH profiles at the right hand side (large high pH plume downstream of the repository in the direction of the ground water flow; smaller pH perturbation upstream of the repository due to diffusion). However, the 2D upstream plume has an asymmetric shape that is a direct consequence of the geometry of different materials in the disposal cell. Similarly, a clear spatial variable leaching pattern of K is visible due the different materials (e.g. backfill mortar and functional concrete). Comparison of the 1D model with a horizontal transect in the 2D model shows that depending on the variable of interest, differences are larger or smaller. For this specific geometry of the disposal cell, a 2D model is in generic terms more representative; however, applying a rigorous model abstraction methodology, 1D simulations might be sufficient depending on the objective of the simulation.

In model 3, the treatment of an inert granite host rock is implemented by excluding it from the simulation domain and applying constant concentration boundary conditions at the granite/cement interface. In models 2 and 3, the main degradation mechanisms in the cementitious material are similar (dissolution of portlandite, decalcification of C-S-H phases, and formation of calcite). However, the cementitious barriers degradation rate is considerably slower when the granitic host rock is explicitly included in the model (model 2) as the formation of the high pH zone at the granite-vault backfill mortar interface plays a significant role. On the other hand, the variant when granitic host rock properties are implemented through the boundary conditions (model 3) with incorporation of porosity-permeability feedback could be treated as a conservative approach; on the other hand, it is a representative representation when the flow is longitudinal along the disposal gallery as was assumed in the 2D model (section 2.4.2.1).

Analysis of spatial and temporal grid size effects on modelling results (model 2 and model 4) indicated that for the analysed system pH can be sufficiently well modelled with the coarser spatial and temporal grid, therefore saving computational resources. The largest differences between the cases were observed for component concentrations in the pore water.

Surrogate modelling was evaluated for a simplified geochemical system [C,Ca,Si,O,H] by comparing a reactive transport model in which the geochemical system is solved with a thermodynamic solver with a model in which the system is solved by a surrogate model using a deep neural network (DNN) algorithm. This illustrated that DNN can substantially speed up reactive transport simulations in cement systems while accurately capturing both dissolution (portlandite and C-SH-) and precipitation (calcite). Increasing the complexity of the geochemical system (e.g., towards [C,Ca,Si,Al,Cl,K,Na,Mg,S,O,H]) significantly increases the requirement to derive extreme high-quality training samples for which different options still have to be investigated (e.g., training sets based on a “cheap” full RT simulation (coarser grid and shorter period (Laloy and Jacques, 2022), physics constraints in DNN training (physics-informed neural networks (PINNs) framework), on line training with an accept/reject mechanism of the kNN-predicted solution or other look-up table approaches (Leal et al., 2020)).

4. What can we learn from ACED about the long-term evolution

Steel is present as an engineered barrier in all studied disposal cells. The type of corrosion products highly depends on the type of dissolved species and several Pourbaix diagrams were calculated in the initial SOTA (Neeft et al, 2022). Apart from pure iron-oxide corrosion products and carbon-containing corrosion products also calcium containing iron products were proposed ($CaFe_2O_4$ i.e. like magnetite a spinel type). ACED learned us that a corrosion product of steel can also contain calcium and silicium. This corrosion product is predicted to be a hydrogarnet and a Pourbaix diagram in section 3.1.2.

Long-term corrosion rates are characterised as steady states, the rates for the dissolution and the generation of the corrosion product are equal. The fate of iron in bentonite is sorption by clay minerals by which the sorption rate may control the corrosion rate of steel. The uptake of iron by clay could be monitored since the sorption is a fast process (see section 3.1.1).

The fate of iron of corroding steel interfacing concrete was unclear. ACED learned us that the uptake of iron is insignificant by the C-S-H minerals but may be incorporated by (Al,Fe)Si-hydrogarnet. This uptake of iron by this hydrogarnet could however not experimentally be monitored since it was too slow (see section 3.1.2).

The rate of processes relevant for the chemical evolution of the disposal cells such as the rate of steel corrosion, are controlled by the access and transport of water. Knowledge of representative physical material properties are therefore crucial in the optimization of the design of the disposal cell.

4.1 Impact of material properties

Physical and chemical properties of materials in disposal cells determine how fast the chemical evolution takes place. A physical property of a material (diffusion value, permeability value, porosity and distribution in size of pores, presence of fractures) in a disposal cell may control the transport of water and exchange of dissolved species and whether or not the chemical processes are microbially induced. The extent of the chemical evolution in a disposal cell is determined by the amounts of materials and differences in chemical properties (reducing conditions, pore water, minerals that can fix dissolved species) of these materials.

There are many materials radioactive. Examples of such materials are concrete, granite and clay due their low radionuclide content or a natural material such as uranium ore (Hamstra, 1975). Radioactive waste is a radioactive material for which no longer use is foreseen. The period that the radiotoxicity of the waste is larger than a radioactive material may be a suitable timescale for assessing the chemical evolution. This period may be larger for HLW than for ILW and the physical properties have a large impact on the chemical evolution. A lot of assumptions are made for determination of the physical properties and verification of the assumed physical properties may increase the confidence in the prediction in the extent of the chemically evolved solid materials such as the waste form.

Granitic host rock has too many water conducting fractures by which the engineered barriers may be assumed to be in contact with ground water. The long-term chemical evolution of engineered barriers is therefore controlled by the evolution of the physical properties of these engineered materials and from the chemical disbalance between engineered barriers materials and the granitic rock. Bentonite and concrete are used in disposal cells investigated in ACED. In both engineered materials, the hydraulic conductivity or permeability is so low that diffusion is assumed as the main transport mechanism. The measurement of the transport properties is challenging and therefore usually not done. Especially for concrete, transport properties used for modelling are calculated or guessed (Samper et al., 2022). Table 4-1 shows that although the permeability of bentonite may be smaller than the one of concrete, its diffusion value is considered higher than concrete. Table 4-1 also shows two examples with the same aggregate content (70 vol%; calculated concrete buffer and calculated functional concrete), water to cement ratio, type of cement (CEM I) but in which different values for porosity and transport properties arise.

Table 4-1: Properties relevant for transport of water in saturated barriers used in modelling in ACED (Samper et al., 2022) except stated otherwise

Buffer	Porosity [%]	Permeability [m^2]	Hydraulic conductivity [m/s]	Effective diffusion coefficient [m^2/s]
Bentonite	40.7	6×10^{-21}	6×10^{-14}	4.07×10^{-11}
COX clay*	18	1×10^{-20}	1×10^{-13} *	3×10^{-11}
Calculated concrete buffer	11.54 8.37 capillary & 3.17 gel			≤10^{-12} but assumed cracks leading 10^{-11} and 10^{-10}
Calculated functional concrete	8.5	1×10^{-19}	1×10^{-12}	2.12×10^{-12}
Measured concrete**	13	7.3×10^{-20}	7.3×10^{-13}	0.8×10^{-11}

* from Levasseur et al. (2021), **from Mladenovic et al. (2024) and Blanc et al. (2024) at 20°C

In ACED, properties of concrete representative for geological disposal facilities, similar aggregate content but different type of cement (CEM III/B) have been obtained by measuring the weight of saturated concrete specimens during drying at controlled relative humidity and temperature conditions for about 1000 days and predicting the measured change in weight as a function of time. The measured evolution in weight of water in the concrete specimen could be well predicted with saturated dependent diffusion values using Millington and Quirk (1961). For the calculation of the evolving weight of water with a saturation dependent permeability, an unrealistic value for the compressibility needed to be assumed (Blanc et al., 2023). What ACED has taught us is that such long-lasting experiments to verify assumed physical properties in modelling are very scarce, perhaps absent in literature. It can be economically valuable to include verified physical properties in the optimization of the disposal cell, especially if the water consumption due to the alteration of waste forms such as glass, steel and organic matter is included. Concrete – if well engineered - appears to be able to handle extremely high suction pressures without dehydration cracks, much higher than clay. Roman concrete is an excellent example that if well engineered, despite chemical changes taking place over more than 2000 years, remains intact. It may therefore not be needed to assume cracks associated with higher diffusion values, provided that the mechanical load on concrete at disposal depth has a negligible impact.

Indurated clay host rock has been known to be dried during the operational phase. The clay host rock is therefore unsaturated at the start of the post-closure phase, and it may take more than 100,000 years to become saturated (Leupin et al., 2016; Samper et al., 2022). Many waste forms consume water during their alteration and alteration processes of some waste forms such as steel and organic matter generate gases. The gas generation rates of these waste forms are currently obtained from experimental set-ups with sufficient access to water. It can be questioned whether these measurements are representative for disposal of waste in clay host rock. This also accounts for experiments performed with cementitious solutions. A diffusion value in water e.g. at 20°C of 2.0×10^{-9} m^2/s (Tofts et al., 2000) is at least 100 times larger than the measured value in concrete of 0.8×10^{-11} m^2/s (see Table 4-1).

4.2 Impact on waste form and RN mobility

The radionuclides, so-called contaminants, in the waste forms together with the long-term behaviour of the solid waste forms and transport of these contaminants in other engineered barriers determine the (type of) ingress of radionuclides into the host rock. This long-term behaviour, in particular how the waste forms react with and dissolve in pore waters in the EBS, contributes to the delay and attenuation of releases by limiting and spreading in time the release of these contaminants.

The long-term behaviour of the waste form can be described as dissolution and dissipation of dissolved constituents (species in Figure 4-1). Species can be a dissolved metallic ion e.g. iron, dissolved silicon, dissolved calcium etcetera. The interaction between the waste form and pore water results in the formation of another solid layer: a Product Layer (PL) with minerals that are hydrated and/or oxidized constituents of the waste form. These layers are developed when materials such as glass (Conradt et al., 1986; Ferrand et al., 2023) and metals such as steel (Mibus et al., 2015) or Zircaloy (Necib et al., 2018) are exposed to water. These layers have a so-called passivation capacity and can delay the release of contaminants from the solid waste form by acting as a diffusion barrier and attenuate the release of contaminants such as radionuclides by uptake such as sorption. A local equilibrium between this solid phase and a dissolved phase will develop. Such a local equilibrium is the solubility of the solid phase. These solubilities can be very small. A diffusional profile develops as long as the water is not stirred (left in Figure 4-1). The dissolution rate of the solid waste form is then controlled by the diffusion rate of dissolved species away from the solid waste form. The dissolution rate becomes larger in case of stirring since the dissipation rate becomes larger and the local equilibrium must be maintained by dissolution of the solid phase.

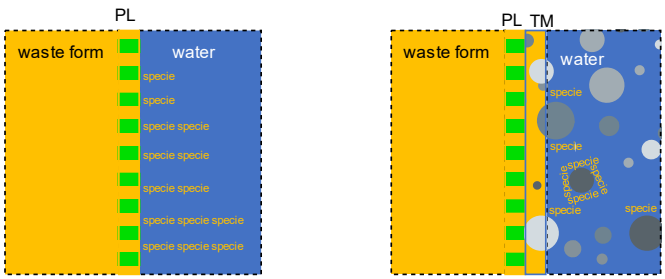

Figure 4-1: Long-term behaviour in terms of solubility and dissipation in water (left) and a porous medium (right) in which the dark 'obstacles' have an opposite charge of the dissolved form, Product Layer (PL) and Transformed Medium (TM). For simplicity, a larger volume fraction of pore water has been drawn than actually is present in any porous media.

A diffusion value of dissolved species in water is larger than a diffusion value of the same species in a porous medium since the dissolved species need to circumvent impermeable obstacles such as a grain of sand and thereby increasing the transport length. The dissipation rate of dissolved species from the solids can therefore be smaller in a porous medium than in water and this smaller dissipation rate may lead to a smaller dissolution rate. Also drying increases the transport length of dissolved species to move away from the waste form.

However, dissolved species are usually charged species. The obstacles present in the porous medium may also have a charge. Sorption occurs if the charge of the obstacle is opposite to the dissolved specie (right in Figure 4-1). The concentration of dissolved species in local equilibrium with the charged obstacle is smaller than the solubility. The dissolution rate of the solids can therefore be larger in a porous medium if sorption occurs. A larger anaerobic corrosion rate of steel in clay than in water (see Neeft et al. (2022)) is an example of the impact of sorption of dissolved iron species by clay minerals that have a negative surface charge. This iron sorption may not only be present in clay. At a pH of lower than 11.7, the surface charge of C-S-H changes from positive to negative (see Figure 2-3). The potential

features and processes of each waste form interacting with pore water and 'obstacles' in a porous medium therefore needs to be known to assess its long-term behaviour.

Apart from a Product Layer (PL), another solid layer may develop at interfaces between two solids by reaction with the dissolved constituents: a so-called Transformed Medium (TM). A TM may have other properties than the virgin properties of the solid porous media such as strength, distribution in size of pores and swelling or self-healing potential. An example is the alteration of the swelling clay minerals into non swelling sheet silicates for iron-affected bentonite. For iron-affected concrete, in the intial SOTA of ACED, reference was made to a more than 30 year old concrete in the vicinity of steel being identified as 'loosely bound material'. The impermeable 'obstacles' can be quartz grains that act as markers of the porous media. Archaeological analogues of steel embedded in clay (Neff et al., 2004) and concrete (Chitty et al., 2005) are examples of porous media in which TMs have been found.

The system with glass is more complicated since the corrosion of iron has shown to have an impact on the glass alteration rate. The positively charged iron species during the corrosion process have an impact on the thickness of the layer of the precipitated phases with clay minerals. Also, the local increase in pH by the corrosion process increases the solubility of silicon. The research performed in ACED shows that the glass alteration rates in the vicinity of (aged) iron both embedded in water saturated clay follows the corrosion process of iron as iron phyllosilicates are formed (Gin et al., 2022). The glass alteration rate is therefore larger in the vicinity of iron.

Stainless steel has dissolved chromium as a species that is released upon corrosion. Dissolved chromium is present as a negatively charged dissolved complex and is therefore expected to have a less detrimental effect on the alteration layer than dissolved iron complexes (Neeft et al., 2022). Also, the corrosion rate of stainless steel is about ten times smaller than that of iron or carbon steel (Swanton et al., 2015). The smaller corrosion rate of stainless steel compared to (aged) iron would lead to a lower glass alteration rate. Preliminary results in ACED of an experiment in which stainless steel and glass were embedded in saturated clay show indeed that the glass alteration rate in the vicinity of stainless is smaller than in contact with (aged) iron. The study of the impact of stainless steel compared to iron in such a system with clay is in progress. The results for a system with a concrete buffer are too preliminary to be included in this update of the SOTA. So far, due to the low corrosion rates of steel in freshly manufactured concrete, it has no impact.

The glass alteration process consumes water. There is more access to water in any experimental set-up considered so far than at disposal scale. What can be assessed is whether the assumed alteration rates are possible with the associated water consumption rates. For a concrete buffer, there is the ingress of bicarbonate. The cementitious mineral portlandite is understood to produce water if reacting with bicarbonate (e.g. Mladenovic et al., 2019). The major component of cement is the C-S-H phase. For unsaturated concrete, the carbonation rate decreases below a certain relative humidity (von Greve-Dierfeld et al., 2020). Based on the mass balance, this decrease has tentatively been attributed to consumption of water to complete carbonation for these C-S-H minerals in ACED (Blanc et al., 2024).

5. Summary and Conclusions

ACED has experimentally investigated in more detail porous media (concrete, clay, cement-clay mixture) interfacing steel. The distribution in size of pores in clay and in concrete minimized microbially induced chemical corrosion while the corrosion of steel might have been controlled by microbial activity for the investigated cement-clay mixture. Uptake of iron from corroding steel could be experimentally monitored for steel interfacing clay but not for steel interfacing concrete as the uptake process was too slow.

ACED has implemented reactive transport codes at different scales – from interfaces between different materials to disposal cells. In general, when experimental data is present, our current modelling capacities are successful in reproducing the main aspects of the interactions and of the geochemical evolution. ACED also demonstrated the power of such types of models to integrate available (process-based) knowledge to have an integrated view on the possible geochemical evolutions of these systems. Reactive transport models, specifically at the larger scale, are also helpful in illustrating the expected geochemical evolution. However, some aspects should retrieve more attention, such as pH dependence of kinetic processes or the two aspects mentioned below.

The saturation degree of porous media and transport of water in porous media may control the alteration rate of the waste forms and its associated release rate of some radionuclides. Other radionuclides may be fixed by the solid layer of minerals formed on the surface of the waste form. In the vicinity of corroding steel in a glass/steel/porous medium system, this solid layer may minimize the alteration rate but this layer is hardly generated for the vitrified waste form.

A conceptual understanding of how fast waste forms may alter requires the virgin physical and chemical properties of the porous media interfacing waste forms as well as how these properties are evolving when chemically interacting with other materials in the disposal cell. The available quantitative information of transport of water in porous media representative for disposal of waste that has been experimentally verified is scarce, especially if the porous medium is unsaturated. The confidence in the modelled chemical evolution of the disposal cell would increase if more verified virgin properties for the transport of water would be available and the knowledge on these properties for chemically evolved increases.

Overall, EURAD-ACED demonstrated the power of reactive transport models to quantitatively assess the geochemical evolution around interfaces in a disposal cell and for the disposal cell, including waste packages, as a whole. Many systems modelled with EURAD-ACED were modelled in an integrated way for the first time, certainly taken into account that the sequence of different processes during the chemical evolution were defined quantitatively during calculations and not qualitatively by a set of “rules” defined prior to the calculations. Said that, the models presented do no aim to predict the exact chemical evolution (scientific knowledge is still evolving) but provides insight on how the chemical evolution is driven by assumptions on processes, properties, parameters and events.

The modeling of the integrated systems with vitrified waste at experimental, waste package and disposal cell scale has demonstrated the possibility to include dissolution rate determining interactions between the glass and its environment (corroding steel, cement buffer, clay buffer, host rock) from the smallest (experimental) level to the largest scale (disposal cell) with simplifications that are supported by a good, but still evolving scientific understanding. The calculations have shown the importance of the assumed evolution scenarios including transient hydric and temperature conditions and dimensioning of the engineered barrier system on the glass dissolution, with effects from the engineered barriers on the glass, but also effects of the glass on the engineered barriers. The experiments on the integrated systems like the ones studied in EURAD-ACED have proven to be essential for the understanding of the basic interaction mechanisms and the parameterization of the evolving system. The modeling at waste package and disposal scale has allowed to quantify the expected glass dissolution rate decrease as a function of time over periods of time far beyond the experimental test durations.

The modelling of the integrated systems for intermediate level waste in largely cement-based repositories highlighted the interplay of waste characteristics (organic waste or metal-based waste), steel of waste drums and the host rock. Waste degradation influences both the water saturation within a repository (both by organic (degradation) and metal (corrosion) waste) and chemical reactivity within the cementitious barriers (carbonation with CO_2 from organic waste degradation). Simultaneously, cementitious materials in direct contact with the host formation will be leached and transformed depending on the geochemical characteristics of the host formation. EURAD-ACED simulated these effects on different scales and showed that it is possible to obtain spatial-temporal information on the heterogeneity and temporal aspects of degradation of the engineered barrier systems and the alterations in the host formation based on the current state-of-the-art knowledge. It forms also a solid basis for further integration of evolving scientific knowledge, specifically to the issues mentioned above.

The variation in modelling approaches together with the new experimental insights obtained within EURAD-ACED are summarized in the current report and detailed in a set of high-quality reports linked to the different tasks in EURAD-ACED. This report together with the set of deliverables produced in EURAD-ACED give an excellent starting point for studies of the geochemical evolution of disposal cells in the scope of national programs at different levels of development and different angles of interest and applications.

References

Altmaier, M. Blin, V., García, D., Henocq, P., Missana, T., Ricard, D., Vandenborre, J, (2021) SOTA on cement-organic-radionuclide interactions. Final version as of 19.05.2021 of deliverable D3.1 of the HORIZON 2020 project EURAD. EC Grant agreement no: 847593.

Alcolea, A., Kuhlmann, U., Lanyon, G.W., and Marschall, P., (2014). Hydraulic conductance of the EDZ around underground structures of a geological repository for radioactive waste – A sensitivity study for the candidate host rocks in the proposed siting regions in Northern Switzerland, NAGRA Arbeitsbericht NAB 13-94 www.nagra.ch.

Águila, J.F., Samper, J., Mon, A. and Montenegro, L. 2020. Dynamic update of flow and transport parameters in reactive transport simulations of radioactive waste repositories. Applied Geochemistry 117.

AREVA, (2007). Specification for standard vitrified waste residue (CSD-v) with high actinide content produced at la Hague (Confidential document not published openly), p. 23.

Atabek, R., Beziat, A., Coulon, H., Dardaine, M., Debrabant, P., Eglem, A., Farcy, C., Fontan, N., Gatabin, C., Gegout, P., Lajudie, A., Landoas, O., Lechelle, J., Plas, F., Proust, D., Raynal, J., and Revertegat, E., (1991). Nearfield behaviour of clay barriers and their interaction with concrete - Task 3 Characterization of radioactive waste forms A series of final reports (1985-89 No 26, Nuclear Science and Technology EUR 13877.

Atkins, M., Beckley, N., Carson, S., Cowie, J., Glasser, F.P., Kindness, A., Macphee, D., Pointer, C., Rahman, A., Jappy, J.G., Evans, P.A., McHugh, G., Natingley, N.J., and Wilding, C., (1991). Medium-active waste form characterization: the performance of cement-based systems Task 3 Characterization of radioactive waste forms A series of final reports (1985-1989) No 1, Nuclear Science and technology EUR 13452, 164 p.:

Atkinson, A., Goult, D.J., and Hearne, J.A., (1985). An assessment of the long-term durability of concrete in radioactive waste repositories, Mat. Res. Soc. Symp. Proc. Materials Research Society, v. 50, p. 239-246.

Ben Zeineb, H., Le Milbeau, C., Blanc, P., Ollivier, P., André, L. and Boussafir, M. 2021 CHEMICAL DEGRADATION OF POLYMERS AND ADDITIVES IN ALKALINE SOLUTION: INFLUENCE OF TEMPERATURE, Goldschmidt 2021, Lyon, France.

Berner, U.R., (1992). Evolution of pore water chemistry during degradation of cement in a radioactive waste repository environment Waste management, v. 12, p. 201-219.

Bildstein, O., Claret, F., and Frugier, P. (2019). RTM for Waste Repositories. Reviews in Mineralogy and Geochemistry 85, 419-457.

Bilke, L., Flemisch, B., Kolditz, O., Helmig, R., Nagel T. (2019). Development of open-source porous-media simulators: principles and experiences. Transport in Porous Media. 130 (1), 337 – 361.

Blanc, P., Debure, M., Goaverts, J., Gu, Y., Jacques, D., Kosakowski, G., Leivo, M., Marty, N.C.M., Neeft, E., Shao, H., and Vehling, F., (to be published in 2024). Description of ILW modelling results and recommendations for future experiments and numerical work: Deliverable 2.15, EC Grant agreement no: 847593, to be published at eurad website.

Bradbury, M.H. and Baeyens, B. 1997. A mechanistic description of Ni and Zn sorption on Na-montmorillonite Part II: modelling. Journal of Contaminant Hydrology 27(3), 223-248.

Bonnet, J., Mosser-Ruck, R., Sterpenich, J., Bourdelle, F., Verron, H., Michau, N., Bourbon, X. and Linard, Y. 2022. Chemical and mineralogical characterizations of a low-pH cementitious material designed for the disposal cell of the high-level radioactive waste (HLW). Cement and Concrete Research 162, 107013.

Brown, A., Small, J., Pimblott, M., Goodacre, R. and Lloyd, J.R. 2014 The impact of ionizing radiation on microbial cells pertinent to the storage, disposal and remediation of radioactive waste. The University of Manchester (United Kingdom).

Červinka, R., Klajmon, M., Zeman, J., Vencelides, T., (2018). Geochemical calculations and reactive transport modelling. SURAO Technical Report 271/2018/ENG.

Chamssedine, F., Sauvage, T., Peuget, S., Fares, T., and Martin, G., (2010). Helium diffusion coefficient measurements in R7T7 nuclear glass by 3He(d,α)1H nuclear reaction analysis, Journal of Nuclear Materials, v. 400, p. 175-181.

Chen, P., Van Loon, L.R., Fernandes, M.M. and Churakov, S. 2022. Sorption mechanism of Fe(II) on illite: Sorption and modelling. Applied Geochemistry 143, 105389.

Chitty, W.-J., Dillmann, P., L'Hostis, V., and Lombard, C., (2005). Long-term corrosion resistance of metallic reinforcements in concrete—a study of corrosion mechanisms based on archaeological artefacts, Corrosion Science, v. 47, p. 1555–1581.

Claret, F., Marty, N., and Tournassat, C. (2018). Modeling the long-term stability of multi-barrier systems for nuclear waste disposal in geological clay formations. In "Reactive Transport Modeling: Applications in Subsurface Energy and Environmental Problems" (X. Yitian, W. Fiona, X. Tianfu and C. Steefel, eds.), pp. 395-451. John Wiley & Sons Ltd.

Claret, F. et al., 2024.DONUT. D4.2 of the HORIZON 2020 project EURAD. EC Grant agreement no: 847593 – in preparation.

Conradt, R., Roggendorf, H., and Ostertag, R., (1986). The basic corrosion mechanisms of HLW glasses, Commission of the European Communities - Nuclear Science and Technology EUR 10680, p. 218.

Dähn, R., Baeyens, B. and Bradbury, M.H. 2011. Investigation of the different binding edge sites for Zn on montmorillonite using P-EXAFS - The strong/weak site concept in the 2SPNE SC/CE sorption model. Geochim Cosmochim Ac 75(18), 5154-5168.

De Windt, L., Miron, G.D., Fabian, M., Goethals, J., and Wittebroodt, C., (2020). First results on the thermodynamic databases and reactive transport models for steel-cement interfaces at high temperature. Final version as of xx.xx.xxxx of deliverable D2.8 of the HORIZON 2020 project EURAD. EC Grant agreement no: 847593., www.ejp-eurad.eu.

De Windt, L., Samper, J., Cochepin, B., Garcia, E., Mon, A., Montenegro, L., Samper, A., Raimbult, L. and Veille, E. 2024 Integrated reactive transport models for assessing the chemical evolution at the disposal cell scale. Final version as of xx.xx.xxxx of deliverable D2.17 of the HORIZON 2020 project EURAD. EC Grant agreement no: 847593.

Debure, M., Linard, Y., Martin, C. and Claret, F. 2019. In situ nuclear-glass corrosion under geological repository conditions. npj Materials Degradation 3(1), 38.

Deissmann, G., Ait Mouheb, N., Martin, C., Turrero, M. J., Torres, E., Kursten, B., Weetjens, E., Jacques, D., Cuevas, J., Samper, J., Montenegro, H., Leivo, M., Somervuori, M., and Carpen, L. (2021). Experiments and numerical model studies on interfaces. D2.5 of the HORIZON 2020 project EURAD. EC Grant agreement no: 847593.

Delage, P., (2013). On the thermal impact on the excavation damaged zone around deep radioactive waste disposal, Journal of Rock Mechanics and Geotechnical Engineering, v. 5, p. 179-190.

Dilnesa, B.Z., Lothenbach, B., Renaudin, G., Wichser, A. and Kulik, D. 2014a. Synthesis and characterization of hydrogarnet Ca3(AlxFe1−x)2(SiO4)y(OH)4(3−y). Cement and Concrete Research 59, 96-111.

Dilnesa, B.Z., Wieland, E., Lothenbach, B., Dähn, R. and Scrivener, K.L. 2014b. Fe-containing phases in hydrated cements. Cement and Concrete Research 58, 45-55.

Duro, L., Altmaier, M., Holt, E., Mäder, U., Claret, F., Grambow, B., Idiart, A., Valls, A. and Montoya, V. 2020. Contribution of the results of the CEBAMA project to decrease uncertainties in the Safety Case and Performance Assessment of radioactive waste repositories. Applied Geochemistry 112, 104479

EURAD, Strategic Research Agenda, Scientific and technical domains and sub-domains and knowledge management needs of common interest between EURAD participants, 2019

Fabian, M., Czompoly, O., Tolnai, I. and De Windt, L. 2023. Interactions between C-steel and blended cement in concrete under radwaste repository conditions at 80 °C. Scientific Reports 13(1), 15372.

Fernández, J., (2017). Reactive Transport Models of low Permeability Structured Porous and Fractured Media. Ph.D. Dissertation. Universidad de A Coruña, Spain.

Ferrand, K., Liu, S., Caes, S., and Lemmens, K., (2023). Topical report on glass dissolution experiments at very high surface area to solution volume, SCK CEN ER-1007.

Frantz, F.K. 1995. Taxonomy of model abstraction techniques. WSC '95: Proceedings of the 27th conference on Winter simulation, 1413–1420.

Frugier, P., Minet, Y., Rajmohan, N., Godon, N. and Gin, S. 2018. Modeling glass corrosion with GRAAL. npj Materials Degradation 2(1), 35.

Furcas, F.E., Lothenbach, B., Isgor, O.B., Mundra, S., Zhang, Z. and Angst, U.M. 2022. Solubility and speciation of iron in cementitious systems. Cement and Concrete Research 151, 106620.

Gaucher, E.C., Tournassat, C., Pearson, F.J., Blanc, P., Crouzet, C., Lerouge, C., and Altmann, S., (2009). A robust model for pore-water chemistry of clayrock, Geochimica et Cosmochimica Acta, v. 73, p. 6470–6487.

Gin, S., Delanoe, A., Tocino, F., Ferrand, K., Goethals, J., Sterpenich, J., and Fabian, M. (2022). High level radioactive waste package – Characterization of glass/steel/buffer interaction experiments. D2.12 of the HORIZON 2020 project EURAD. EC Grant agreement no: 847593.

Glaus, M.A. and Van Loon, L.R. 2008. Degradation of Cellulose under Alkaline Conditions: New Insights from a 12 Years Degradation Study. Environmental Science & Technology 42(8), 2906-2911.

Goethals, J., De Windt, L., Wittebroodt, C., Abdelouas, A., de la Bernardie, X., Morizet, Y., Zajec, B. and Detilleux, V. 2023. Interaction between carbon steel and low-pH bentonitic cement grout in anoxic, high temperature (80 °C) and spatially heterogeneous conditions. Corrosion Science 211, 110852.

Govaerts, J., Jacques, D., Samper, J., Neeft, E. and Montoya, V. 2022 Model abstraction methods for upscaling and integration of process knowledge in reactive transport models for geological disposal of radioactive waste. Final version as of 10.01.2022 of deliverable D2.18 of the HORIZON 2020 project EURAD. EC Grant agreement no: 847593.

Gruppelaar, H., Kloosterman, J.L., and Konings, R.J.M., (1998). Advanced technologies for the reduction of nuclear waste, Petten, Netherlands Energy Research Foundation ECN-R--98-008.

Hadi, J., Wersin, P., Serneels, V. and Greneche, J.-M. 2019. Eighteen years of steel–bentonite interaction in the FEBEX in situ test at the Grimsel Test Site in Switzerland. Clays and Clay Minerals 67.

Hamstra, J., (1975). Radiotoxic Hazard Measure for Buried Solid Radioactive Waste, Nuclear Safety, v. 16, no. 2, p. 180-189.

Havlova, V., Kiczka, M., Mendoza Miranda, A., Klajmon, M., Wersin, P., Pekala, M., Jenni, A., Hadi, J., Samper, J., Montenegro, L., Mon, A., Fabian, M., Osan, J., Dauzeres, A., and Jacques, D., (2021). Modelling of the steel-clay interface – approaches, first results and model refinements. Final version as of 28 08 2020 of deliverable D2.6 of the HORIZON 2020 project EURAD. EC Grant agreement no: 847593., www.ejp-eurad.eu.

Helfferich, F., (1962). Ion exchange, United States of America, McGrawhill-Hill Book company, McGraw-Hill Series in advanced chemistry, 624 p.

Huang, Y., Shao, H., Wieland, E., Kolditz, O. and Kosakowski, G. 2018. A new approach to coupled two-phase reactive transport simulation for long-term degradation of concrete. Construction and Building Materials 190, 805-829.

Huang, Y., Shao, H., Wieland, E., Kolditz, O. and Kosakowski, G. 2021. Two-phase transport in a cemented waste package considering spatio-temporal evolution of chemical conditions. npj Materials Degradation 5(1).

Jackson, M.D., Mulcahy, S.R., Chen, H., Li, Y., Li, Q., Cappelletti, P., and Wenk, H.-R., (2017). Philipsite and Al-tobermite mineral cements produced through low-temperature water-rock reactions in Roman marine concrete, American Mineralogist, v. 102, no. 7, p. 1435-1450.

Jollivet, P., Gin, S. and Schumacher, S. (2012). Forward dissolution rate of silicate glasses of nuclear interest in clay-equilibrated groundwater. Chemical Geology 330, 207-217.

Kempl, J., and Copuroglu, O., 2015, The interaction of pH, pore solution composition and solid phase composition of carbonated blast furnace slag cement paste activated with aqueous sodium monofluorophosphate, 15th Euroseminar on Microscopy Applied to Building Materials: Delft, the Netherlands, p. 287-296.

Kosakowski, G., Huang, Y. and Wieland, E. 2020 Influence of material heterogeneities, process couplings and aggregate reactivity on the geochemical evolution of the L/ILW repositor. Nagra Arbeitsberichte NAB 20-11. Wettingen, Switzerland.

Laloy, E. and Jacques, D. 2022. Speeding up reactive transport simulations in cement systems by surrogate geochemical modeling: deep neural networks and k-nearest neighbors. Transport in Porous Media (accepted).

Lanson, B., Lantenois, S., Aken, P.A.v., Bauer, A. and Plançon, A. 2012. Experimental investigation of smectite interaction with metal iron at 80 °C: Structural characterization of newly formed Fe-rich phyllosilicates. American Mineralogist 97(5-6), 864-871.

Leal, A.M.M., Kyas, S., Kulik, D.A. and Saar, M.O. 2020. Accelerating Reactive Transport Modeling: On-Demand Machine Learning Algorithm for Chemical Equilibrium Calculations. Transport in Porous Media 133(2), 161-204.

Lemmens, K., Debure, M., Ferrand, K., Goethals, J., Liu, S. and Marty, N. 2024 Results of modelling and recommendations for future experimental and numerical work (HLW disposal system). Final version as of xx.xx.xxxx of deliverable D2.14 of the HORIZON 2020 project EURAD. EC Grant agreement no: 847593.

Leupin, O.X., Smith, P., Marschall, P., Johnson, L., Savage, D., Cloet, V., Schneider, J., Senger, R. (2016) Low- and intermediate level waste repository induced effects, NAGRA Technical report 14-14.

Levasseur, S., Collin, F., Daniels, K., Dymitrowska, M., Harrington, J., Jacops, E., Kolditz, O., Marschall, P., Norris, S., Sillen, X., Talandier, J., Truche, L., and Wendling, J., (2021). Initial State of the Art on Gas Transport in Clayey Materials. Deliverable D6.1 of the HORIZON 2020 project EURAD, Work Package Gas. EC Grant agreement no: 847593., www.ejp-eurad.eu.

Liu, S., Ferrand, K., Aertsens, M., Jacques, D. and Lemmens, K. 2019. Diffusion models for the early-stage SON68 glass dissolution in a hyper-alkaline solution. Applied Geochemistry 111.

Mibus, J., Swanton, S., Suzuki-Muresan, T., Rodríguez Alcalá, M., Leganés Nieto, J.L., Bottomley, D., Herm, M., de Visser-Týnová, E., Cvetković, B.Z., Sakuragi, T., Jobbágy, V., and Heikola, T., (2015). WP2 Annual Progress Report - Year 2 - Deliverable 2.5 Carbon-14 Source Term (CAST), p. 98.

Millington, R.J. and Quirk, J.P. 1961. Permeability of porous solids. Transactions of the Faraday Society 57, 1200-1207.

Miron, G.D., Kulik, D.A. and Lothenbach, B. 2022a. Porewater compositions of Portland cement with and without silica fume calculated using the fine-tuned CASH+NK solid solution model. Materials and Structures 55(8), 212.

Miron, G.D., Kulik, D.A., Yan, Y., Tits, J. and Lothenbach, B. 2022b. Extensions of CASH+ thermodynamic solid solution model for the uptake of alkali metals and alkaline earth metals in C-S-H. Cement and Concrete Research 152, 106667.

Miron, G.D., Leal, A.M.M., Dmytrieva, S.V. and Kulik, D.A. 2023. ThermoFun: A C++/Python library for computing standard thermodynamic properties of substances and reactions across wide ranges of temperatures and pressures. Journal of Open Source Software 8, 4624.

Mladenovic, A., Markku, L., Neeft, E., Dähn, R., and Kosakowski, G., (to be published). ILW: Report describing the results of characterisation performed during the project. Final version as of XX.XX.202X of deliverable D2.13 of the HORIZON 2020 project EURAD. EC Grant agreement no: 847593.

Mladenovic, A., Neeft, E., Deissmann, G., Dähn, R., Geng, G., Koskowski, G., and Markku, L., (2019). ILW: Report describing the selected experiments and the existing/expected experimental results. Final version as of 24.12.2019 of deliverable D2.11 of the HORIZON 2020 project EURAD. EC Grant agreement no: 847593.

Montenegro, L., Samper, J., Mon, A., De Windt, L., Samper, A.-C. and García, E. 2023. A non-isothermal reactive transport model of the long-term geochemical evolution at the disposal cell scale in a HLW repository in granite. Applied Clay Science 242, 107018.

Müller-Vonmoos, M., and Kahr, G., (1983). Mineralogische unterschungen von Wyoming Bentonit MX-80 und montigel, NAGRA Technischer bericht 83-12 www.nagra.ch.

Nardi, A., Idiart, A., Trinchero, P., De Vries, L.M. and Molinero, J. 2014. Interface COMSOL-PHREEQC (iCP), an efficient numerical framework for the solution of coupled multiphysics and geochemistry. Computers & Geosciences 69, 10–21.

Naumov, D.Y., Fischer T., Bilke, L., Rink, K., Watanabe, N., Wang, W., Lu, R., Grundwald, N., Zill, F., Huang, Y, Bathmann, J., Chen, C., Shao, H., Chen, S., Miao, X., Meng, B., Walther, M., Buchwald, J., Boog, J., Zheng, T Yoshioka, K., Zhang, N., Thiedau, J., Parisio, F., Nagel, T., Helbig, C., Kalbacher, T., Lehmann, C., Wanlong C., Herfurth, J., Montoya, V., (2020) ufz/ogs: 6.2.2, June, 2020.

Necib, S., Bucur, C., Caes, S., Cochin, F., Cvetković, B.Z., Fulger, M., Gras, M., Herm, M., Kasprzak, L., Legand, S., Metz, V., Perrin, S., Sakuragi, T., and Suzuki-Muresan, T., (2018). Overview of 14C release from irradiated Zircaloys in geological disposal conditions, Radiocarbon, v. 60, no. 6, p. 1757-1771.

Neeft, E., Jacques, D., and Deissmann, G., (2022). Initial State of the Art on the assessment of the chemical evolution of ILW and HLW disposal cells. D 2.1 of the HORIZON 2020 project EURAD. EC Grant agreement no: 847593., http://www.ejp-eurad.eu

Neeft E., de Bruin T., van Kleef R., Phung Q T., Perko J., Seetharam S., Mijnendonckx K., Li X., Hausmannová L., Vašíček R., Večerník P., Hlaváčková V., Černá K., Černoušek T., Helson O., Bourbon X., Zghondi J., Vidal T., Sellier A., Shao J., Rougelot T., Jantschik K., Kulenkampff J., Deissmann G., Griffa M., Churakov S, Gimmi T., Ma B. (2021): Selected experiments for assessing the evolution of concrete, their mechanical safety function and performance targets. Final version as of 28.01.2022 of deliverable D16.3 of the HORIZON 2020 project EURAD. EC Grant agreement no: 847593.

Neeft, E., Weetjens, E., Vokal, A., Leivo, M., Cochepin, B., Martin, C., Munier, I., Deissmann, G., Montoya, V., Poskas, P., Grigaliuniene, D., Narkuniene, A., García, E., Samper, J., Montenegro, L., and Mon, A., (2019). Treatment of chemical evolution in National Programmes. D 2.4 of the HORIZON 2020 project EURAD. EC Grant agreement no: 847593., http://www.ejp-eurad.eu

Neff, D., Reguer, S., Bellot-Gurlet, L., Dillmann, P., and R., B., (2004). Structural characterisation of corrosion products on archaeological iron. An integrated analytical approach to establish corrosion forms, Journal of Raman Spectroscopy, v. 35, no. 8-9, p. 739-745.

Pachepsky, Y.A., Guber, A., van Genuchten, M.T., Nicholson, T.J., Cady, R.E., Simunek, J. and Schaap, M.G. 2006 Model Abstraction Techniques for Soil-Water Flow and Transport. pp. NUREG/CR-6884.

Pally, D., Le Bescop, P., Schlegel, M.L., Miserque, F., Chomat, L., Neff, D. and L'Hostis, V. 2020. Corrosion behavior of iron plates in cementitious solution at 80 °C in anaerobic conditions. Corrosion Science 170, 108650.

Pointeau, I., Coreau, N., and Reiller, P.E., (2008). Uptake of anionic radionuclides onto degraded cement pastes and competing effect of organic ligands, Radiochimica Acta, v. 96, no. 6, p. 367-374.

Pointeau, I., Reiller, P.E., Macé, N., Landesman, C., and Coreau, N., (2006). Measurement and modeling of the surface potential evolution of hydrated cement paste, Journal of Colloid and Interface Science, v. 300, p. 33-44.

Prasianakis, N.I., Laloy, E., Jacques, D., Meeussen, J.C.L., Tournassat, C., Miron, D.A., Kulik, D.A., Idiart, A., Demirer, E., Coene, E., Cochepin, B., Leconte, M., Savino, M., Samper II, J., De Lucia, M., Churakov, S.V., Kolditz, O., Yang, C., Samper, J. and Claret, F. 2024. Geochemistry and Machine Learning: review of methods and benchmarking (in preparation).

Razavi, S., Tolson, B.a. and Burn, D.H. 2012. Review of surrogate modeling in water resources. Water Resources Research 48(7), W07401.

Samper, J., Mon, A., Montenegro, L., De Windt, L., Govaerts, J., Laloy, E., Jacques, D., Grigaliuniene, D., Povilas, B., Povilas, P., Shao, H. and Vehling, F. 2024 Report on comparison of model abstraction results, D 2.19 of the HORIZON 2020 project EURAD. EC Grant agreement no: 847593.

Samper, J., Xu, T. and Yang, C. 2009. A sequential partly iterative approach for multicomponent reactive transport with CORE2D. Computational Geosciences 13(3), 301-316.

Samper, J., Montenegro, L., De Windt, L., Montoya, V., Garibay-Rodriguez, J., Grigaliuniene, D., Narkuniene, A., Poskas, P., and Cochepin, B., (2022). Conceptual model formulation for a mechanistic based model implementating the initial SOTA knowledge (models and parameters) in existing numerical tools. Final version as of 15.07.2022 of deliverable D2.16 of the Horizon 2020 project EURAD. EC agreement no: 847593, http://www.ejp-eurad.eu

Samper, J., Naves, A., Montenegro, L. and Mon, A. 2016. Reactive transport modelling of the long-term interactions of corrosion products and compacted bentonite in a HLW repository in granite: Uncertainties and relevance for performance assessment. Applied Geochemistry 67, 42-51.

Savage, D., (2014). An Assessment of the Impact of the Long Term Evolution of Engineered Structures on the Safety-Relevant Functions of the Bentonite Buffer in a HLW Repository, NAGRA Technical Report 13-02.

Seymour, L.M., Maragh, J., Sabatini, P., Di Tommaso, M., Weaver, J.C., and Masic, A., (2023). Hot mixing: Mechanistic insights into the durability of ancient Roman concrete, Sciences Advances v. 9, p. 1-3.

Small, J.S., Nykyri, M., Vikman, M., Itävaara, M. and Heikinheimo, L. 2017. The biogeochemistry of gas generation from low-level nuclear waste: Modelling after 18 years study under in situ conditions. Applied Geochemistry 84, 360-372.

Soltermann, D., Baeyens, B., Bradbury, M.H. and Marques Fernandes, M. 2014. Fe(II) Uptake on Natural Montmorillonites. II. Surface Complexation Modeling. Environmental Science & Technology 48(15), 8698-8705.

Stein, M., (2014). Erläuterungen zur Verpackung radioaktiver Abfälle im Endlagerbehälter, Arbeitsbericht NAB 14-104.

Stefanoni, M., Angst, U.M., and Elsener, B. (2018). Electrochemistry and capillary condensation theory reveal the mechanism of corrosion in dense porous media. Scientific Reports 8, 7407.

Stroes-Gascoyne, S. and West, J.M. (1997). Microbial studies in the Canadian nuclear fuel waste management program. Federation of European Microbiological Societies. (FEMS) Microbiology reviews 20, 573-590.

Stumm, W., (1992). Chemistry of the solid-water interface. Processes at the mineral-water and particle water interface in natural systems, Canada, A Wiley interscience publication, 428 p.

Swanton, S.W., Baston, G.M.N., and Smart, N.R., (2015). Rates of steel corrosion and carbon-14 release from irradiated steels – state of the art review D2.1 from CArbon-14 Source Term project from the European Union's Seventh Framework Programme for research, technological development and demonstration under grant agreement no. 604779.

Tecon, R. and Or, D. 2017. Biophysical processes supporting the diversity of microbial life in soil. FEMS microbiology reviews 41(5), 599-623.

Tofts, P.S., Lloyd, D., Clark, C.A., Barker, G.J., Parker, G.J.M., McConville, P., Baldock, C., and Pope, J.M., (2000). Test Liquids for Quantitative MRI Measurements of Self-Diffusion Coefficient In Vivo, Magnetic Resonance in Medicine, v. 43, p. 368-374.

Trotignon, L., Thouvenot, P., Munier, I., Cochepin, B., Piault, E., Treille, E., Bourbon, X. and Mimid, S. 2011. Numerical Simulation of Atmospheric Carbonation of Concrete Components in a Deep Geological Radwaste Disposal Site During Operating Period. Nuclear Technology 174(3), 424-437.

Turrero, M.J. et al. (2024). Final technical report on the steel/cement material interactions. D2.7 of the HORIZON 2020 project EURAD. EC Grant agreement no: 847593.

Uras, S., Zovini, C., Paratore, A., Tits, J., Pfingsten, W., Dahn, R., Meeussen, H. and Seetharam, S.C. 2021 State of the art in packaging, storage, and monitoring of cemented wastes (Deliverable 7.1 of the Predis project), EC Grant Agreement No. No 945098.

van der Lee, J., De Windt, L., Lagneau, V. and Goblet, P. 2003. Module-oriented modeling of reactive transport with HYTEC. Computers & Geosciences 29(3), 265-275

van Eijk, R.J., and Brouwers, H.J.H., (2000). Prediction of hydroxyl concentrations in cement pore water using a numerical cement hydration model, Cement and Concrete Research, v. 30, no. 11, p. 1801-1806.

Van Humbeeck, H., De Bock, C., and Bastiaens, W., (2007). Published, Demonstrating the construction and backfilling feasibility of the supercontainer design for HLW (2B.14), in Proceedings Radioactive waste disposal in geological formations, Braunschweig, Place, Published, Reposafe, p. 336-354.

Vehmas, T., and Itälä, A., (2019). Compositional parameters for solid solution C-S-H and the applicability to thermodynamic modelling, KIT Scientific reports 7752 : Proceedings of the Second Workshop of the Horizon 2020 Cebama project, p. 293-300.

von Greve-Dierfeld, S., Lothenbach, B., Vollpracht, A., Wu, B., Huet, B., Andrade, C., Medina, C., Thiel, C., Gruyaert, E., Vanoutrive, H., Saéz del Bosque, F., Ignjatovic, I., Elsen, J., Provis, J.L., Scrivener, K., Thienel, K.-C., Sideris, K., Zajac, M., Alderete, N., Cizer, O., Van den Heede, P., Hooton, D.H., Kamali-Bernard, S., Bernal, S.A., Zhao, Z., Shi, Z., and De Belie, N., (2020). Understanding the carbonation of concrete with supplementary cementitious materials: a critical review by RILEM TC 281-CCC, Materials and Structures, v. 53, no. 136, p. 34.

Warthmann, R., Mosberger, L. and Baier, U. 2013 Langzeit-Degradation von organischen Polymeren unter SMA-Tiefenlagerbedingungen. Nagra, Wettingen, Switzerland.

Wersin, P., and Kober, F. (2017). FEBEX-DP − Metal corrosion and iron-bentonite interaction studies. Nagra Arbeitsbericht NAB 16-16, Nagra, Wettingen, Switzerland.

Wieland, E., Kosakowski, G., Lothenbach, B. and Kulik, D.A. 2020. Geochemical modelling of the effect of waste degradation processes on the long-term performance of waste forms. Applied Geochemistry 115, 104539.

Wieland, E., Kosakowski, G., Lothenbach, B., Kulik, D.A. and Cloet, V. 2018 Preliminary assessment of the temporal evolution of waste packages in the near field of the L/ILW repository Nagra Arbeitsbericht NAB 18-05. Nagra, Wettingen, Switzerland.

Wieland, E., Miron, G.D., Ma, B., Geng, G. and Lothenbach, B. 2023. Speciation of iron(II/III) at the iron-cement interface: a review. Materials and Structures 56(2), 31.

Wittebroodt, C., Turrero, M.J., Torres, E., Gomez, P., Garralon, A., Notario, B., Sanmiguel, M., Cuevas, J., Mota, C., Ruiz, A.I., Fernandez, R., Ortega, A., Samper, J., Mon, A., Montenegro, L., Hadi, J., Kizcka, M., Jenni, A., Goethals, J., Greneche, J.M., David, K., Wersin, P., Havlova, V., Klajmon, M., Dobrev, D., Vecernik, P., Fabian, M., Jacques, D. (2024a). Final technical report on the steel/clay material interactions. Final version as of xx.xx.xxxx of delivrable D2.7 of the HORIZON 2020 project EURAD. EC Grant agreement no: 847593.

Wittebroodt C., Goethals J., De Windt L., Fabian M., Miron G.D., Zajec B., and Detilleux, V. (2024b): Final technical report on the steel/cement material interactions. D2.9 of the HORIZON 2020 project EURAD. EC Grant agreement no: 847593.

Zhang, G., Yang, Z., Yan, Y., Wang, M., Wu, L., Lei, H., and Gu, Y., (2021). Experimental and theoretical prediction model research on concrete elastic modulus influenced by aggregate gradation and porosity, Sustainability, v. 13, no. 1811, p. 16.